FALL/WINTER 2014
VOLUME 6, NUMBER 2

Print ISSN: 2152-4157
Online ISSN: 2152-4165

WWW.IJERI.ORG

International Journal of Engineering Research & Innovation

Editor-in-Chief: Mark Rajai, Ph.D.
California State University Northridge

Published by the
International Association of Journals & Conferences

CUTTING EDGE JOURNAL OF RESEARCH AND INNOVATION IN ENGINEERING

Print ISSN: 2152-4157
Online ISSN: 2152-4165

www.ijeri.org

www.iajc.org

INTERNATIONAL JOURNAL OF ENGINEERING RESEARCH AND INNOVATION

ABOUT IJERI:

- IJERI is the second official journal of the International Association of Journals and Conferences (IAJC).
- IJERI is a high-quality, independent journal steered by a distinguished board of directors and supported by an international review board representing many well-known universities, colleges, and corporations in the U.S. and abroad.
- IJERI has an impact factor of **1.58**, placing it among an elite group of most-cited engineering journals worldwide.

OTHER IAJC JOURNALS:

- The International Journal of Modern Engineering (IJME) For more information visit www.ijme.us
- The Technology Interface International Journal (TIIJ) For more information visit www.tiij.org

IJERI SUBMISSIONS:

- Manuscripts should be sent electronically to the manuscript editor, Dr. Philip Weinsier, at philipw@bgsu.edu.

  For submission guidelines visit www.ijeri.org/submissions

TO JOIN THE REVIEW BOARD:

- Contact the chair of the International Review Board, Dr. Philip Weinsier, at philipw@bgsu.edu.

  For more information visit www.ijeri.org/editorial

INDEXING ORGANIZATIONS:

- IJERI is indexed by numerous agencies. For a complete listing, please visit us at www.ijeri.org.

Contact us:

Mark Rajai, Ph.D.

Editor-in-Chief
California State University-Northridge
College of Engineering and Computer Science
Room: JD 4510
Northridge, CA 91330
Office: (818) 677-5003
Email: mrajai@csun.edu

www.tiij.org

www.ijme.us

INTERNATIONAL JOURNAL OF ENGINEERING RESEARCH AND INNOVATION

The INTERNATIONAL JOURNAL OF ENGINEERING RESEARCH AND INNOVATION (IJERI) is an independent and nonprofit publication, which aims to provide the engineering community with a resource and forum for scholarly expression and reflection.

IJERI is published twice annually (fall and spring issues) and includes peer-reviewed research articles, editorials, and commentary that contribute to our understanding of the issues, problems, and research associated with the engineering and related fields. The journal encourages the submission of manuscripts from private, public, and academic sectors. The views expressed are those of the authors, and do not necessarily reflect the opinions of the IJERI or its editors.

EDITORIAL OFFICE:

Mark Rajai, Ph.D.
Editor-in-Chief
Office: (818) 677-2167
Email: ijmeeditor@iajc.org
Dept. of Manufacturing Systems Engineering & Management
California State University-Northridge
18111 Nordhoff Street
Northridge, CA 91330-8332

THE INTERNATIONAL JOURNAL OF ENGINEERING RESEARCH AND INNOVATION EDITORS

TABLE OF CONTENTS

IN THIS ISSUE (P.5)
USING SOFTWARE ENGINEERING BEST PRACTICES TO CREATE AN APP TO TEST TOUCHSCREEN COMPATIBLE PROSTHESES

Philip Weinsier, IJERI Manuscript Editor

Touchscreen technology is ubiquitous. Sure, easy to say, but rather subjective. By some estimates, 2013 alone saw the shipment of over one billion smartphones, which accounted for a little more than half of the mobile phones shipped. According to the Pew Research Center, 90% of Americans have a cell phone and 58% have smartphones. And that is just the adult population. Nor do these numbers take into account other touchscreen-compatible devices like tablet computers: another 42% of us own one. So, I feel quite comfortable saying that this technology touches most of us, while at the same time acknowledging that there are undoubtedly some people who do not use the technology. In most of those cases, though, I would guess the issue is, more often than not, related to an inability to afford the devices. I also feel it safe to say that, in most of those cases, the people have previously owned or at least used the technology at some point and are likely to own a touchscreen-compatible device in the future. But it is not this greater portion of our population that is being addressed in this article (see *Using Software Engineering Best Practices to create an App to Test Touchscreen Compatible Prostheses* on p.5). Rather, the focus is on that portion of the population not physically able to interact with the technology: those with prosthetic arms, hands, and/or fingers.

It would be hard to find an active member of our society who is not aware of the field of prosthetics. By the same token, it would be hard to find an active member of our society who is familiar with how the technology works, and the fact that there are different technologies at work here. Herein lies the reason why I am focusing on this article. I feel that it is important for us, given the ubiquity of touchscreen devices, to understand how they work and how researchers are helping to make such devices accessible to people with prostheses. Did you know that current technology offers us a spray with nano particles to help the material of the prosthesis react with the touchscreen device; resistive-type screens that can respond to materials beside human skin; and, touchscreen-compatible leather and textiles that work with capacitive-type touchscreen devices? Additionally, other researchers are developing prosthetic devices with graspable bodies that include pointers, which can be configured to selectively contact the touchscreen display based on movements by the user, and which contain heating elements that can selectively warm the electrically conductive display.

In this current study, participating students touched a number of "app" targets with their index fingers and recorded the number of errors generated by the app. Average error and standard deviations were calculated for each student. Average student performance (touch error) and standard deviations were 1.22% and 0.28%, respectively. The testing was then conducted using items other than human skin such as a Band Aid, the fingertip of a glove, and a rubber-tipped stylus designed for tablets and smartphones. These tests were also conducted 10 times each and averaged. The Band Aid and glove proved to be much worse than the bare human fingertip, with a percentage of error greater than 5% for each and a huge standard deviation greater than 12% for each. The stylus recorded better accuracy than the human finger, with an average error under 1% and a standard deviation of 0.29%. This provided both a baseline for normal human interaction and a range of responses for artificial materials that interact with the touchscreen. This study and the results can aid in the development process for prosthetic fingertips to give people the ability to reliably activate touchscreens. It is the authors' hope that this work will lead to enhanced usability of currently available products, or even as-yet undiscovered products, available to the minority portion of the population not currently able to adequately and efficiently use touchscreen devices.

Editorial Review Board Members

USING SOFTWARE ENGINEERING BEST PRACTICES TO CREATE AN APP TO TEST TOUCHSCREEN COMPATIBLE PROSTHESES

Andrew James Trapp, Robert Morris University; Sushil Acharya, Robert Morris University; Benjamin Campbell, Robert Morris University

Abstract

Touchscreen technology in society today is obvious. However, such technology is not usable for an important minority population, namely those with prostheses. Medical technology has advanced to the point where the missing body part can be replaced with a convincingly realistic prosthesis. However, not all functionality or normality is restored. The individual would be unable to utilize capacitive touchscreens with the prosthesis, and such touchscreens are becoming more and more commonplace. This can be mitigated by the development of touchscreen-compatible prostheses. Development of such a device should consider current uses of touchscreens as well as the future of such technology, while also meeting a standard of accuracy defined by the natural accuracy of a human finger. This study was devoted to devising an Android app using software engineering best practices that would assist in developing prosthetics capable of resolving issues like accuracy and interactivity faced by the prosthetics in use today. Accuracy can be tested, analyzed, and adjusted through use of a custom-built Android application. The application will help ensure proper development for a functional and useful prosthesis. Once developed, such a prosthesis would then provide users with the freedom to interact with capacitive touchscreens.

Introduction

Touchscreens are beginning to shape many different fields of technology in use in society, and smart phones and tablet PCs are some of them. Smart phones are the new wave for cellular communication and tablet PCs are widely used for a variety of computing needs. Smart phones are powerful devices that offer people an incredible capability to access information when needed [1]. Most smart phones feature touchscreens, partially because touchscreens are a popular new technology for companies to exploit [2]. For the first time, in 2013, over a billion smart phones had been shipped [3]. Table 1 depicts this growth. Tablet PCs operate as a small computer with an entirely touchscreen-based interface and have become a favorite for all generations. Figure 1 depicts the rapid growth of the tablet PC market; reaching the level of desktop and notebook PCs in an incredibly short amount of time [4]. While touchscreens have their roots as musical synthesizers [5], they have evolved over the decades to become a multipurpose technology that allows for many different forms of interaction such as swipe keyboard typing and pinch-to-zoom. Though smart phones are the most common instances of touchscreen usage, the device list goes beyond phones to everyday things such as coffee machines, appliances, and service kiosks. Touchscreen voting machines are becoming more and more commonplace [6], though many are currently resistive, meaning they do not require skin contact. Regardless of the touchscreen style, the screens are becoming something that most people interact with frequently, if not daily, and are comfortable with.

Table 1. Top Five Smartphone Vendors, Shipments, and Market Share, 2013 (in Millions)

Vendor	2013 Shipment Volumes
Samsung	313.9
Apple	153.4
Huawei	48.8
LG	47.7
Lenovo	45.5
Others	394.9
Total	1,004.2

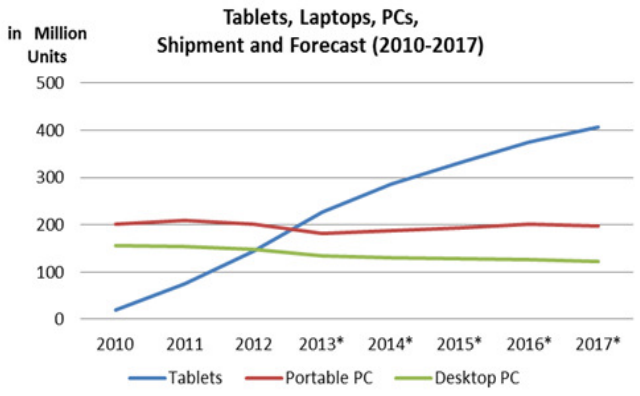

Figure 1. Tablets Shipment and Forecast

Although teenagers are likely the largest group of touchscreen users in society today, it must also be recognized that touchscreen users can come from nearly the full age spectrum. For example, touchscreen devices are being used in schools to teach children [7]. Cost of tablets and easily available/downloadable apps are contributing to such usage. The apps are being used to supplement learning and even teach new things, while the children play games. At the opposite end of the age spectrum are the elderly users. For those in assisted living, touchscreen devices such as digital agendas can help the elderly keep track of events, calendars, contact information, medicine, etc. [8]. In both nursing homes and hospitals, touchscreen devices are rapidly replacing standard paper-and-pencil forms for those who may not be able to properly manipulate a normal writing device. This seemingly simple act restores some degree of independence lost when one comes to have difficulty with non-electronic tools.

In between and including these two groups of users is a wide range of users with many different professions. While all careers are fundamentally different, most can find some use for touchscreen devices, and apps can be developed for almost all jobs. For example, airlines have started equipping pilots with tablets loaded with all the many different flight schedules and manuals they require for flight operations, instead of the bulky manuals weighing 35 pounds or more they are seen carrying around [9]. Many if not all professions can find such an advantage, allowing touchscreens to be a wide-reaching tool. Unfortunately, despite the large range of touchscreen users, there are also a good number who cannot make use of them; most prominent are those with prosthetic arms, hands, and/or fingers.

In this paper, the authors discuss the development of an Android app using software engineering best practices to test the accuracy of artificial fingertips; some are available commercially, while others were developed in the authors' institute lab. The resulting data can then be used to refine or redesign prosthetic fingertips in order to ensure that the user has the best possible range of accuracy and can be involved in interactivity. First, work carried out on touchscreens to make them usable for those with disabilities must be studied. Touchscreens must then be analyzed in order to determine what needs to be addressed when creating an accuracy application. Issues and limitations must be specifically and individually addressed. Also presented here are touchscreen issues and limitations, specifically accuracy and interactivity. Second, the application must be well designed. The design must encompass the issues and limitations that were found in the touchscreen analysis. The authors further discuss the software engineering artifacts that are created to support the app development like the software requirements document, software design document, use-cases, etc. Software engineering best practices must be used to create such artifacts.

Next, the application should be developed. It should follow the design to make sure it covers all bases and purposes. Once complete, the application must be tested for accuracy to make sure that it performs to the necessary standard. This can be done in the development stage of the application itself by utilizing displays of the mathematics the system uses on the backend to calculate the target values. Finally, the application must be reviewed against the requirements specification to ensure that all required components are present in the application. This will ensure that the application does what it is intended to do. At this point, the application will be ready for production use, and testing of artificial fingertips can begin. Preliminary results from this study were promising.

Related Work on Touchscreens

The proliferation of touchscreen-based devices has led researchers to investigate the possibility of the technology for users with physical disabilities. McGookin et al. [10] investigated the usability of touchscreen being used by those with visual impairments. They investigated ways of overcoming touchscreen accessibility problems by comparing a raised paper overlay touchscreen-based MP3 player with a touchscreen gesture-based player. Trewin et al. [11] explained that the potentials of touchscreen devices like Smart Phones and Tablets are not yet fully realized for those with dexterity impairment. They observed that the dexterity demands of important accessibility features made such devices unusable for many users with this impairment. Oh et al. [12] proposed techniques to teach touchscreen gestures to the visually impaired. The first technique uses corrective verbal feedback using text-to-speech and automatic analysis of the user's drawn gesture.

The second technique uses gesture sonification to generate sound based on finger touches, creating an audio representation of a gesture. Anthony et al. [13] studied YouTube videos to investigate touchscreen interaction for people with motor impairments. They studied the video to characterize the interaction, the challenges encountered, and the adaptations being adopted in daily use to find that, while many people with motor impairments find touchscreen devices empowering, accessibility issues still exist. Cheng and Takatsuka [14] proposed a new approach for fingertip interaction with large display systems using monocular computer vision. By taking into account the location of the user and the interaction area available, they are able to estimate an interaction surface—virtual touchscreen—between the dis-

play and the user. Ongoing research on touchscreen usability issues to a minority population strengthens the case to develop an Android app for artificial fingertip research.

Understanding Touchscreens

There are two types of touchscreen technology in consumer electronics: Resistive and Capacitive. Resistive touchscreens operate on the basis of screen pressure. A user presses the touchscreen glass panel to register inputs. The glass panel is covered with two metallic layers, one of which is conductive, whereas the other is resistive. Between the layers are spacers; when the touchscreen is in the on-mode, there is an electrical current. When pressure is applied to the glass panel, the two layers come into contact at that spot. A change in the electric field occurs and the coordinates of this touch point are then translated by a device driver to register an input. This input is then interpreted by the operating system to execute a function. These touchscreens are used on some Samsung, HTC, and LG phones, and are typical of ATMs, supermarket checkout stations, and the electronic UPS signature pad for deliveries. [15]

Capacitive touchscreens operate by making use of the conductive property of human fingers. Like resistive touchscreens, these also have a glass panel. However, the glass panel is covered by a transparent conductor. An electrical charge is stored in this conductor. When a user touches the screen with his/her finger, the electrical field gets distorted. The device driver uses this distortion to register the contact point. This input is then interpreted by the operating system to execute a function. These touchscreens are used on the iPhone, Droid Eris, and Blackberry Storm [15]. A major drawback in these types of screens is that either they do not accurately register inputs or they fail to register inputs altogether when the normal human finger does not make screen contact.

Due to the design of capacitive touchscreens, prostheses do not possess the necessary conductance to complete the alternating current circuit. Standard prostheses run into the same issue as a normal pair of gloves: without the physical skin contact, the ability to interact with the capacitive touchscreen is taken away. Further, prostheses, by nature, are not as coordinated as natural fingers, so an issue of accuracy develops as well. There are tools such as styli and other things that can interact with and increase the accuracy of capacitive touchscreens. Unfortunately, a number of these tools face similar problems of conductance, thus making progress on the accuracy front but not much on the more pressing interactivity front. Research has shown that accuracy and interactivity are two major, interrelated issues with touchscreens. This study took into consideration these two issues when designing the Android app.

The problem with any form of touchscreen aid is accuracy. If an item or tool is not accurate, then it does not really do much to help the user interact. This problem carries into any attempt at creating a touchscreen-compatible prosthetic fingertip. So, accuracy must be factored into such a prosthetic. Testing of accuracy is best done on the same kind of screens that the fingertip will eventually be used for. To this end, the authors developed an Android application that can gather and analyze touchscreen accuracy data. This data can then be analyzed and manipulated in order to extrapolate results that can then be used to refine the fingertip. The application provides a valuable design and development tool. Without it, accuracy can only be determined through blind trial and error, which is both inefficient and likely ineffectual. As such, the application will not only help make the fingertip more useable, but it will also help make the fingertip development process faster and more efficient with raw, physical data to guide changes and improvements.

Accuracy results in interactivity. To develop interactivity, the fundamental issue of conductance must be addressed. There are two possible solutions that come to the surface. The first is to develop new smartphones, tablets, and other touchscreen devices that rely on resistive touchscreens, rather than capacitive. This would enable any kind of implement to utilize the screen. Unfortunately, this would require companies to pour time and funding into a limited market that is not, by any measure, a majority. Further, this brings back issues that face resistive technology, such as unintended interaction (as through “pocket-dialing”). The secondary solution, the arguably more viable of the two, is to develop a means for prostheses to interact with capacitive touchscreens. This can be possibly accomplished through prosthetic add-ons, special implants, or even a new prosthetic material.

Android App Design Methodology

It was realized that the development of an application of such significance would benefit from the use of software engineering best practices. Making prostheses compatible with touchscreens is only part of the challenge. Due to the often small surfaces that devices feature, accuracy is an important issue that must be considered. Without an accurate system, the user would have a rather limited range for interactivity. In order to provide usability to someone with an artificial hand, prostheses must be as accurate as possible.

For developing accuracy in such prostheses, the best medium for testing purposes would be the very devices that

such prostheses would likely interact with, like smart phones and tablets. To measure accuracy, special applications can be developed to measure, record, and analyze the contact points of whatever is touching the screen. Then, informed changes can be made to the prosthesis in order to improve its accuracy. Developing accuracy in an artificial fingertip is an iterative process. The first step is baseline testing. This should be done with a normal human finger so as to determine a normal level of accuracy. Next, the artificial fingertip should be tested to observe its accuracy in comparison to the baseline. After this has been done, modifications can be made as needed. These modifications can be in size, composition, design, point of contact, etc. The process should then enter an iterative process of comparison and modification until a sufficient threshold of accuracy is reached. A customized application would allow developers to monitor, administer, and track tests in a uniform, central manner. Further, the application could be customized and/or adapted into other tests if the researchers and developers need more than basic accuracy.

Once the domain was understood in detail, software requirements were identified. Research and iterative requirements elicitation meetings with faculty advisors led to the identification of five key features for the app. These features were: visual targets, touch-event detection, coordinate display, recording, and exporting. Table 2 lists these features with requirement statements as well as implementation thoughts.

Table 2. Requirements Specification

Feature	Requirement	Implementation
Visual Targets	R1: Users shall use predefined targets on the touchscreen to aim for accuracy.	Implement a graphical target interface in app layout.
Touch Event Detection	R2: App shall know when the screen is touched	Implement onTouchEvent listeners in code to detect touch points and their coordinates.
Coordinate Display	R3: App shall display the screen point where the user has touched.	Implement Toast function to display coordinates of each touch event.
Recording	R4: App shall know the coordinates of the point where the screen is touched.	Implement write functions in order to record touch events and coordinates to a data file.
Exporting	R5: Users shall export touch data points.	Implement email function to send data files to user-defined address.

A graphical target system allows the tester to take advantage of uniform, set points to touch in order to gauge accuracy. A touchscreen's size is measured in pixel density, so the accuracy must be tested at this pixel level. Targets can encompass several groupings of pixels and will allow the device to determine a relatively sizeable range of points. For the baseline, the tester can see how many pixels are impacted with each touch event. Then, for the fingertip's testing, the application can find the same measurement of pixel interaction and help the tester determine the level of overlap between the two tests. Once that overlap is found, the tester can determine the accuracy of the artificial fingertip. In essence, the more overlap, the higher the level of accuracy.

The app is developed using the Android programming language, as it is arguably the best mobile application platform to use because of the ease of access to the development software (free and downloadable from the official Android development site) and because it is easier to become a published application developed for Android, as opposed to Apple's iOS. In order to determine, record, and analyze the pixel points, the application will need to have a built-in coordinate system, which, through the hard code foundation of the Android programming language, allows applications to function at the pixel level. Applications can include code to display, record, and otherwise access/manipulate the coordinate locations of touch events; it is these features that can be implemented in a prosthesis testing application for the purposes of recording and gauging accuracy. The class diagram depicted in Figure 2 illustrates the interactions of the various code functions that such an application would require.

Once the target and coordinate systems facilitate touch events, the coordinates and other data should be stored in a database. In the case of Android, arrays can act as databases that allow for a slim, relatively easy, and somewhat "built-in" system for an application. This database should also be exportable so that developers and/or researchers can have better access to the data for the purposes of analysis and interpretation. Once the app is built, a tester will be able to initiate trials. These trials, upon startup, will allow the user to record a set number of touch events, have them exported, and then analyze them outside of the application so that the fingertips can be calibrated, adjusted, or even redesigned. Figure 3 depicts a use-case diagram that illustrates this flow of the touch data and calculations.

The application itself is designed to be relatively easy to navigate; unnecessary clutter was omitted and the buttons were designed for simplicity. As seen in Figure 4(a), the Homepage is restricted to only three buttons for navigating to each of the three pages of the application. And, there are

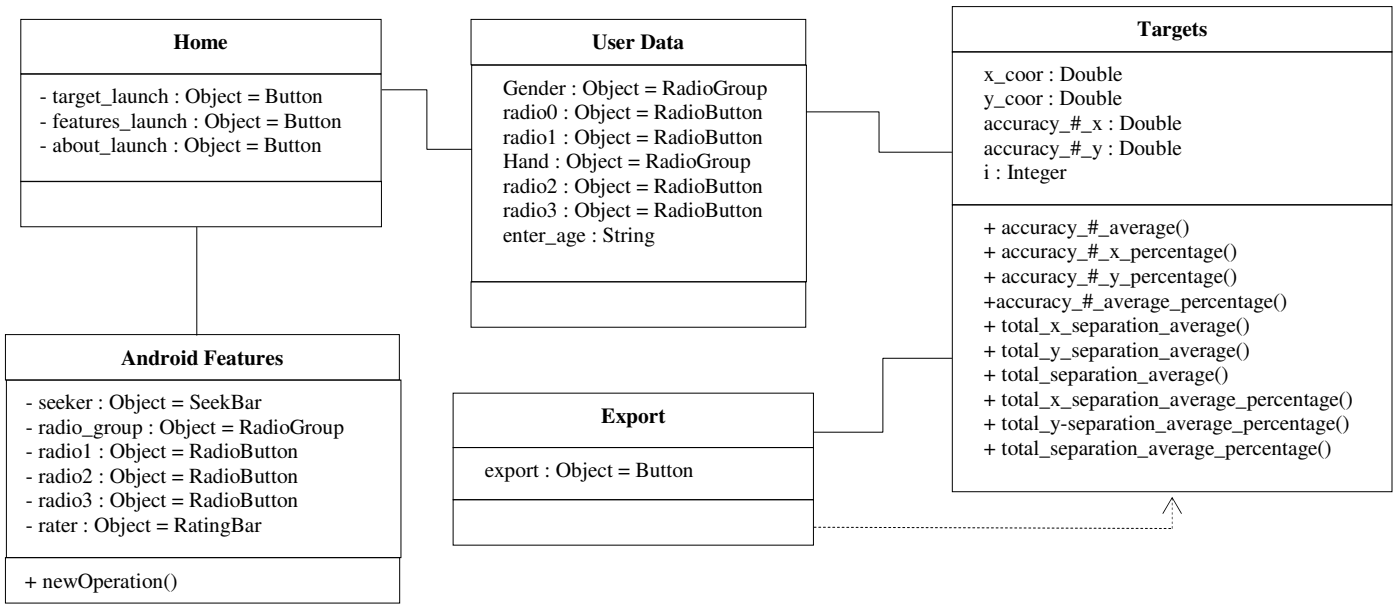

Figure 2. Class Diagram

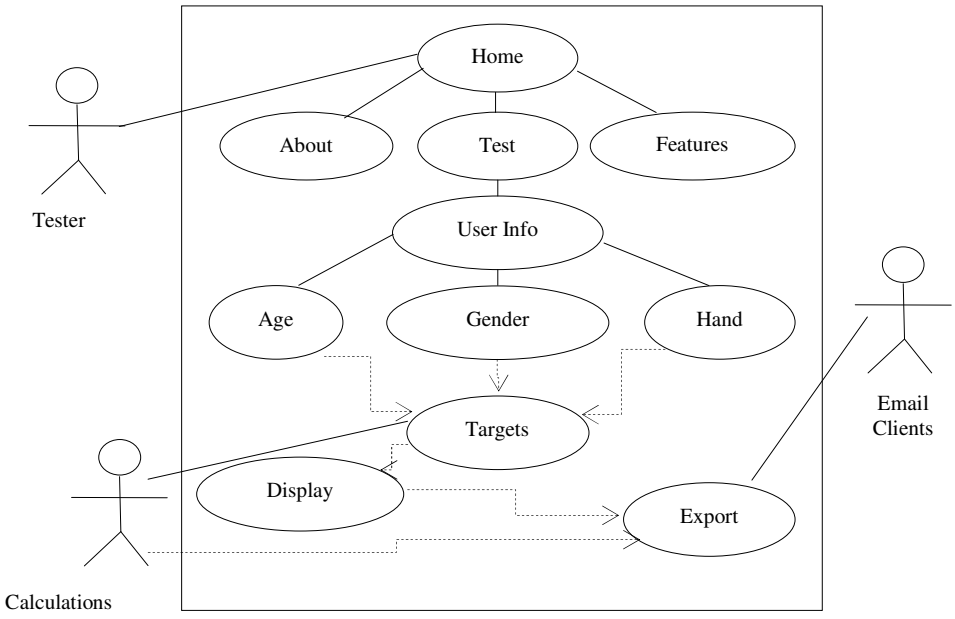

Figure 3. Use-case Diagram

no loading times. Figure 4(b) illustrates the actual target test page. The targets are overlaid with their numbers so that users can easily tell which targets they need to touch at any given point. All page elements on all pages of the application are placed on a blank white background in order to ensure adequate visibility.

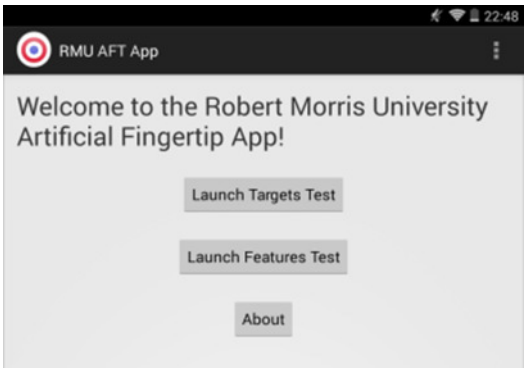

(a) Welcome Window

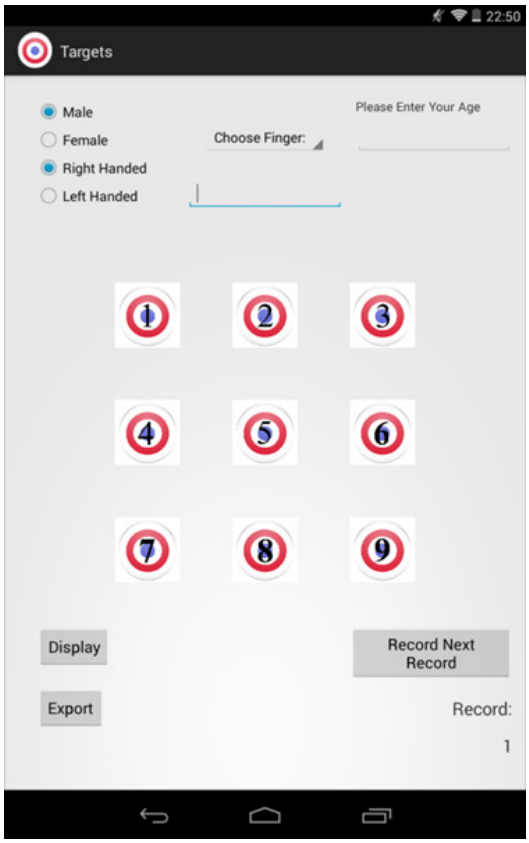

(b) Contact Points

Figure 4. App Windows

App Validation

In order for the app to perform as required, the software must undergo a validation test. This test is split into two parts. First, the application itself must be using the correct data in its calculations. The individual target center points must be correct in order for the accuracy data to be valid. This was implemented by displaying the variables calculated by the device. Android has built-in methods for accessing the device's screen size; this information was used to calculate the exact center points of the targets. These results were then used in the second part of the validation. Once the application itself is determined to have the correct "control points", the system is then hand-tested by real users in order to determine that a) the application is producing the proper, required data, and b) that the data being produced are actually useful. This testing was done by the development team.

Validation testing of the application showed that the system performed as required. The trials were performed with both human fingers and with a basic touchscreen stylus. The data were then exported, consolidated, and analyzed to produce visual results in the form of two graphs. The graphs depicted in Figures 5(a) and 5(b) take averages of five separate tests, compared against the defined center points of each of the five targets. The two tests produced similar results, but each test arrived at the same conclusion in different ways. The human finger testing showed that the subjects had a varying distance of separation from the target center points, but were less than two percentage points off the average. Conversely, the stylus testing showed much more consistent separation from the center pixels; but, because the touch points were further away, the overall accuracy ended up being within one to two percentage points of the separation shown by the human finger trials. A possible explanation is that the users were holding the tablet at an angle. As they touched the targets with the stylus, because of the angle, the top of the stylus touched the screen first and rocked upwards, causing the touch to be registered as further off center. Meanwhile, the finger tests were more of a direct touch; so, while the distances were more varied, they were altogether closer. This may affect the prostheses, and it will be a point of interest to see if the prostheses act similarly to real fingers or more like a stylus.

Figures 6(a) and 6(b) show the average coordinates of the test touches (triangles) in relation to the actual position of the center points of the targets (squares). The graphs illustrate the earlier point about the human touches being overall closer to center than the stylus touches. Figures 6(a) and 6 (b) show the consistency of the touch distances. As Figure 6 (a) shows, the human testing varied more than the much smoother stylus line of Figure 6(b).

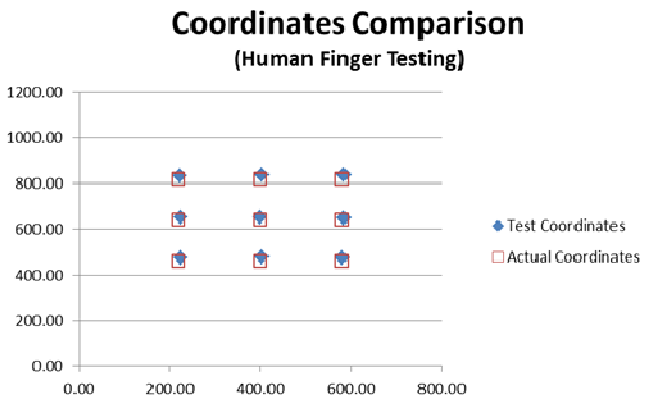

(a) Coordinates Comparison with Human Fingers

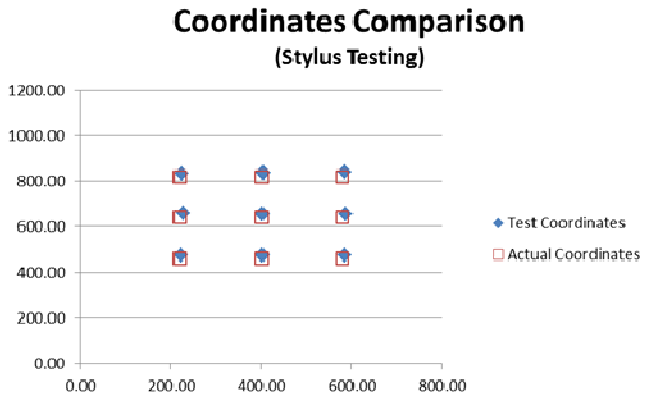

(b) Coordinates Comparison with Stylus

Figure 5. Coordinates Comparisons

Preliminary App Results

The preliminary data collected through the app showed promising results. The app was used to measure human touch accuracy compared with a few materials commonly used to interact with a touchscreen. Students participating in this project touched the nine app targets with their index finger and recorded the error number generated by the app. This was repeated 10 times (90 total touches, 10 output error numbers). The average error and standard deviation were calculated for each student, showing very similar accuracy. The average student performance (touch error) and standard deviation calculated combining the readings of five students were 1.22% and 0.28% , respectively (see Table 3). The testing was then conducted using items other than human skin that normally contact touchscreens, such as a Band Aid, the conductive touch pad on the fingertip of a glove, and a rubber-tipped stylus designed for tablets and smartphones. These tests were also conducted 10 times and then averaged. The Band Aid and glove proved to be much worse than the bare human fingertip, with a percentage of error greater than 5% for each, with a huge standard deviation greater than 12% each. The stylus recorded better accuracy than the human finger, with an average error under 1% and a standard deviation of 0.29% (see Table 4). This provided both a baseline for normal human interaction and a range of responses for artificial materials that interact with the touchscreen. This method and data can aid in the development process for prosthetic fingertips to give people with disabilities the ability to reliably activate touchscreens.

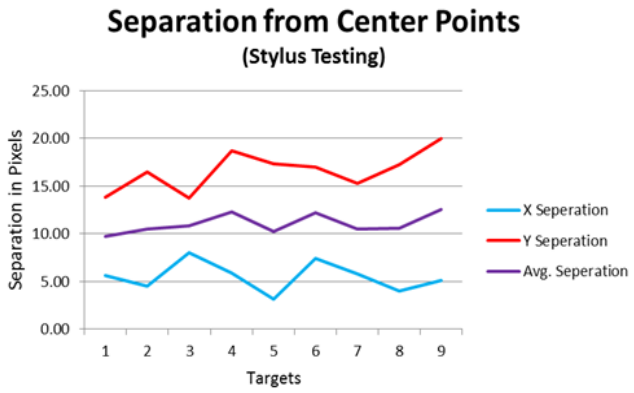

(a) Results of Human Finger Testing

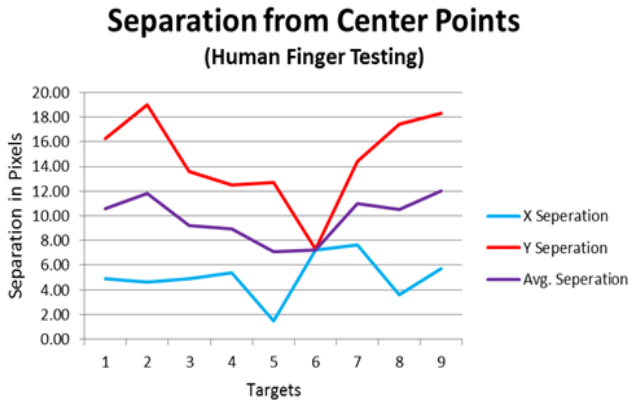

(b) Results of Stylus Testing

Figure 6. Testing Results

Conclusions and Future Directions

Smart phones and tablets are some of the current forerunners of touchscreen technology, but the future could get even more advanced. For example, the field of augmented

reality is one that is beginning to grow rapidly and is penetrating the mobile industry [16]. Unfortunately, despite the large range of touchscreen users, such technology is not usable for the population of amputees that use hand prostheses. In this paper, the authors described the use of domain knowledge and software engineering best practices to design and develop an Android app to test the accuracy of prostheses on touchscreens. Using software engineering best practices, the app was designed, developed, and validated. The application's design covered all listed requirements and was found to produce the necessary data in a valid format. The data are fully exportable and formatted in such a way as to facilitate easy manipulation and analysis outside of the application. The validation test determined that everything was working as designed and that the data produced were both informative and useful. Preliminary data were collected and analyzed. The app was being used with more diverse prosthesis materials. It is expected that this analysis will lead to a material that will be able to provide usability to the minority population referred to in this study.

Table 3. Results from Five Students using the Touch Test App with Their Index Finger, Averaged over 10 Trials

	Error percentage	Standard deviation
Student J.H.	1.17%	0.46%
Student D.P.	1.24%	0.36%
Student K. S.	1.21%	0.41%
Student D.K	1.26%	0.45%
Student Z.B.	1.24%	0.22%
	Average Student touch error	Combined standard deviations
Student Total	1.22%	0.28%

Table 4. Results from Common Materials on Touch Test App, Averaged over 10 Trials

	Error percentage	Standard deviation
Band-Aid on finger	5.57%	12.60%
Winter glove with conductive patch over finger	5.05%	12.20%
Rubber tipped Stylus designs for tablets	0.91%	0.29%

No matter what type of system touchscreens become a part of, they represent a technology that is very likely to persist for a long time to come. Perhaps one day, medicine will advance to the point of restoring limbs and body parts in their natural form. But until then, once touchscreen-compatible artificial fingertips and other prostheses are developed, those that need them will have options to be able to interact with touchscreens accurately if they so choose, giving them the same freedom of choice as those with fully functioning hands, fingers, etc.

References

[1] Ho, S., Sun, W., & Wang, Y. (2011). Investigation of factors influencing the adoption of mobile data services. *Proceedings of the 13th International Conference on Electronic Commerce*, Article No. 11.

[2] Yang, Y., Zhang, Y., Hou, Z., & Lemaire-Semail, B. (2011). Adding haptic feedback to touchscreens at the right time. *Proceedings of the 13th international conference on multimodal interfaces*, (pp. 73-80).

[3] Worldwide Smartphone Shipments Top One Billion Units for the First Time, According to IDC, IDC Analyze the Future, Retrieved from getdoc.jsp?containerId=prUS24645514

[4] The Statistics Portal. Retrieved from http://www.statista.com/statistics/272595/global-shipments-forecast-for-tablets-laptops-and-desktop-pcs/

[5] Cohen, N. (2011). *Timeline: A History Of Touch-Screen Technology: NPR*. Retrieved from http://www.npr.org/2011/12/23/144185699/timeline-a-history-of-touch-screen-technology

[6] Jones, M. (2005). The pedagogic opportunities of touch-screen voting. *Proceedings of the 10th annual SIGCSE conference on Innovation and technology in computer science education, 37*(3), 223-226.

[7] McKnight, L., & Fitton, D. (2010). Touch-screen technology for children: giving the right instructions and getting the right responses. *Proceedings of the 9th international conference on interaction design and children*, (pp. 238-241).

[8] Iglesias, R., De Segura, N. G., & Iturburu, M. (2009). The elderly interacting with a digital agenda through an RFID pen and a touchscreen. *Proceedings of the 1st ACM SIGMM international workshop on media studies and implementations that help improving access to disabled users*, (pp. 63-70).

[9] Sheryl, J. (2013). *American Airlines has completed the rollout of computer tablets to pilots*. Retrieved from http://aviationblog.dallasnews.com/2013/06/american-airlines-has-completed-rollout-of-computer-tablets-to-pilots-15143.html/

[10] McGookin. D, Brewster, S., & Jiang, W. (2008), Investigating Touchscreen Accessibility for People with Visual Impairments. *Proceedings of the 5th Nordic conference on Human-computer interaction: building bridges* (NordiHI 2008), (pp. 298-307), ACM Digital Library

[11] Trewin, S, Swart, C. & Pettick, D. (2013). Physical Accessibility of Touchscreen Smartphones, *Proceedings of the 15th International ACM SIGACCESS*

Conference on Computers and Accessibility (ASSETS '13), Article # 19, ACM Digital Library

[12] Oh, U., Kane, S., & Findlater, L. (2013). Follow That Sound: Using Sonification and Corrective Verbal Feedback to Teach Touchscreen Gestures. *Proceedings of the 15th International ACM SIGACCESS Conference on Computers and Accessibility* (ASSETS '13), Article # 13, ACM Digital Library

[13] Anthony, L., Kim, Y., & Findlater. L. (2013). Analyzing user-generated YouTube videos to understand touchscreen use by people with motor impairments. *Proceedings of the SIGCHI Conference on Human Factors in Computing Systems* (CHI'13), (pp. 1223-1232), ACM digital Library

[14] Cheng, K., & Takatsuka, M., (2006). Estimating Virtual Touchscreen for Fingertip Interaction with Large Displays. *Proceedings of the 18th Australia conference on Computer-Human Interaction: Design: Activities, Artefacts and Environments* (OZCHI 2006), (pp. 397-400), ACM Digital Library

[15] Soniak, M (2012). How do touchscreens work? Retrieved from http://mentalfloss.com/article/31378/how-do-touchscreens-work

[16] Karlsson, N., Li, G., Genc, Y., Huenerfauth, A., & Bononno, E. (2012). iAR: an exploratory augmented reality system for mobile devices. *Proceedings of the 18th ACM symposium on virtual reality software and technology*, (pp. 33-40).

Biographies

ANDREW TRAPP is an undergraduate Honors Software Engineering senior at Robert Morris University. Andrew is also pursuing an integrated Master's degree in Information Security and Assurance with a concentration in Enterprise Systems. Andrew can be reached at ajtst19@mail.rmu.edu

DR. SUSHIL ACHARYA is an Associate Professor of Software Engineering at Robert Morris University. His teaching involvement and research interests are in the areas of Software Engineering education, Software Verification and Validation, Data Mining, Neural Networks, and Enterprise Resource Planning. He is a member of the Nepal Engineering Association, ASEE, and ACM. He has published several papers in peer-reviewed journals and co-authored textbooks. In 2013, he received a National Science Foundation (NSF) Grant to develop course materials through an industry-academia partnership in the area of Software Verification and Validation. Dr. Acharya can be reached at acharya@rmu.edu

DR. BENJAMIN CAMPBELL is an Assistant Professor of Engineering at Robert Morris University. At RMU he has assisted with the Biomedical Engineering Program and is currently developing Mechatronics curriculum options. Previously, he worked as a laser engineer at the Penn State Electro-Optics Center specializing in laser micromachining with ultrashort pulse lasers for which he received an NSF grant in 2011. He holds a B.S. in Physics, an M.S. in EE from Penn State, and a Ph.D. in Engineering from Robert Morris University. Dr. Campbell can be reached at campbellb@rmu.edu

IMPROVING THE ROLLER SHAFT SUBASSEMBLY PROCESS USING DISCRETE-EVENT MODELING AND SIMULATION: A CASE STUDY

Ali Alavizadeh, Indiana University Purdue University-Fort Wayne; Robert Palevich, Indiana University Purdue University-Fort Wayne

Abstract

The objective of the study was twofold: 1) to identify sources of waste, if any, in terms of materials and man-hours in order to reduce the flow time of parts and the operational costs; and, 2) to conduct simulation experiments to compare three scenarios—one-, two-, and three-operator workstations—under the operational conditions of regular production versus ramp-up production (e.g., order size is doubled). The goal was to determine which scenario resulted in higher profitability. ARENA software was used to model the system, and statistics such as queue time and flow time and cost were analyzed to see which scenario would be optimum. The results suggested that, although for regular production one operator is enough, for ramp-up production, two operators would be more efficient in terms of cost.

Introduction

Modeling and simulation play a vital role in systems design and business process improvement. A model is a representation of a system or a concept. Models are built to help researchers better understand system behavior and run simulation experiments in order to observe system behaviors under various scenarios. In essence, simulation is "the imitation of the operation of a real-world process or system over time" [1]. In some cases, one may be able to study the actual system and modify it to observe the outcome (e.g., testing the impact of expanding the number of automated check-in kiosks on reducing passenger wait time) [2]; however, changing the setting of a real emergency room to study the impact on serving the patients is not a viable option.

Depending on the nature of the problem, one may need to use discrete-event or continuous simulation. For example, a typical queuing problem may be modeled using discrete-event modeling and simulation, while continuous modeling is suitable for heat transfer analysis in a conductor. Generally speaking, there are several important steps in building and simulating a model [3], [4]:

1. Problem statement and initial information gathering: The problem is clearly formulated and stated based on the information obtained through initial study.
2. Objectives and overall project plan: This includes the question(s) of interest, plan of study (i.e., number of people to include, cost, etc.), and scope.
3. Data collection: Current data relevant to the problem are collected. If data are lacking, an estimated range of input parameters will be used (i.e., typical cycle time for a process).
4. Model building: The model will be constructed using a specialized software package (e.g., ARENA, ProModel, etc.); although, if needed, one may use such programs as MATLAB or C++.
5. Verification and validation: The model should be verified and validated to ensure that it represents the system and its outputs appropriately.
6. Conducting simulation experiments: Depending on the problem, several scenarios are typically developed and run to compare the results.
7. Output analysis: The simulations outputs are compared and contrasted in order to identify the optimal solution among various alternatives.
8. Developing recommendations: A report is generated to discuss the identified solution and to make recommendations.

In this paper, the authors present the application of discrete-event modeling and simulation in a manufacturing company. The roller shaft operation was the primary focus of the study, used to analyze the impact of ramp-up production (e.g., a sudden increase in demand) on workstation flow time, utilization, and operational costs. Three different scenarios were considered: one-operator, two-operator, and three-operator workstations.

Literature Review

Modeling and simulation of manufacturing systems have been extensively studied and discussed. Smith [5] and Negahban and Smith [6] reported the results of a survey on the use of simulation in design and operation of manufacturing systems. Ferreira et al. [7] reported the results of modeling and simulation of an automobile assembly line using ARENA in which they studied the impact of changing the production sequence on line throughput. In another study to examine the usefulness of discrete-event modeling and simulation in small companies, Patterson et al. [8] used a different software package (Witness) to redesign a manufacturing

system. They considered the relative lack of spare resource capacity as a characteristic of small companies that was taken into account. They conducted simulation experiments to study the impact of purchasing a lathe machine on the bottleneck that exited in the manufacturing system; the results indicated an improvement in the bottleneck, though they required further validation.

The Case

Shuttleworth [9] is a manufacturing company in the area of material handling solutions and packaging products. Its customers range from the food industry to automobiles, medical, and pharmaceuticals, to name a few [10]. The company's manufacturing facility was visited as part of this current study in order to evaluate their roller shaft workstation. The workstation consisted of three subsections wherein processes were completed sequentially: chopping, chamfering, and cleaning. Figure 1 shows each of these subsections.

Data Collection and Analysis

Orders arrive on a daily basis and vary in quantity. According to the general manager, they could range from one to 4000 in a typical month. It was also mentioned that although the operators knew how to run each subsection and could run the workstation alone, depending on order size, more operators needed to be added in order to finish the orders more quickly. The general manager was asked to send a spreadsheet including the order quantity and dates that the company had received in the past three years. Using ARENA's built-in input analyzer, the authors noticed that, except for Weibull, none of the available probability distributions (exponential, gamma, normal, longnormal, uniform, beta, Erlang, and triangular) fit the data appropriately. Each of these distributions resulted in p-values less than 0.05. Figure 2 shows the best fit using Weibull distribution.

The fit was made based on a histogram with 40 bins. However, as shown in Figure 2, this fit would still result in a p-value close to 0.05 with a 95% confidence level. The authors, therefore, decided to use the real data to fit the data empirically using ARENA's input analyzer. Table 1 includes the cycle time for each subsection (in seconds). These were obtained from the general manager and based on their historical day-to-day operations.

Table 1. Cycle Time for the Three Subsections (in seconds)

Subsection	Chopping	Chamfering	Cleaning
Cycle time	8 - 15	10 - 14	10 - 14

(a) Chopping

(b) Chamfering

(c) Cleaning

Figure 1. The Subsections of the Roller Shaft Workstation

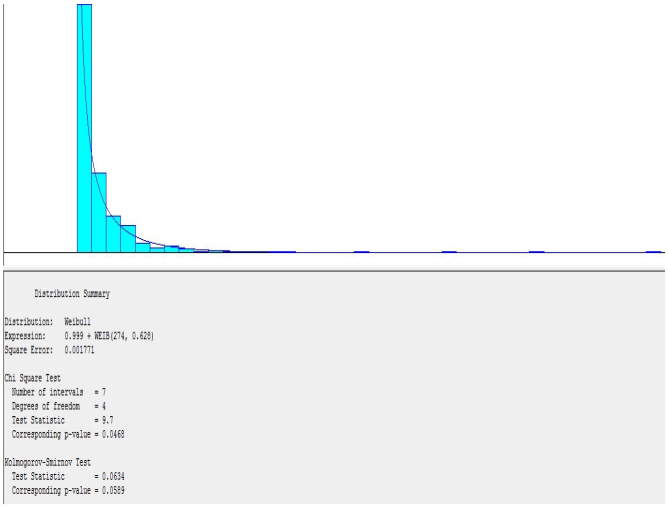

Figure 2. The Probability Distribution Function Estimated by ARENA's Input Analyzer

Model Building and Simulation

For the purpose of the simulation, three scenarios were considered:

1. One operator handles all three subsections—chopping, chamfering, cleaning;
2. Two operators handle all three subsections. In this case, one operator works only on the chopping subsection; the second operator switches between chamfering and cleaning, once s/he finishes 50 parts in each subsection; and,
3. Three operators, one for each subsection.

The computer model was built using ARENA 14.00.00000. Figure 3 shows the generic flowchart used to build the model for all of the scenarios. New orders arrived according to the empirical probability distribution calculated by ARENA's input analyzer, as discussed earlier. The interarrival time was modeled using a uniform distribution function with one and 30 as the number of days between two consecutive orders. The model consisted of two segments: the actual workstation model and a controller. The job of the controller was to shift the operator from one subsection to the other in the case of one- and two-operator scenarios. The three-operator scenario did not include the controller segment, since each subsection had only one operator. Figures 4-6 show each segment. The model was verified by analyzing its output and comparing the model components and parameters with the ones provided by the company. The verification was not completed as the experiments were hypothetical. A total of five replications were run for an 8-hour shift for one full year (365 working days).

Discussion

The authors compared two hypothetical operational conditions: Shuttleworth receiving a contract with a typical (normal) volume order (one to 4000 per month), and one with double that amount (ramp-up production). Furthermore, the workstation ran under the following conditions:

- Originally, there was one operator that ran the entire workstation (one-operator scenario).
- The average work week was 50 to 60 hours per week for one operator. The normal work week was composed of 10 hours per day with the extra on Saturday.
- The salary for the operator with no overtime was $36,400 per year. With time-and-a-half after 40 hours, the operator was paid $96,005 per year for an average work week of 57 hours. This was producing the product at a $59,605 overrun on a standardized pay level for the operator. Such an operation could result in a potential problem: the operator would become burned out (working too many hours). Operator morale could be also very low, due to the lack of planning.

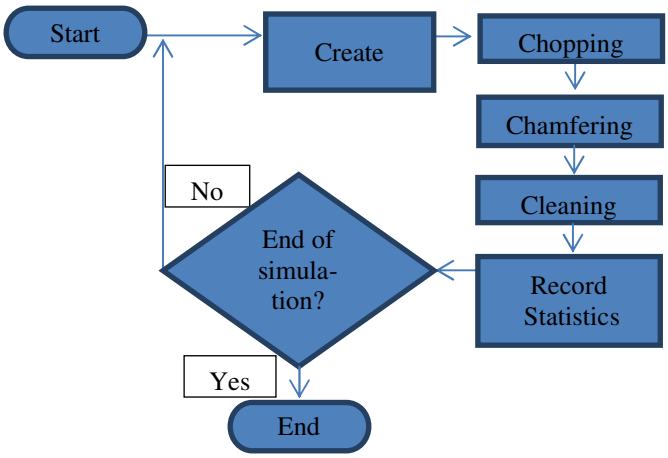

Figure 3. The Overall Simulation Flowchart

The challenge to management was to see what the profit opportunities were in relation to:

- Improving the process
- Adding revenue
- Improving return on its investment(ROI)
- Offsetting the aforementioned overloaded operation (one-operator scenario) with the new ones (two- and three-operator scenarios) and gain management acceptance
- Offsetting new employment costs with added internal revenue
- Offsetting the cost of new equipment with better process economies of scale

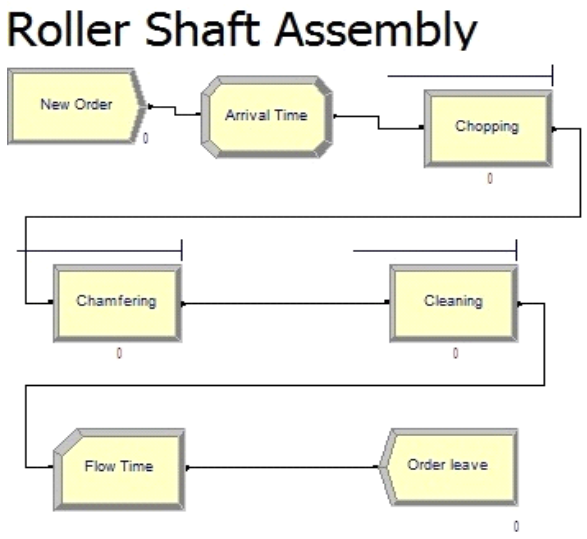

Figure 4. The Workstation Segment (the same for all of the scenarios)

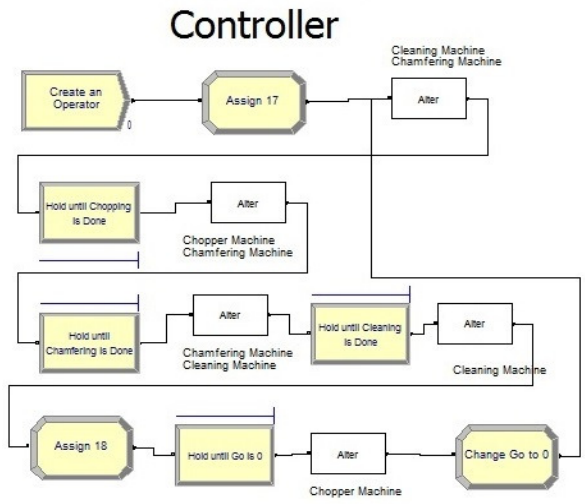

Figure 5. The Controller Segment (for the one-operator scenario)

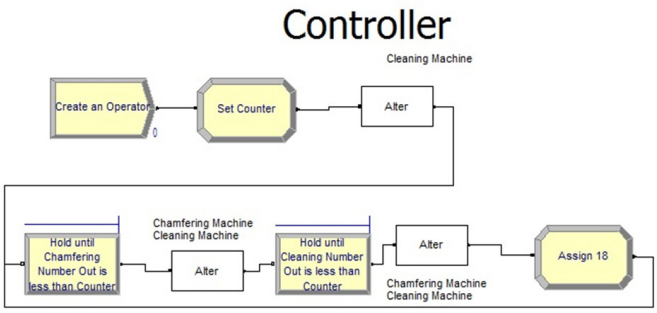

Figure 6. The Controller Segment (for the two-operator scenario)

The following is a summary of the results of the simulation for each of the three scenarios, under normal and ramp-up operations:

First Scenario—One Operator Handling All Three Subsections

Normal operation

- The value-added time = 0.0098600 hours
- The orders' quantity (number in) = 13,634
- The finished order (number out) = 13,634
- Work in progress = 67.96
- The average wait time in the queue = 12.2197 hours
- The total time = 12.2296 hours

Ramp-up operation

- The value-added time = 0.00985994 hours
- The orders' quantity (number in) = 15,912
- The finished order (number out) = 15,864
- Work in progress = 199.33
- The average wait time in the queue = 34.0025 hours
- The total time = 34.0124 hours

Second Scenario—Two Operators: One for Chopping, the Other for Chamfering and Cleaning

Normal operation

- The value-added time = 0.00985991 hours
- The orders' quantity (number in) = 13,831
- The finished order (number out) = 13,871
- Work in progress = 59
- The average wait time in the queue = 10.7737 hours
- The total time = 10.7836 hours

Ramp-up operation

- The value-added time = 0.00986178 hours
- The orders' quantity (number in) = 18,532
- The finished order (number out) = 18,511
- Work in progress = 64
- The average wait time in the queue = 9.6623 hours
- The total time = 9.6722 hours

Third Scenario—Three Operators: One for each Subsection

Normal operation

- The value-added time = 0.00986821 hours
- The orders' quantity (number in) = 13,634

- The finished order (number out) = 13,634
- Work in progress = 14
- The average wait time in the queue = 2.4948 hours
- The total time = 2.5046 hours

Ramp-up operation

- The value-added time = 0.0098601 hours
- The orders' quantity (number in) = 18,291
- The finished order (number out) = 18,291
- Work in progress = 20
- The average wait time in the queue = 2.7965 hours
- The total time = 2.8063 hours

By comparing the results, the authors found that, under normal operation, the ratio of value-added work to the total time (also called VSM) had significant variance depending on the scenario. In the first scenario, and under normal operation, the VSM is 0.0098600/12.2296 = 0.0806%. The VSM for this scenario, under the ramp-up operation was 0.0290%. For the second scenario, the VSM was 0.0914% and 0.1020% for normal and ramp-up operation, respectively. For the third scenario, the VSM was 0.2919% and 0.3514% for normal and ramp-up operation, respectively. The highest VSM, which was the case of the ramp-up operation with three operators, illustrates the most efficient use of the workforce. In terms of the average wait time in the queue for the ramp-up operation, the one-operator scenario had the highest amount (34.0025 hours), followed by the second scenario (9.6722 hours), and the third scenario (2.7965 hours). The same order was also observed for normal operational conditions.

The final decision ultimately will be based on the highest profit model utilizing a more uniform work schedule. There is a saying that it is a privilege to make a profit in corporate America, and the second scenario yields the highest profit. Only the mindset of upper management needs to be changed by running the second scenario to prove the point. This is discussed in the next section. Table 2 includes cost and revenue analysis of each scenario under the two operational conditions. Based on these results, the third scenario with a ramp-up operation seemed to be dominant with the highest revenue and best profit, which was 15% better than the first scenario with a ramp-up operation.

A Change in Management Opinion

Throughout the evaluation process, the authors were sold on the idea of three operators. Prior to conducting this study, the company's management was in the hiring process to add two additional operators, thus implementing the third scenario. The simulation showed that the three operators would be significantly underutilized. The three operators would work 3.3802 hours per day and 2.8063 hours per day under normal and ramp-up operation, respectively. The results supported the authors' convictions that a two-operator workstation would be the best alternative. Under the ramp-up operation, this scenario gave the operators the best schedule to work with and also benefited them.

In the third scenario, under normal conditions, each operator received an annual salary of $36,400 and was tremendously underutilized. For the ramp-up operation, the two-

Table 2. Financial Calculation for each Scenario

	Scenario					
	One operator		Two operators		Three operators	
	Normal	Ramp-up	Normal	Ramp-up	Normal	Ramp-up
Average Inventory	$339.78	$996.65	$296.40	$319.52	$121.28	$99.29
Cost of Production per Day	$136,338	$159,118	$138,716	$185,324	$209,530	$182,910
Cost of Employee and Overtime per Day	$251.03	$822.83	$353.07	$323.90	$420.00	$420.00
Hourly Rate per Day	$17.50	$17.50	$17.50	$17.50	$17.50	$17.50
Revenue per Day	$218,144	$253,824	$221,296	$296,176	$218,140.80	$292,659.20
Inventory Cost per Day	$0.41	$1.20	$0.36	$0.38	$0.15	$0.12
Profit Cost per Day	$81,554.57	$93,882.77	$82,226.52	$110,527.70	$8,190.39	$109,326.79
Value-added ×Revenue	$2,150.89	$2,502.69	$2,181.96	$2,920.82	$2,152.66	$2,885.65

operator scenario allowed the operators to work 9.67722 hours per day. This equated to eight hours per day at $17.5/ hour plus 1.67722 hours per day at 1.5 x $17.5/hour = $36,400 + $10,920 (overtime) = $47,320. This was a 30% increase in pay.

Conclusions

The fundamental decision came down to the final valuation of profitability. The third scenario resulted in the lowest total time, 2.5046 hours and 2.8063 hours for normal and ramp-up operations, respectively. However, as shown in Table 2, the revenue of the second scenario was $221,296 and $296,176 for normal and ramp-up operations, respectively, which are higher than other scenarios under similar operational conditions. The additional profit can be invested partially in new capital equipment and in training the new operator, should the company decided to implement the two -operator scenario.

In terms of resource utilization, the ARENA reports indicated that in the first scenario, for either operational condition, all the subsections' scheduled utilization was almost 100%. For the second scenario and under normal operation, the scheduled utilization for the cleaning subsection was close to 100%, while for chopping and chamfering it was 1.5% and 1.6%, respectively. Under a ramp-up operation, the chopping and chamfering subsections had 2.1% and 2.0% scheduled utilization, while the cleaning subsection had close to 100%. As far as the third scenario, all three subsections had scheduled utilization of about 1.5% for normal operation and around 2.0% for ramp-up operation. At first glance, most of the scheduled utilizations seemed very small. The reason was that the orders might arrive several days apart, with various quantities. The model considered that the chopping operator, for example, stays with the machine even on the days when there is no order. This is not the case in reality, as operators move to other workstations in the factory to do other tasks. Nonetheless, these estimates suggested that, while the one-operator scenario was overloaded and the three-operator scenario was underutilized, the two-operator scenario seemed to be the optimal solution for both normal and ramp-up operations. As far as waste in terms of materials, the authors did not observe any significant waste in the workstation.

Acknowledgments

The authors would like to express their gratitude to Shuttleworth, Inc. for providing the necessary information and sharing the knowledge.

References

[1] Banks, J. (Ed.). (1998). *Handbook of Simulation: Principles, Methodology, Advances, Applications, and Practice.* Danvers, MA: John Wiley & Sons, Inc.

[2] Kelton, W. D., Sadowski, R. P., & Sturrock, D. T. (2007). *Simulation with ARENA.* (4th ed.). New York, NY: McGraw-Hill.

[3] Altiok, T., & Melamed, B. (2007). *Simulation Modeling and Analysis with ARENA*. Burlington, MA: Academic Press.

[4] Banks, J., Carson II, J. S., Nelson, B. L., & Nicol, D. M. (2009). *Discrete-Event System Simulation*. (5th ed.). Upper Saddle River, NJ: Prentice Hall.

[5] Smith, J. S. (2003). Survey on the Use of Simulation for Manufacturing System Design and Operation. *Journal of Manufacturing Systems, 22*(2), 157-171.

[6] Negahban, A., & Smith J. S. (2014). Simulation for Manufacturing System Design and Operation: Literature Review and Analysis**.** *Journal of Manufacturing System, 33*(2), 241-261.

[7] Ferreira, L. P., Ares, E., Peláez, G., Marcos, M., & Araújo, M. (2012). A Methodology to Evaluate Complex Manufacturing Systems through Discrete-Event Simulation Models. In M. Marcos, J. Salguero, & A. Pastor (Eds.). *Key Engineering Materials, 502*, 7-12.

[8] Patterson, T., Dalgarno, K. W., & Murgatroyd, S. (2009). Using Discrete Event Simulation to Redesign Manufacturing Systems in Small Manufacturing Firms. *Technical paper of the Society of Manufacturing Engineers, 2*, 1-13.

[9] Shuttleworth Integrated Product Handling Solutions. (n.d.). Retrieved from http://www.shuttleworth.com/

[10] Solutions by Industry. (n.d.). Retrieved from http://www.shuttleworth.com/products/solutions-by-industry/

Biographies

ALI ALAVIZADEH is an Assistant Professor of Industrial Engineering Technology and director of the Master of Science in Technology at Indiana University-Purdue University, Fort Wayne, IN. He received his Ph.D. from Indiana State University in Technology Management and his B.S. degree in Physics from Sharif University of Technology. Dr. Alavizadeh has worked in various domestic and international companies, holding positions such as software engineer and systems architect. His areas of interest include complex systems modeling and simulation, mathematical modeling, and nonlinear dynamics. Dr. Alavizadeh may be reached at alavizaa@ipfw.edu

ROBERT PALEVICH is currently an Associate Professor of the Deormer School of Business at Indiana University -Purdue University, Fort Wayne, IN. He is an internationally recognized expert in supply chain management and has over 25 years of experience in this area. He earned a B.S. degree from Purdue University, an M.S. degree in Business Process Management in 1985, and an MBA from Indiana University in 1990. His interests are lean manufacturing and the lean service industries, lean hospital and hospital services, Six Sigma and process analysis, RFID, the sustainable green supply chain, and disruptive emerging technologies. Professor Palevich can be reached at palevicr@ipfw.edu

NUMERICAL SIMULATION OF DIRECT CONTACT MEMBRANE DESALINATION (DCMD): PART II

Isam Janajreh, Masdar Institute of Science and Technology, UAE; Dana Suwwan, Masdar Institute of Science and Technology, UAE

Abstract

A steady state performance of low-energy direct contact membrane distillation (DCMD) was conducted. The 2-D numerical model of the DCMD setup consisted of two uniform fluid flows separated by a thin PVDF membrane of hydrophobic nature. The flow was governed by the Navier-Stokes flow coupled with the energy equation in conjugate heat transfer formulation. The performance of the DCMD setup was influenced greatly by the membrane characteristics including permeability, thickness, pore size and conductivity. The mechanism lies within the fact that local temperature difference was created and, hence, caused a driving pressure gradient responsible for phase change of the feed at the surface, transporting the vapor through the pores, and condensing it at the permeate side where it was flushed out. During this analysis, mass and heat transfer modules were examined with varying flow properties and membrane parameters. As a function, temperature polarization, mass flux, heat flux were studied under different flow velocities and parametric configurations. Results showed a good agreement with published theoretical work. In view of these plausible results, a sensitivity study of the flow rates was carried out in order to gain better insight to temperature polarization, heat flux (convective and conductive), associated latent heat, as well as effects on process metrics and yield.

Introduction

Direct contact membrane distillation (DCMD) is gaining popularity because of the required low-grade energy compared to other technologies such as multistage flash (MSF) or reverse osmosis (RO) [1]. The advantages of DCMD lies in its simplicity, utilization of a low-grade temperature difference and the potential for achieving near 100% rejection of dissolved solids [2]. In addition, membrane processes can be modular and flexible for scale-up, while keeping the advantage that separation is occurring under mild conditions [3]. Another benefit lies in the variable membrane properties, which can be adjusted. A review of the design of membrane distillation can be found elsewhere [4], [5], and includes, in addition to the DCMD, air gap membrane distillation (AGMD), vacuum membrane distillation (VMD), and sweeping gas membrane distillation (SGMD) with a clear comparative analysis in terms of potential applications. The four membrane configurations are illustrated in Figure 1.

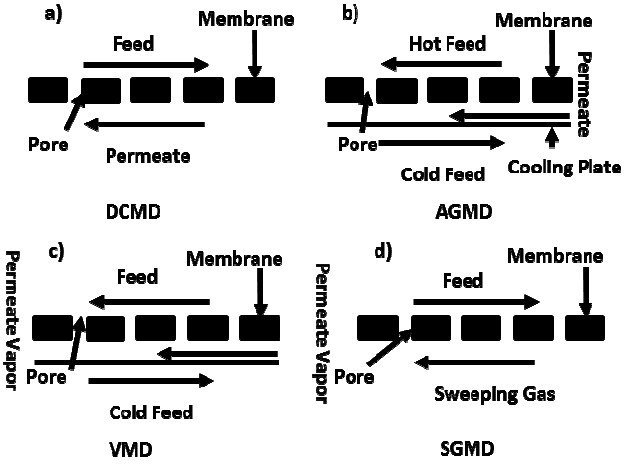

Figure 1. Different DCMD Configurations

The DCMD incorporates a phase-change at the feed side, transmembrane flux towards the permeate side, and condensation at the permeate side [4]. It is different from the classical multistage flash (MSF), multi-effect distillation (MED), vapor compression (VC), freezing, and humidification/ dehumidification, solar stills electro-dialysis (ED), reverse osmosis (RO), and common membrane distillation (MD) [1]. Many of these common techniques are operated by the consumption of large amounts of fossil fuels to power dedicated desalination plant or indirectly through co-generation. DCMD is a well-known water production application providing separation and purification.

The anatomy of the DCMD consist of two-flows with different temperatures and species separated by a hydrophobic membrane, which is in direct contact to the flows. The feed flow is typically the flow with a higher temperature than the permeate flow. The temperature difference between the two flows across the contacting membrane surface creates a difference in the potential vapor partial pressure. This difference drives the transport of vapor mass and energy transfer from the hotter feed side to the cooler permeate side.

This study aimed to obtain a fundamental understanding of the DCMD setup and its pronounced parameters through a high-fidelity flow simulation and sensitivity study. DCMD's pure water productivity was presented in several macroscopic models. Several empirical and semi-empirical

models were also proposed [3]. Recently, a model that includes the temperature polarization for a flat DCMD was proposed, this model was helpful in understanding the transmembrane flux mechanism.

Hui et al. [5] conducted a numerical study considering the transmembrane heat and mass fluxes of the DCMD membrane in a hollow fiber tube. They utilized similar conjugate heat transfer model and studied the influence of the mass flow and length of the membrane, but with less emphasis on the combined width, length, and velocity effects. Others utilized less-accurate semi-empirical correlations, constant mass flux coefficients, a single side of the flow, or a stack of thermal resistances in order to arrive at the prediction of the driving process temperature distribution [2], [6-9]. Zhang et al. [6] and Zhang [10] are among the pioneer who modeled the DCMD as conjugate heat considering the sandwiched a low thermally conductive membrane and its surrounding fluids, yet without consideration of any phase change. The mean spatial temperature was also estimated by Phattaranawik et al. [11] and Schofield [12], who used the boundary layer analogy. However, due to strong coupling of the two flow sides and the semi conductive membrane and its transmembrane flux these empirical models fell short to provide reliable and comprehensive flow information on the two-dimensional temperature distribution and, thereby, on the special heat transfer coefficients [4], [13].

These findings considered both parallel and counter flow arrangements. Results of CFD simulations and experimental work were compared in terms of mass fluxes and temperature distributions. It was found that temperature polarization decreased upstream and then increased downstream. The local heat fluxes increased and then decreased with the flow direction. Nusselt numbers were also reported to be highest at the entrance, due to thin thermal boundary layer and prior to the developing flow.

Most importantly, the thermal efficiency, which defined as the heat carried by the transmembrane flux to the total heat, was studied and it was found that higher velocities do in fact enhance the transmembrane mass flux but decrease the efficiency due to heat loss on the permeate side due conduction. On the other hand, a high fidelity analysis and rather complicated fluid dynamics modeling combined with the Ergun model for pressure drop, Knudson-diffusion for transmembrane flux, was introduced by Charfi et al. [13] for the modeling of the DCMD. The brought complexity of this model, however, hindered its practicality.

Therefore, only limited literature on the high fidelity CFD modeling of the DCMD presents today. This current study intended to enrich this literature gap by considering a comprehensive arrangement of the flow in two dimensional laminar Navies-stokes flow coupled with the energy conservation for the membrane in a conjugate heat transfer. This model was equally applied to parallel (or counter flow) channels as well as axisymmetric of two concentric cylindrical flow separated by the membrane. Such model can be used as conceptual design tool for innovative design and development in the new emerging field of DCMD.

Theoretical Modeling

The mathematical modeling technique was built upon previous work by the authors, where the flow regimes were studied; that is, parallel and counter configuration, along with temperature effects. Therefore, this study would undergo the same steps of theoretical modelling and formulation as the previous studies [14].

Overall, an aqueous hot feed enters the top side (outer cylinder in axisymmetric) of the membrane, whereas the permeate enters the bottom, cold side of the membrane (inner cylinder axisymmetric). Evaporation of the feed first occurs at the top/outer membrane surface in the form of pure water; the vapor is then transported within the membrane towards the bottom surface. Finally, this vapor condenses on that surface as pure permeate [15]. The performance of the DCMD depends on the temperature and pressure of the feed/permeate flows, properties and physical membrane characteristics including permeability, conductivity, pour size distribution, and geometry. For modeling purposes, the model assumed a two-dimensional (2D) flow along the x and perpendicular to y Cartesian coordinate directions, as illustrated in Figure 2. The incoming velocity profiles were considered uniform and steady parallel flows at fixed velocity and temperature values.

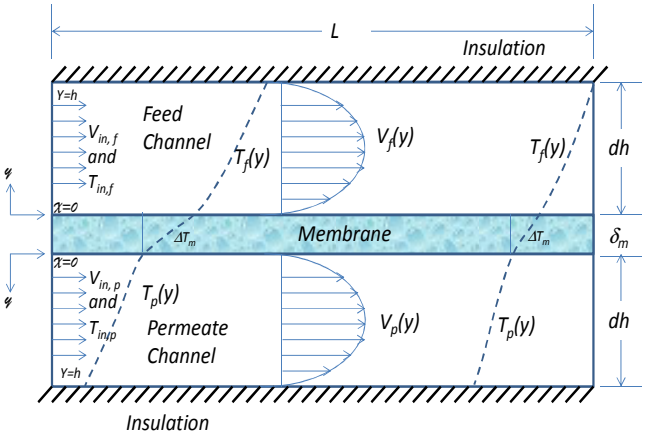

Figure 2. Schematic Diagram of the Parallel Flow DCMD and Schematics of the Velocity and Temperature Profiles

Governing Equations

For the steady state heated flow process, the mass and x and y Navies-stokes (momentum) conservation are given in Equations (1), (2), and (3) respectively.

$$\frac{\partial(\rho u)}{\partial x} + \frac{\partial(\rho v)}{\partial y} = 0 \tag{1}$$

$$u\frac{\partial(\rho u)}{\partial x} + v\frac{\partial(\rho u)}{\partial y} = -\frac{\partial P}{\partial x} + \mu\left(\frac{\partial^2 u}{\partial x^2} + \frac{\partial^2 u}{\partial y^2}\right) \tag{2}$$

$$u\frac{\partial(\rho v)}{\partial x} + v\frac{\partial(\rho v)}{\partial y} = -\frac{\partial P}{\partial y} + \mu\left(\frac{\partial^2 v}{\partial x^2} + \frac{\partial^2 v}{\partial y^2}\right) + \rho g_y \tag{3}$$

where, $\rho\left(\frac{kg}{m3}\right), u\left(\frac{m}{s}\right), v\left(\frac{m}{s}\right), P(pa), \text{and } \mu\ (pa.s)$ are the density, velocity in x, velocity in y, pressure, and dynamic viscosity, respectively.

The scalar energy is given by Equation (4):

$$u\frac{\partial(\rho CpT)}{\partial x} + v\frac{\partial(\rho CpT)}{\partial y} = k\left(\frac{\partial^2 T}{\partial x^2} + \frac{\partial^2 T}{\partial y^2}\right) + S_h \tag{4}$$

where,

Cp is the specific heat $\left(\frac{w}{kg.K}\right)$
T is the temperature (K)
k is the thermal conductivity $\left(\frac{w}{m.K}\right)$
u is the velocity in x
v is the velocity in y

The term S_h signifies the sink/source heat that is attributed to the latent heat of evaporation at both the feed and permeate membrane surface, respectively, and is defined in Equation (5):

$$S_h = \begin{cases} \frac{q_{md}}{\delta_y}.\frac{y_{mo}}{y_{mi}} \; for\; y = y_{mi} \\ -\frac{q_{md}}{\delta_y} for\; y = y_{mi} \\ 0\; otherwise \end{cases} \tag{5}$$

where,

q_{md} is the membrane's feed side latent heat flux
y is the vertical distance
mo, *mi* are the locations of the top and bottom membrane surfaces, respectively. The term S_h also holds the heat boundary conditions attributed to the flow and implicitly applied to the membrane surface.

Mass Transfer Module

In the DCMD process, evaluating the transport of mass through the membrane constitutes the process productivity. Due to the temperature gradient, a driving pressure force is created which is responsible for the mass transfer across the membrane [3]. The general form of the mass flux is illustrated by Greenlee et al. [1] and Tsung and Chii [3], and is given in Equation (6):

$$J'' = c_m\left(P_{mf}^{sat} - P_{mp}^{sat}\right) \tag{6}$$

where,

c_m is the intrinsic mass membrane coefficient
P_{mf}^{sat} is the saturated pressure of water on the feed
P_{mp}^{sat} is the permeate membrane's surface

The beauty of Equation (6) is that for a given pressure-temperature association, the mass flux temperature dependency can be inferred by Equation (7):

$$J'' = c_m\frac{d}{dT}\left(P_{mf}^{sat} - P_{mp}^{sat}\right) * (T_{mf} - T_{mp}) \tag{7}$$

The pressure-temperature relationship was tabulated in steam tables according to the Antoine equation [11], which follows a monotonic form within the operational desalination temperature range. Equation (8) is written as:

$$P_{pure}^{sat} = \exp\left(23.238 - \frac{3841}{T_m - 45}\right), i \in \{f, p\} \tag{8}$$

This equation was adjusted for none-pure saline or wastewater [14] and is shown here in Equation (9):

$$P_i^{sat}(x, T) = x_w a_w P_{i\,(pure)}^{sat}, i \in \{f, p\} \tag{9}$$

where,

x_w is the mole fraction of the water in saline solution
a_w is the water activity in NaCl solutions

The water activity in NaCl solutions is estimated using correlations by Lawson and Lloyd [2] and Khayet [4], and given by Equation (10):

$$a_w = 1 - 0.5x_{NaCl} - 10x_{NaCl}^2 \tag{10}$$

where, x_{NaCl} is the mole fraction of NaCl in the brine solution. Therefore, an increase in temperature will definitely lead to an increase in the transmembrane mass flux. This can be achieved either by operating at a higher feed temperature condition or by targeting a higher temperature distribution along the membrane. The mass coefficient was obtained from the simulation following either Knudson-diffusion, molecular diffusion, Poiseuille flow, or Monte Carlo simulation [16-18]. Equation (11) shows a suitable combination of the Knudson and Poiseuille models, as was presented by Khayet [4]:

$$c_m = c_k + c_p = 1.064\,\alpha(T)\frac{\varepsilon r}{\tau \delta_m}\sqrt{\frac{M_w}{R\,T_{mt}}} + 0.125\;\beta(T)\frac{\varepsilon r^2}{\tau \delta_m} \quad (11)$$

where,

- $\alpha(T)$ is the Knudsen diffusion model
- $\beta(T)$ is the Poiseuille flow model contributions
- M_w is the molar mass of the water in (kg/mol)
- T_{mt} is the mean membrane temperature (C)
- R is the gas constant
- P_m is the mean pressure
- δ_m is the thickness of the membrane
- r is the radius of the pores
- ε is the porosity of the membrane
- τ is the tortuosity factor, which can be estimated for hydrophobic membranes, according to Iversen et al. [19], and is expressed here as Equation (12).

$$\tau = \frac{1}{\varepsilon} \quad (12)$$

The transmembrane heat flux is described by the latent heat flux and conduction through the membrane. The former is shown in Equation (13):

$$q_m = j''.\Delta H_m \quad (13)$$

where, ΔH_m is the latent heat of the permeated transmembrane fluid. The conduction is described by the Nusselt number (*Nu*) and written as shown in Equation (14):

$$Nu = \frac{h.d}{k}\ or\ \frac{q.d}{k(T_b - T_m)} \quad (14)$$

where,

- *h* is the heat transfer coefficient
- *d* is the characteristic length
- *k* is the thermal conductivity
- *q* is the heat flux
- *T* is the local temperature, where the subscripts *b* and *m* signify the bulk and the membrane, respectively.

Heat Transfer Module

The heat transfer in the DCMD process can be described via these following three steps: The heat transfer through the feed boundary layer, heat transfer through a membrane, and heat transfer through the permeate boundary layer [15]. The total heat flux for the membrane is either due to the convection through the feed membrane surface, or the convection through the permeate membrane surface or a combination of the conduction (Q_m) and latten heat of evaporation through the membrane. The conduction across the membrane material is in part due to the bulk membrane material conduction (Q_c) and the other is due to the vapor-filled pores (Q_v). The total membrane heat flux can be described via Equation (15):

$$Q_m = Q_c + Q_v \quad (15)$$

The transmembrane heat flux can be written as shown in Equation (16):

$$q_m = j''.\Delta H_m \quad (16)$$

where, ΔH_m is the latent heat of the transmembrane flux of the fluid. According to Termpiyakul et al. [20], this enthalpy can be fitted from the enthalpy data of saturated water vapor and liquid, according to Equation (17):

$$H_{m,i} = 1.7535\,T_{m,i} + 2024.3 \quad i \in \{f, p\} \quad (17)$$

Hence, the conduction can be expressed by Equation (18):

$$Q_{m,i} = \frac{k_m}{\delta_m}(T_{m,f} - T_{m,p}) \quad \text{with} \quad K_m = (1-\varepsilon)K_b + \varepsilon K_V \quad (18)$$

where,

- km represents the membrane conduction coefficients,
- T is the temperature
- f and p are feed and permeate, respectively
- K_m is the membrane conductivity, which is the volume weighted average of the bulk conductivity, K_v
- K_b is the vapor conductivity, which can be estimated from the work of Tsung and Chii [3].

DCMD Performance: Parameter Effects

The DCMD thermal efficiency metric, η, is governed by the fraction of the heat used as latent heat of evaporation instead of the lost conduction fraction. This efficiency can be written as shown in Equations (19) and (20):

$$\eta = j''.\Delta H_m / q_f \quad (19)$$

and

$$q_f = j''.\Delta H_m + K_m(T_{mf} - T_{mp})/\delta_m \quad (20)$$

Therefore, low membrane conductivity is desirable in order to increase the thermal efficiency. Dividing by the latent heat enthalpy ΔH_m defines the "equivalence" conductive mass flux (j''_{keq}) ; the efficiency can, then, be rewritten as Equation (21):

$$\eta = j''/(j'' + j''_{keq}) \quad (21)$$

Temperature polarization, θ, measures the ratio of boundary layer resistance over the total heat transfer resistance, and is expressed in Equation (22):

$$\theta = \frac{T_{m,f} - T_{m,p}}{T_{b,f} - T_{b,p}} \quad (22)$$

where, the subscripts *m, b, f,* and *p* signify the membrane, bulk, feed flow and permeate flow, respectively. For small values of θ (≤ 0.2), the DCMD is considered heat transfer limited, meaning the module design is poor. For larger values of θ (≥ 0.6), the DCMD enters the mass transfer limitation that is hindered because of the low membrane permeability [20]. The presented mathematical and CFD models were applied to determine the mass flux, heat flux, temperature polarization, and membrane coefficient for the parallel flow.

Flow Properties and Boundary Conditions

The baseline 2D geometry consisted of 21 cm by 0.1 cm channels. The membrane was sandwiched between the two channels with a 0.130 mm thickness. A parallel flow was considered, entering at a nominal Reynolds number of 500, and inlet feed and permeate temperatures of 40°C and 25°C, respectively. A quadrilateral mesh type was used for the whole geometry, the feed and permeate channels, and the membrane. A boundary layer mesh was used at the membrane surface targeting the y+ value of one unit to capture the smooth growth of the kinematic and thermal boundary layer. It progressively and smoothly expanded towards the center channel. The mesh size was 2100 x 64 and 2100 x 8 for the membrane. Initially, the property of the membrane was evaluated using a void-solid weighted average, according to Equation (23):

$$\emptyset_m = (1-\varepsilon)\emptyset_o + \varepsilon\emptyset_v \qquad (23)$$

where, Ø is the equivalent permeable membrane property and the subscripts *o* and *ϑ* signify the core membrane material, typically polyvindeline fluoride or polyvinyl alcohol with cellulose reinforcements/enhancements, and the vapor, which occupies the membrane pores. Material properties of each of the membranes, saline feed, and fresh water permeate are summarized in Table 1.

Table 1. Properties of the of Membrane and Flow Materials

Material	Density (kg/m^3)	Specific heat (J/kg.k)	Conductivity (w/m.k)	Viscosity (Pas)
PVDF [21]	1175	1325	0.2622	-
Vapor	0.554	2014	0.0261	-
Membrane	302.2	1896.9	0.0662	-
Saline sea water* [22]	1013.2	4064.8	0.642	5.86E-4
Pure water** [23]	995.2	4182.1	0.613	8.38E-4
*At 3.5% salinity and 323 K **At 303 K				

Results and Discussion

Results of the temperature profile are depicted in Figure 3 (a) and are in agreement with the work by Chen et al. [15]. It can be inferred that a considerable influence exists of the flow velocity on the temperature distribution at the membrane surface and this difference grows larger as the velocity is increased/doubled and it became more pronounced when the velocity was quadrupled, as depicted in Figure 3 (a). The difference in temperature was maintained until the flow exited. It is, however, not easy to state the optimal velocity values as both the one sided bulk and membrane surface temperatures are decrease asymptotically.

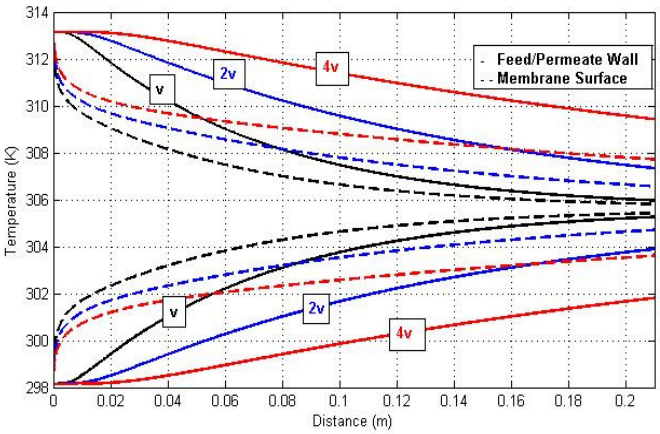

(a) Temperature Profiles for Feed-permeate Velocities of 1v, 2v, and 4v

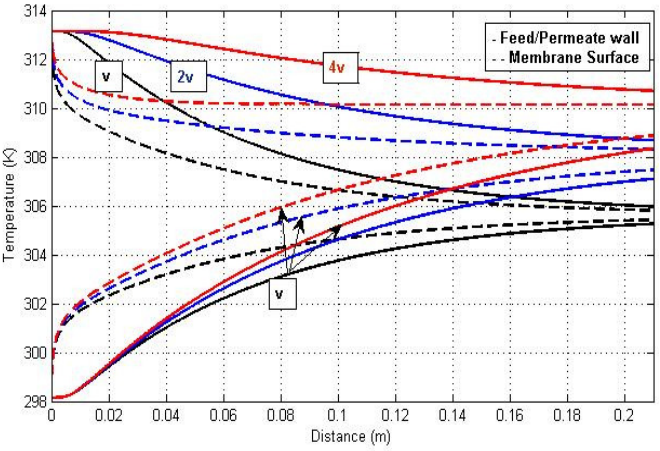

(b) Temperature Profiles with Varying Feed Velocities of 1v, 2v, and 4v, but Fixed Velocity Permeate

Figure 3. Temperature Profiles Correspond to Different Inlet Velocities of Parallel Flow in which the Feed is Entering at 40° C and the Permeate is at 25° C

The shorter residence time for the flow to cool down at the feed side, or to heat up at the permeate side, however, delays the reduction at higher velocities. It is worth mentioning that the mean membrane temperature was almost constant and nearly identical for the parallel flow in the DCMD model at the three velocity values. As the permeate velocity can be controlled independently and kept constant, there is some interest in investigating this effect on the resulting mass flux. The membrane and bulk temperature line plots are depicted in Figure 3(b), which shows that the temperature across the membrane decreased as the velocity of the permeate remained fixed. Thus, one anticipates lower performance for inferior permeate feed velocity flow.

The Nusselt number is depicted in Figure 4 and shows a similar asymptotic decreasing trend as seen for the temperature. The Nusselt values of the permeate side dominate initially and exceeding twice the value of the feed side. The difference, however, decreases and comes closer at midstream and nearly it converges near the exit at the downstream particularly for low inlet velocities. The equal channel velocities exhibit more spread values, while for fixed permeate velocities, the Nusselt values are more converged. It should be noted that the low values of Nusselt suggesting both convection and conduction are in the same order of magnitude and slightly in favor of the convection heat transfer for the single digit value. Also, note the amount of heat transfer, due to top membrane surface convection or membrane conduction and latent heat of evaporation or bottom membrane wall convection are equal. These values are characteristic of laminar flow and are comparable to those obtained by the work of Hui et al. [5].

Figure 5 depicts the resulting polarization temperature factor, θ. In addition to the thermal boundary resistance, it provides the operational range of the parallel configuration. An asymptotic decreasing trend is fast reaching at lower velocity values. It appears that higher velocities resulted in an extended mass limitation range and reaching nearly 1/10 of the channel length before it descended to the favorable range of 0.6-0.2. The lower velocity appeared to descend to the normal range faster and remained operational within the favorable range. In keeping the permeate at lower velocities, while increasing the feed velocity, caused an extended mass limitation in the entry region but averaging higher and favorable θ.

Mass flux, j" , is directly affected by the incremental increase of velocity, temperature, change of configuration, and membrane characteristics. The distributed local and accumulative mass flux for the equal two-sided velocity values are depicted in Figure 6(a), and those at constant permeate velocities are depicted in Figure 6(b). It is clearly shown that as the velocity increased the flux also increased. It tends to reach to asymptotic values at low velocities, while it is delayed and not reached at higher velocities. It implies that the length velocity combination additional to other system properties (membrane, channel height, inlet temperature, etc.) is less tuned for higher velocities than lower velocities. This was also observed at constant permeate velocities, as depicted in Figure 6(b), which shows that the mass flux was opted to reach the asymptotic plateau faster because of the lower permeate velocity. It should be noted that for the current membrane properties and configuration of a maximum of 5.76 kg /m^2.hr, whereas for the same high velocity of feed and lower permeate value, the total flux was 4.05 kg /m^2.hr. These values, corresponding to their velocity values, are summarized in Table 2.

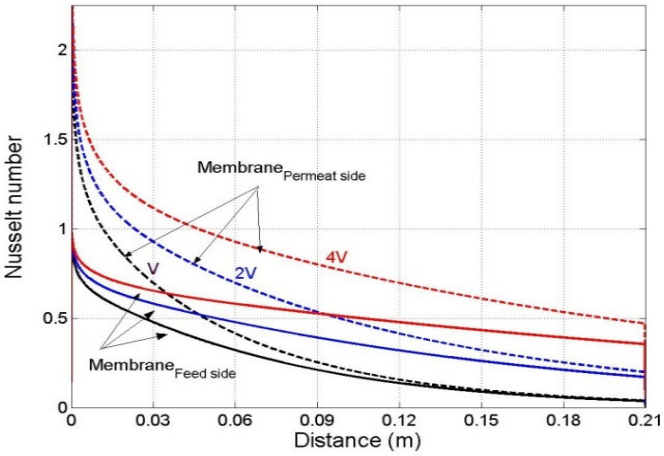

(a) Nusselt Number of the Feed and Permeate Membrane Surfaces at Equal Feed and Permeate Velocities

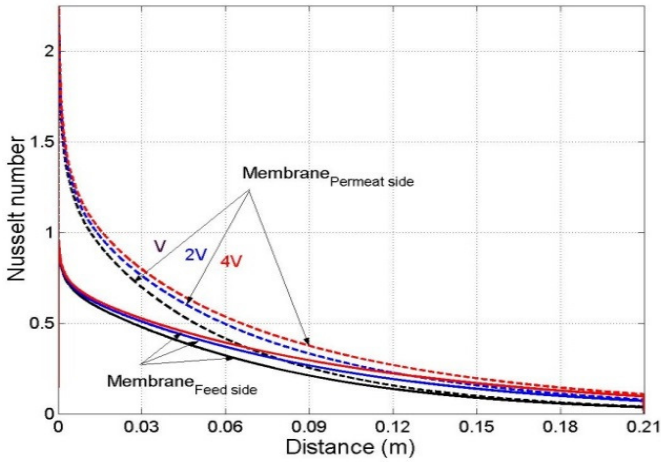

(b) At Fixed Permeate Velocity and Varying Feed Velocity

Figure 4. Nusselt Number of the Feed and Permeate Membrane Surfaces

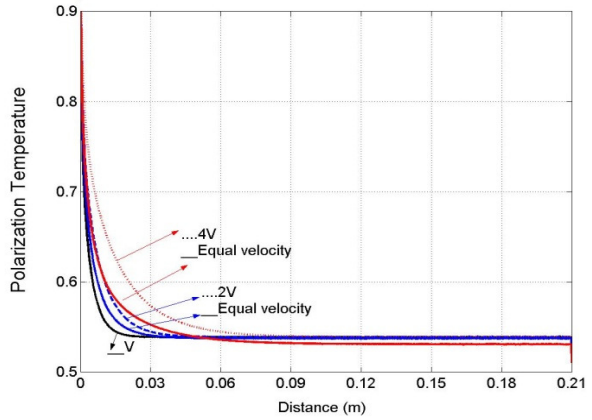

Figure 5. Polarization Temperature Factor for Varying Velocities

Table 2. Summary of Mass Fluxes at Corresponding Flow Velocities

Feed Re* / velocity (m/s)	Permeate Re* / velocity (m/s)	Accumulative mass flux ($kg/m^2.hr$)**
12.5 / 0.01 m/s	12.5 / 0.01 m/s	2.38
25.0 / 0.02 m/s	25.0 / 0.02 m/s	3.57
50.0 / 0.04 m/s	50.0 / 0.04 m/s	5.76
25.0 / 0.02 m/s	12.5 / 0.01 m/s	3.24
50.0 / 0.04 m/s	12.5 / 0.01 m/s	4.05

*Re is based on a channel height of 1 m
**Values are renormalized for lengths of 1 mm instead of 0.21 m

The heat flux and temperature difference across the membrane are depicted in Figure 7. Higher heat was injected into the membrane at higher velocities and a similar trend was observed for the temperature difference. This difference is indicative of the conductive heat which also equal to the same convective heat flux for zero transmembrane flux. The latent heat associated with the transmembrane flux in DMCD is typically very low compared to the conductive flux in which the former is the effective absorbed heat and the latter is considered as conduction loss. This defines the efficiency of the DMCD system, which is the ratio of the latent heat to that of the total convective heat or total conductive and latent heat.

The evaluated efficiency of the DCMD is depicted in Figure 8, which reveals very low efficiency; this constitutes the current and main drawback of the process. Interestingly, the fixed feed resulted in higher efficiency at double and quadruple feed velocities. Nevertheless, there is more room to improve this efficiency 5- or even 10-fold by combining optimal flow conditions and membrane characteristics. This includes optimal flow velocities and inlet temperature, optimal channel height and upper and lower surface temperatures. As for the membrane parameters, optimal porosity, tortuosity, and membrane thickness as well as very low conductivity are the chief membrane parameters to enhance the DCMD process metrics.

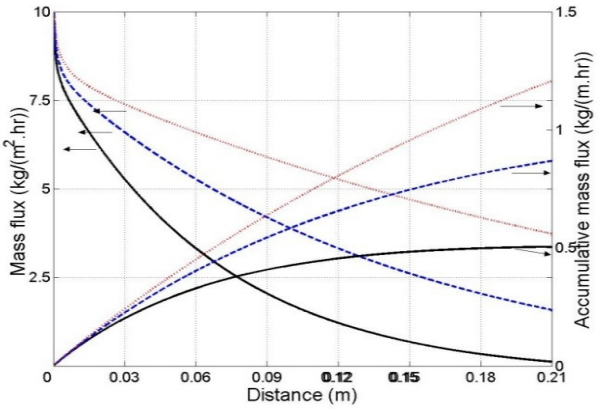

(a) At Equal Feed and Permeate Velocities

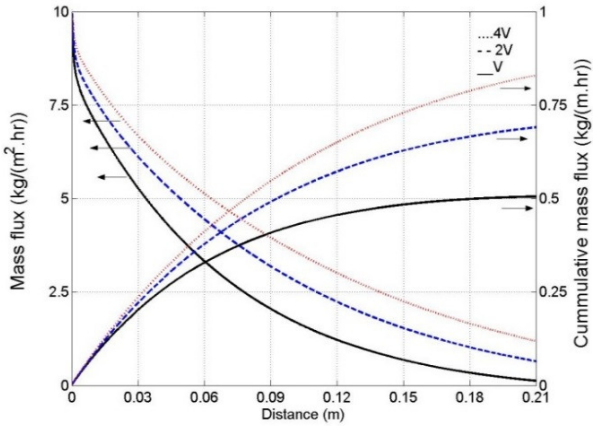

(b) At Fixed Permeate Velocity and Varying Feed Velocity

Figure 6. Incremental and Accumulative Mass Flux

Figure 9 displays the temperature profiles across the upper and lower channels of the DCMD. The temperatures on the positive axis represent the feed side, while the temperatures on the negative axis represent the permeate side. These results were obtained as a function of the vertical distance that is the height of the channels (1 mm each). The four temperature profiles in each graph represent four points along the horizontal distance chosen randomly which are 0.0525, 0.105, 0.1575, and 0.21. It can deduced from these graphs that with increasing velocities from 1v to 4v, the temperature trend gets closer at all points along the channel. Moreover, at the higher velocity of 6v, temperatures tended to increase. For example, at 6v, at point 0.0525, the temper-

atures were higher at the feed side and lower at the permeate side, in comparison with the 4v velocity graph. Also, at higher velocities, the temperature range across the membrane was higher, indicating that most of the heat transfer occurred within the membrane.

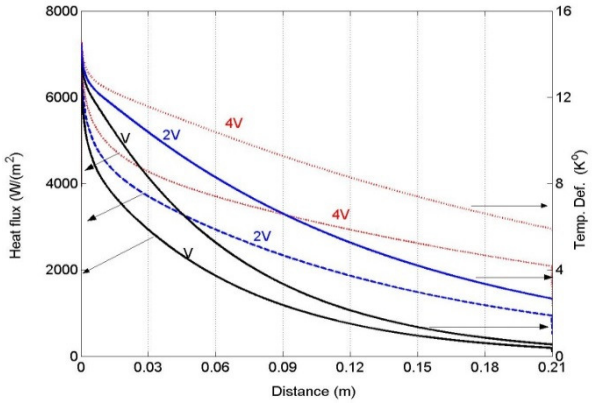

(a) At Equal Feed and Permeate Velocities

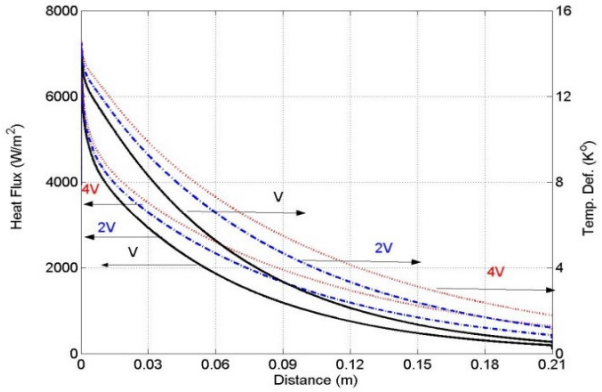

(b) At Fixed Permeate Velocity and Varying Feed Velocity

Figure 7. Heat Flux and Temperature Difference across the Membrane

To complement the above analysis, a parametric analysis was carried out to assess the effect of varying the geometry of the DCMD on system performance.

a) System length: This study involved altering the horizontal distance of the two shallow channels and examining its impact. Six cases were chosen (see Table 3) for four velocities where the mass flow and average temperature polarization were determined. Figure 10(a) shows the effects of total accumulative mass flow and Figure 10(b) depicts the average temperature polarization for varying length and velocities. It can be seen that a higher mass flux is achieved with higher velocities; the highest reported was above 4 kg/m^2.hr. In addition, the accumulative mass flow slowly increased with an increase in horizontal distance. That is, for velocities v and 2v, the mass flux was barely increasing from 0.5x to 6x. At higher velocities (e.g., 6v), increasing the length from 0.5x to 6x resulted in an increase of almost 3 kg/m^2.hr, which was quiet notable. This study helped optimize the performance of the DCMD, keeping in mind the cost effectiveness of the DCMD geometry. The temperature polarization shown in Figure 10(b) is a function of velocity and distance. Generally, as heat is lost, a minimal temperature exchange occurs, particularly near the exit. However, lower velocities (e.g., 1v) are associated with a higher temperature polarization in comparison with velocity 6v, adding that higher velocities trigger unnecessary frictional flow losses.

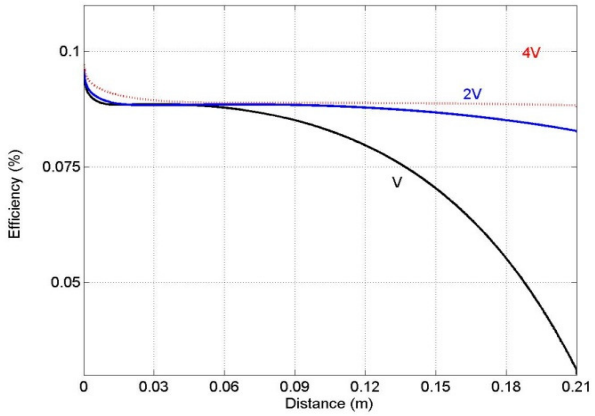

(a) At Equal Feed and Permeate Velocities

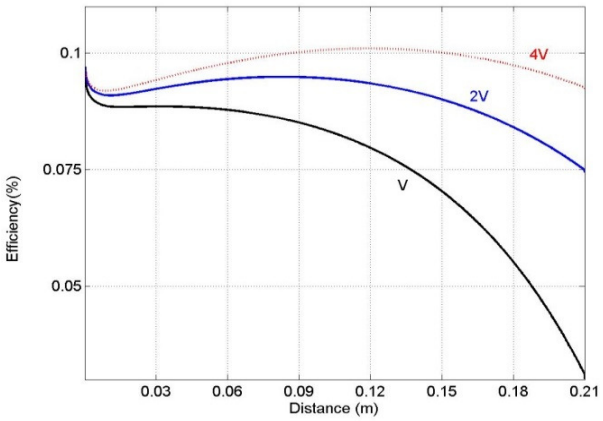

(b) At Fixed Permeate Velocity and Varying Feed Velocity

Figure 8. The DCMD-evaluated Efficiency

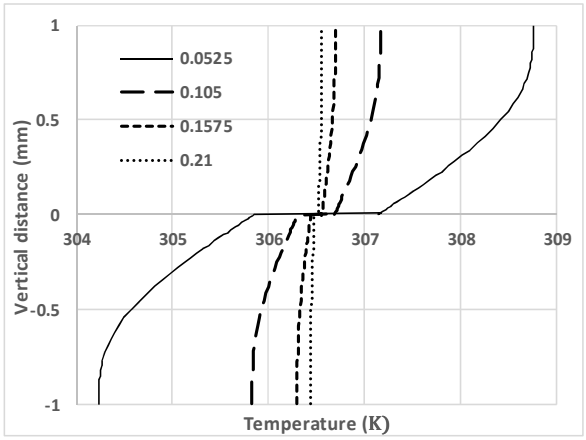

(a)Temperature Distributions for Velocity 1v

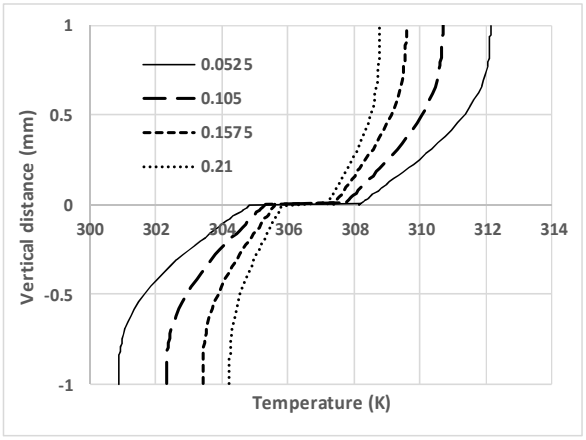

(b) Temperature Distributions for Velocity 2v

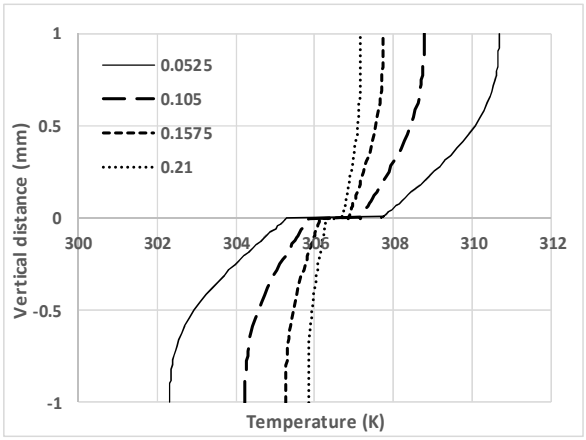

(c) Temperature Distributions for Velocity 4v

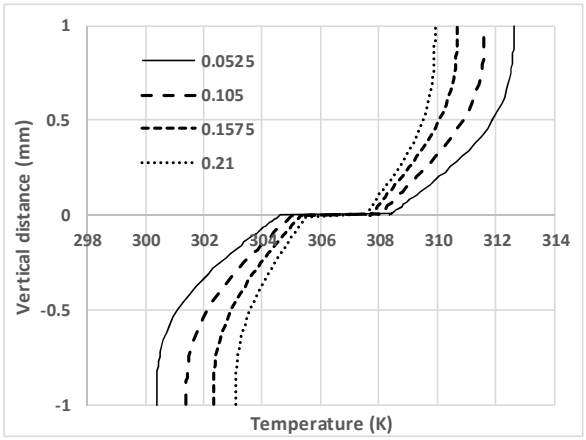

(d) Temperature Distributions for Velocity 6v

Figure 9. Temperature Profiles across the DCMD Setup for Velocities 1v, 2v, 4v, and 6v

Table 3. Horizontal Length Scaling and Flow Velocities

Horizontal length	(m)	Velocity (m/s)
0.5x	0.105	1v (0.01m/s), 2v (0.02m/s), 4v (0.04m/s), and 6v (0.6 m/s)
0.75x	0.1575	
1x	0.21	
2x	0.42	
4x	0.84	
6x	1.26	

Table 4. Vertical Length Scaling and Flow Velocities

Vertical Length	(mm)	Velocity (m/s)
0.5y	0.5	1v (0.01m/s), 2v (0.02m/s), 4v (0.04m/s), 6v (0.6 m/s)
0.75y	0.75	
1y	1	
2y	2	

b) Vertical depth: The same study was conducted for vertical distance, keeping four velocities and four vertical lengths, as listed in Table 4. Figure 11(a) and 11(b) represents both mass flux and temperature polarization for varying vertical distances and velocities. For the mass flux, the increasing trend was similar to the trend spotted for the horizontal study. However, for velocity 6, a higher mass flux was achieved with the horizontal study at 6x than the vertical study at 2y. In addition, there was a marginal increase with every vertical distance studied, unlike with the horizontal study, extreme distances like 6x resulted in higher flux. For the temperature polarization, it seems that it is less affected by the velocity in comparison with the polarization ratios in the horizontal study. However, it is worth noting that the decrease in temperature polarization is more linear and drastic with increasing the vertical distance compared to the horizontal distance which suffered lower decrease.

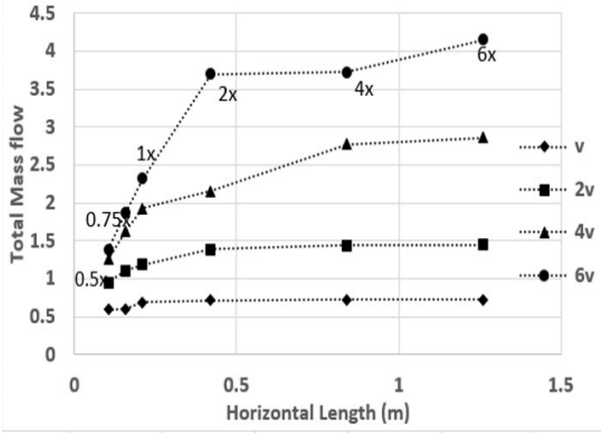

(a) Total Mass Flow Rate versus Velocity for Different Horizontal Channel Lengths

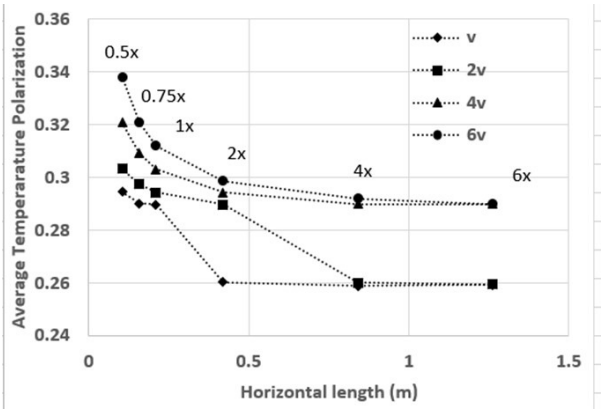

(b) Average Temperature Polarization Velocity Associated with Higher Temperature Polarization

Figure 10. Determination of Mass Flow and Average Temperature

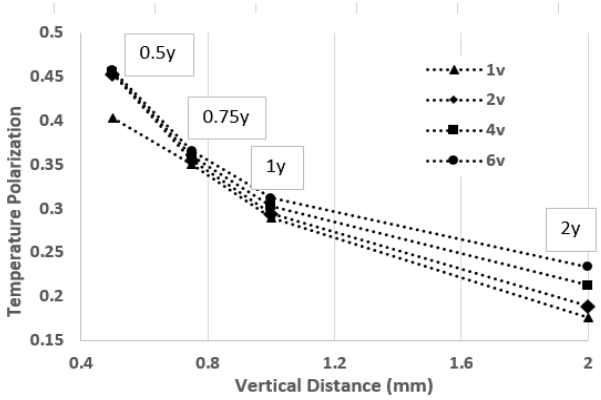

(a) Total Mass Flow Rate versus Velocity for Different Vertical Channel Lengths

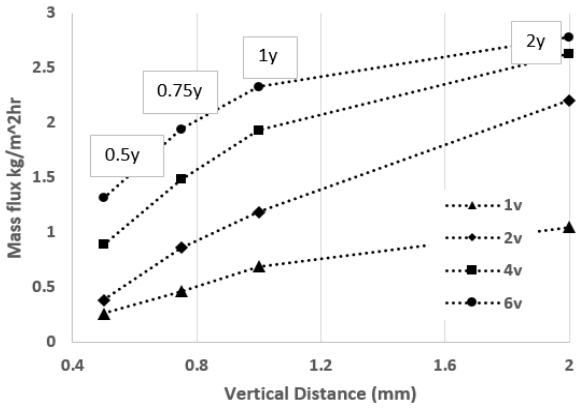

(b) Average Temperature Polarization

Figure 11. Mass Flux and Temperature Polarization for Varying Vertical distances and Velocities

Conclusions

The conjugate heat computational fluid dynamics was applied in order to determine a high fidelity analysis for the DCMD. The model evaluates and returns the bulk and membrane temperatures at the two sides of the two parallel flows, representing the hot feed and cooler permeate. The temperature gradient across the membrane created a difference in the saturation pressure across the membrane fluid, which drives mass and energy transfer through the membrane from the feed to the permeate side. The model was utilized to investigate local and accumulative flow parameters including the mass flux, the heat flux, and the DCMD metrics. The increase in the inlet flow resulted in a higher yield of mass flux. This was due to the higher convective heat flux, as illustrated by the higher values of Nusselt number.

Temperature polarization was investigated beyond the entry region and neither heat nor mass transfer limitation occurred, as the values remained within the allotted values {0.2, 0.6}. In view of these results, the efficiency of the process was evaluated and found to be extremely low. Therefore, a detailed sensitivity analysis was suggested to find the optimal yield and process metrics. Lastly, the parametric study reflected that velocity change could produce pronounced effects on both the mass flux and temperature polarization. In addition, the highest mass flux achieved was above 4 kg/m^2.hr and was in the horizontal study at velocities 6v and 6x. However, to draw quantitative conclusions on whether to vary the horizontal or vertical distance will need more in-depth case studies and will be tackled in the near future.

Acknowledgments

The authors are grateful for the financial support from MASDAR Institute of Science and Technology and for all Waste to Energy Lab to their support throughout this research.

References

[1] Greenlee, L. ., Lawler, D. ., Freeman, B. ., Marrot, B, & Moulin, . (2009). Reverse Osmosis Desalination: water sources, technology, and today's challenge. *Water Research, 43*(9), 2317–2348.

[2] Lawson, K. W., & Lloyd D. R. (1996). Membrane distillation (II) Direct contact MD. *Journal of Membrane Science, 120*(1), 123–133.

[3] Tsung, C. ., & Chii, D. H. (2010). Immediate assisted solar direct contact membrane distillation in saline water desalination. *Journal of Membrane Science, 358*(1), 122-130.

[4] Khayet, M. (2011). Membranes and theoretical modeling of membrane distillation: A review. *Membrane Separation and Colloid Science, 164* (1-2), 56-88.

[5] Hui, Y., Xing Y., Rong, W., & Anthony, G. F. (2011). Numerical simulation of heat and mass transfer in direct membrane distillation in a hollow fiber module with laminar flow. *Journal of Membrane science, 384*(1-2), 10-116.

[6] Zhang, L. Z., Liang C. H., & Pei L. X. (2010). Conjugate heat and mass transfer in membrane-formed channels in all entry regions. *International Journal of Heat and Mass Transfe, 53*(5–6), 815–824.

[7] Gryta, M., & Tomaszewska, M. (1998). Heat transport in the membrane distillation process. *Journal of Membrane Science, 144*(1–2), 211–222.

[8] Aravinth, S. (2000). Prediction of heat and mass transfer for fully developed turbulent fluid flow through tubes. *International Journal of Heat and Mass Transfer, 43*(8), 1399–1408.

[9] Qtaishat, M., Matsuura, T., Krucze, B. K., & Khayet, M. (2008). Heat and mass transfer analysis in direct contact membrane distillation. *Desalination, 219*(1–3), 272–292.

[10] Zhang, L. Z. (2010). Heat and mass transfer in a quasi-counter flow membrane-based total heat exchanger. *International Journal of Heat and Mass Transfer, 53*(23–24), 5478–5486.

[11] Phattaranawik, J., Jiraratananon, R., & Fane, A.G. (2003). Heat transport and membrane distillation coefficients in direct contact membrane distillation. *Journal of Membrane Science, 212*(1), 177-193.

[12] Schofield, R. W., Fane, A.G., & Fell C. J. D. (1987). Heat and mass transfer in membrane distillation. *Journal of Membrane Science, 33(3), 299–313.*

[13] Charfi, K., Khayet, M., & Safi, M. J. (2010). Numerical simulation and experimental studies on heat and mass transfer using sweeping gas membrane distillation. *Desalination, 259*(1), 84–96.

[14] Janajreh, I. M., Suwwan, D., & Faith, H. (2014). Flow analysis of low energy direct contact membrane desalination: Part I. *International Journal of Technology Enhancements and Emerging Engineering Research, 8*(2), 1-6.

[15] Chen, T., Ho, C., & Yeh, H. (2009). Theoretical modeling and experimental analysis of direct contact membrane distillation. *Journal of Membrane Science 330*(1), 297-287.

[16] Ding, Z., Liu, L., El-Bourawi., M S., & Ma, R. (2005). Analysis of a solar-powered membrane distillation system. *Desalination, 172*(1), 27-40.

[17] Bui, V.A., Vu, L. T. T., & Nguyen, M. H. (2010). Modelling the simultaneous heat and mass transfer of direct contact membrane distillation in hollow fiber modules. *Journal of Membrane Science, 353* (1), 85–93.

[18] Imdakm, A.., & Matsuura, . (2005). Simulation of Heat and Mass Transfer in Direct Contact Membrane Distillation (MD): The Effect of Membrane Physical Properties. *Journal of Membrane Science, 262(1), 117-128.*

[19] Iversen, S. B., Bhatia, V. K. K., & Jonsson D. G. (1997). Characterization of micro porous membranes for use in membrane contactors. *Journal of Membrane Science. 130*(1), 205-217.

[20] Termpiyakul, P., Jiraratananon, R., & Srisurichan, S. (2009). Heat and mass transfer characteristics of a direct contact membrane distillation process for desalination. *Desalination, 177*(1), 133-141.

[21] Iguchi, C. Y., dos Santos, W. N., & Gregorio, R. Jr. (2007). Determination of thermal properties of pyroelectric polymers, copolymers and blends by the laser flash technique. *Polymer Testing, 26* (6), 788-792.
[22] Sparrow, B. S. (2003). Empirical equations for the thermodynamic properties of aqueous sodium chloride. *Desalination, 159* (2), 161–170.
[23] Yaws, C. L. (1998). *Chemical Properties Handbook*. (1st ed.). McGraw-Hill.

Biographies

ISAM JANAJREH received his Ph.D. and Masters from Virginia Tech in Engineering Science and Mechanics and Mechanical Engineering, respectively. He received his B.S. in Mechanical Engineering from Jordan University of Science and Technology. Dr. Janajreh's focus is on solid-fluid interactions, turbulence modeling and mixing, and thermo-mechanical coupling. He was a Visiting Professor at Virginia Tech at the Engineering Science and Mechanics and Math departments through 1998 and later joined Michelin R&D, USA as a Tire and Automotive Research Engineer, analyzing wet tire traction and nonlinear structure analysis, vehicle dynamics, and rubber material modeling. Dr. Janajreh joined Masdar in 2007, continuing his research while also teaching Advanced Renewable Energy Conversion Systems, Fundamentals of Combustion, Advanced Fluid Dynamics, and Computational Fluid Dynamics. He has authored over 15 referenced publications on fluid dynamics and structure interaction, made more than 35 contributions to international conferences, and is a key contributor to three Michelin patents (Catamaran, Primacy, X-one) and three books (traction, rolling, resistance noise). Dr. Janajreh can be reached at ijanajreh@masdar.ac.ae

DANA SUWWAN is a Master's students and a Research Assistant in her first year in the Waste to Energy Lab at Masdar Institute of Science and Technology. Her interests lie within developing a full-fledged study on the possible ways to enhance the productivity of the DCMD, be it energy wise or on a molecular development level. Dana can be reached at dsuwwan@masdar.ac.ae

ROTATIONAL MACHINE FAULT DETECTION WITH ENSEMBLE EMPIRICAL MODE DECOMPOSITION BASED ON A THREE-ORTHOGONAL CHANNEL SENSOR

Li Tan, Purdue University North Central; Alexander Mussa, Purdue University North Central;
Justin Poling, Purdue University North Central; Kai Justice, Purdue University North Central;
Hongbo Xu, Nanjing University of Science and Technology

Abstract

Rotational machine fault detection and condition monitoring can prevent harmful conditions and ensure reliable operations of equipment. In order to achieve fault detection and conditional monitoring, many signal processing techniques, such as short-time Fourier transform (SFFT), wavelet transform, and empirical mode decomposition (EMD), have been developed. Among these methods, the EMD process has been a very promising and effective technique. In this paper, the authors propose an EMD-based algorithm that consists of two stages. The first stage processes vibrational signals using three orthogonal channel recordings in order to obtain a principal component signal. At the second stage, the ensemble empirical mode decomposition (EEMD) is applied to the principal component signal in order to obtain the intrinsic mode functions (IMF). The Hilbert-Huang transform spectrum, based on IMFs for various operating load conditions, was examined for fault diagnosis. The proposed algorithm alleviates the computational load by using the principal component signal instead of three individual x-, y-, and z-channel recordings. The experimental validations of the proposed algorithm were demonstrated using vibration signals acquired from a three-phase electric induction motor for both healthy and fault conditions under various loads.

Introduction

In the past, time-frequency and time-scale analysis methods such as short-time Fourier transform (STFT) and wavelet transform [1-3] were investigated for analysis of non-stationary or non-linear signals with applications in rotational machine fault detection and health monitoring to prevent harmful conditions and ensure the reliable operation of equipment. Although these techniques were successfully applied to machine health diagnosis and fault detection, the results depended on the selection of window type or the use of a base wavelet. More recently, the Hilbert-Huang transform (HHT) [4], [5] was proposed for decomposing a signal into a set of intrinsic mode functions (IMF) via the empirical decomposition (EMD) process [6-10]. The EMD is an adaptive approach and is effective for decomposing the non-stationary or non-linear signals. However, the EMD process suffers from a problem of mode mixing due to signal intermittency [11], [12]. The problem may cause the decomposed results to be vague and inappropriately interpreted. To eliminate the mode mixing problem, the ensemble empirical mode composition (EEMD) algorithm [11], [12] was proposed. This method essentially processes the original signal with an added white noise sequence into a set of IMFs using the standard EMD repetitively. The ensemble mean of the corresponding IMFs, which are obtained from the standard EMD, is used as the final EEMD decomposed IMF. Although the EEMD is effective for removing the mixing mode problem, the computational load is huge due to the ensemble process. Specially, when applying multi-channel signals, such as those from a sensor that provides three-orthogonal channel information, processing each channel's data sequence via the EEMD process requires even more computations and hinders practical applications.

Presented here, then, are the principles of the standard EMD, the Hilbert-Huang transform, and the EEMD. In order to reduce the computational load by using the EEMD for multichannel signals, a principal component empirical decomposition (PCEEMD) algorithm was proposed. The PCEEMD process consists of two stages: the first stage constructs the principal component signal based on the data sensed from three orthogonal channels; the second stage applies the standard EEMD process to the principal component signal. After obtaining the IMFs in the principal direction, they can be directly employed for rotational machine fault detection by the HHT spectrum, or, as an option, the obtained IMFs can be projected into three orthogonal axes.

Principles of the EMD, the HT Spectrum, and the EEMD

The EMD is an adaptive decomposition approach, which is applied to decompose nonlinear and non-stationary signals. The EMD process extracts a set of IMFs from the original signal. Each IMF must meet two conditions [4]: the number of extrema and the number of zero crossings must be either equal or differ at most by one; the mean value of the envelope defined by the local maxima and the envelope defined by the local minima at any point must be zero. The

steps of the EMD algorithm [4-6] to decompose a signal $x(t)$ are described as follows:

Step 1: Initialize $r_0(t) = x(t)$ and set $i = 0$

Step 2: Extract the i[th] IMF with the following sifting procedure:

a. Initialize $h_{i(k-1)}(t) = r_{i-1}(t)$ with $k = 1$;
b. Find the local maxima and local minima of signal $h_{i(k-1)}(t)$;
c. Interpolate the local maxima and local minima by cubic splines to construct the upper and lower envelopes of $h_{i(k-1)}(t)$;
d. Calculate the mean $m_{i(k-1)}(t)$ of the upper and lower envelopes of $h_{i(k-1)}(t)$;
e. Calculate $h_{ik}(t) = h_{i(k-1)}(t) - m_{i(k-1)}(t)$; and,
f. If the stop criterion for iteration k is given, Equation (1) is satisfied:

$$\sum_{t=0}^{T} \frac{[h_{i(k-1)}(t) - h_{ik}(t)]^2}{h_{i(k-1)}^2(t)} \leq SD \tag{1}$$

where, SD is a predefined value and usually set to 0.1; that is, if Equation (1) is satisfied, $h_{ik}(t)$ is an IMF and then set $c_i(t) = h_{i(k)}(t)$; else set $k = k + 1$ and then go to step (b).

Step 3: Calculate sequence: $r_{i+1}(t) = r_i(t) - c_i(t)$

Step 4: If $r_{i+1}(t)$ has at least 2 extrema then set $i = i + 1$ and go to step 2; else the decomposition is completed and $r_{i+1}(t)$ is the residual signal. The decomposition results are:

$$x(t) - c_1(t) = r_1(t)$$
$$r_1(t) - c_2(t) = r_2(t)$$
$$\ldots\ldots$$
$$r_{N-1}(t) - c_N(t) = r_N(t)$$

Summing the decomposition results yields Equation (2):

$$x(t) = \sum_{i=1}^{N} c_i(t) + r_N(t) \tag{2}$$

It can be seen that signal $x(t)$ is decomposed into N intrinsic mode functions and a residue signal $r_N(t)$. Once signal $x(t)$ is decomposed to N IMFs, the Hilbert transform (HT) [4], [5] can be applied to each IMF in order to obtain an instantaneous frequency, as given by Equation (3):

$$y_i(t) = \frac{1}{\pi} \int_{-\infty}^{\infty} \frac{c_i(t)}{t - \tau} d\tau \tag{3}$$

The analytical signal, $z_i(t)$, which is constructed using both IMF $c_i(t)$ and its HT $y_i(t)$, can be expressed by Equation (4):

$$z_i(t) = c_i(t) + jy_i(t) \tag{4}$$

Then, the instantaneous envelope of the analytic signal for the i[th] IMF can be found by Equation (5):

$$a_i(t) = \sqrt{c_i^2(t) + y_i^2(t)} \tag{5}$$

and the corresponding phase angle can be determined by Equation (6):

$$\theta_i(t) = \tan^{-1}\left(\frac{y_i(t)}{c_i(t)}\right) \tag{6}$$

Notice that instantaneous envelope $a_i(t)$ indicates the signal energy variation, while the phase angle $\theta_i(t)$ is the instantaneous phase. The instantaneous frequency for the i[th] IMF can be found by taking the derivative of the phase angle, as in Equation (7):

$$\omega_i(t) = \frac{d\theta_i(t)}{dt} \tag{7}$$

The Hilbert transform based on the IMF is referred to as the Hilbert-Huang transform (HHT); and, the time-frequency plot of the HHT is referred to as the HHT spectrum. Although the EMD demonstrates the effectiveness in decomposing nonlinear and non-stationary signals, the method has a problem of mode mixing; that is, a single IMF may contain oscillations of dramatically disparate scales, or a component of a similar scale resides in different IMFs, due to signal intermittency. The intermittence could cause serious signal aliasing in time-frequency distributions as well as make the physical meaning of the individual IMF unclear.

The noise-assisted data analysis [11], [12] of adding noise to the original signal was then proposed. This method is referred to as the ensemble empirical mode decomposition (EEMD). The principle of the EEMD can simply be described as follows: The EEMD adds white noise to the original signal before applying the EMD. Since the added white noise in the background populates the whole time-frequency space uniformly, the signal components at different scales can automatically be projected onto proper scales of the references, established by the white noise in the background. Although each trail may produce noisy results, the noise in the results can be cancelled out by using the ensemble mean with a significant number of trials. Hence, each IMF obtained using EEMD is the ensemble mean of trials.

The EEMD can then be summarized as:

Step 1: Add a white noise sequence to the original signal (the standard deviation of noise =10~20% of the standard deviation of the original signal).
Step 2: Decompose the signal with an added white noise sequence into the IMFs [$c_{i,m}(t)$ at the mth trial] using EMD.
Step 3: Repeat Steps 1-2 with different white noise sequences M times.
Step 4: Calculate the ensemble mean for each IMF from Equation (8):

$$c_i(t) = \frac{1}{M}\sum_{m=1}^{M} c_{i,m}(t) \quad , \quad i = 1, 2, \cdots, N \tag{8}$$

Obviously, the EEMD algorithm has a large computational load.

Development of a Principal Component EEMD

In many applications, a sensor [13] acquiring signals may contain multiple components. Figure 1 depicts an accelerometer (single station) consisting of three orthogonal channels: x, y, and z. Channels x and y are designated to record accelerations in the x and y directions, respectively. Channel z measures vertical acceleration. An incoming signal has angles α, β, and γ relative to the x, y, and z axes, respectively. Applying the EEMD algorithm for each channel requires a significant amount of computational load.

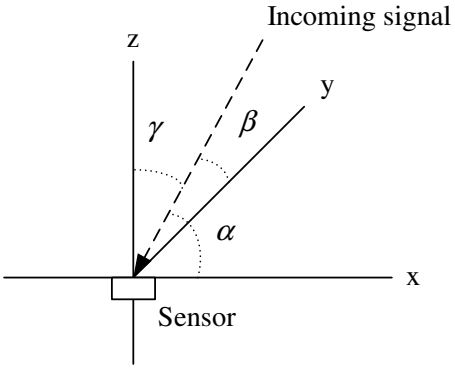

Figure 1. A Sensor with x-, y-, z- Channel Recordings

Assuming that $s(n)$ is the incoming signal with a direction of [cosα cosβ cosγ], while $x(n)$, $y(n)$, and $z(n)$ are the sensor recordings, the incoming signal can be estimated by a linear combination, as given by Equation (9):

$$s(n) = U^T X = \begin{bmatrix} u_1 & u_2 & u_3 \end{bmatrix} \begin{bmatrix} x(n) \\ y(n) \\ z(n) \end{bmatrix} \tag{9}$$

where, $U^T = [\, u_1\ u_2\ u_3\,]$ and $X^T = [x(n)\ y(n)\ z(n)]$.

Again, the sensor signals are assumed to be zero mean process, as given by Equation (10):

$$E(X) = \begin{bmatrix} E(x(n)) \\ E(y(n)) \\ E(z(n)) \end{bmatrix} = \begin{bmatrix} 0 \\ 0 \\ 0 \end{bmatrix} \tag{10}$$

then Equation (11):

$$E(s(n)) = E(U^T X) = 0 \tag{11}$$

where, $E(\ )$ is the expectation operator. Note that the power of the incoming signal can be expressed by Equation (12):

$$\sigma_s^2 = E(s^2(n)) = U^T E(XX^T) U = U^T C U \tag{12}$$

where, C is a 3x3 covariance matrix defined by Equation (13):

$$C = E(XX^T) = \begin{bmatrix} \sigma_x^2 & \sigma_{xy} & \sigma_{xz} \\ \sigma_{xy} & \sigma_y^2 & \sigma_{yz} \\ \sigma_{xz} & \sigma_{yz} & \sigma_z^2 \end{bmatrix} \tag{13}$$

with,

$$\sigma_x^2 = E(x^2(n))$$

$$\sigma_y^2 = E(y^2(n))$$

$$\sigma_z^2 = E(z^2(n))$$

$$\sigma_{xy} = E(x(n)y(n))$$

$$\sigma_{xz} = E(x(n)z(n))$$

$$\sigma_{yz} = E(y(n)z(n))$$

Based on Figure 1, it can be seen that

$$X = \begin{bmatrix} x(n) \\ y(n) \\ z(n) \end{bmatrix} = \begin{bmatrix} \cos\alpha \\ \cos\beta \\ \cos\gamma \end{bmatrix} s(n) \tag{14}$$

If U^T = [cosα cosβ cosγ] is found, the estimated incoming signal becomes that of Equation (15):

$$s(n) = U^T X = \left(\cos^2\alpha + \cos^2\beta + \cos^2\gamma\right) s(n) = 1 \cdot s(n) \quad (15)$$

Equation 15 indicates that U^T = [u_1 u_2 u_3] should be a unitary vector; that is, $U^T U = 1$ and the best unitary vector is the one to maximize the power of the incoming signal with the constraints of Equations (16) and (17):

$$\max_{U,\lambda} \ \sigma_s^2 \quad (16)$$

$$\sigma_s^2 = U^T C U - \lambda^L (U^T U - 1) \quad (17)$$

Taking the derivative of σ^2_s to U and setting the result to zero, Equation (18) follows:

$$(C - \lambda^L I)U = 0 \quad (18)$$

Taking the derivative of σ^2_s to the Lagrange multiplier λ^L and setting the result to zero yields the unitary vector constraint $U^T U = 1$. It is clear that the Lagrange multiplier λ^L is essentially an eigenvalue of the covariance matrix C; that is, $\lambda^L \in \lambda_1^C, \lambda_2^C, \lambda_3^C$. To ensure that σ^2_s is the maximum value, taking the second-order derivative of σ^2_s to U leads to the matrix of Equation (19):

$$\frac{\partial^2 \sigma_s^2}{\partial U^2} = \frac{\partial (C - \lambda^L I)U}{\partial U} = C - \lambda^L I = H \quad (19)$$

where, H must be semi-negative definite. Letting λ^H and U^H be an eigenvalue and an eigenvector of matrix H, respectfully, then Equation (19) becomes Equation (20):

$$(H - \lambda^H I)U_H = [C - (\lambda^L + \lambda^H)I]U_H = 0 \quad (20)$$

Equation 20 indicates that $\lambda^L + \lambda_i^H$ is an eigenvalue of matrix C, or Equation (21):

$$\lambda_i^C = \lambda^L + \lambda_i^H \ \ i = 1,2,3 \quad (21)$$

where, $U_H = U$. The eigenvalue of matrix H can be determined by Equation (22):

$$\lambda_i^H = \lambda_i^C - \lambda^L, \ \ i = 1,2,3 \quad (22)$$

To ensure that $\lambda_i^H \leq 0$ (H must be semi-negative definite), $\lambda^L = \lambda_{max}^C$. The corresponding unitary vector U for λ_{max}^C is the optimal vector which represents the signal principal direction. With the obtained optimal unitary vector of U, the principal component signal is achieved as $s(n) = U^T X$. Therefore, the proposed principal component ensemble empirical mode decomposition (PCEEMD) algorithm is summarized below:

Step 1: Compute the covariance matrix C.

Step 2: Determine the maximum eigenvalue, λ_{max}^C, and its corresponding unitary eigenvector, U.

Step 3: Compute the principal component signal as $s(n) = U^T X$.

Step 4: Apply the EEMD algorithm to the principal component signal as $s(n) = U^T X$ in order to obtain the IMFs.

Step 5: (optional) Project the IMFs onto the x, y, and z axes, respectively, that is:

$$IMFx_i = u_1 \times IMF_i$$

$$IMFy_i = u_2 \times IMF_i$$

$$IMFz_i = u_3 \times IMF_i$$

Experimentation and Validation

To validate the proposed PCEEMD method for non-stationary or non-linear signal analysis, vibrational signals from the accelerometer, based on three orthogonal channels, were acquired from the three-phase induction motor with an adjustable load (Figure 2). As shown in Figure 2, an accelerometer was attached to the three-phase induction motor. The accelerations measured in the x, y, and z axes were obtained via the LabView data acquisition platform at a sampling rate of 10 kHz with a 16-bit data resolution. The acquired data sequence from each channel was preprocessed to remove its mean (DC component). The adjustable load via the belt was coupled to the motor via a rubber coupler. A fault in the rubber coupler was introduced. Figure 3 shows healthy and fault coupler conditions. The coupler in the fault condition had worn-out inner and outer teeth on the driving side. The experiments were carried out with no load (0% load), medium load (50% load), and full load (100% load) with the motor running at 1800 rpm. The speed of the shaft was monitored by an optical encoder.

Notice that for the healthy condition validation experiment, the healthy coupler was installed, while for the fault condition validation, the healthy coupler was simply replaced by the fault coupler. It was also assumed that the condition for the healthy coupler or the fault coupler would stay the same during testing. The transition condition between the healthy coupler and the fault coupler was not considered in this study and will be investigated in the future. Figure 4 shows x-y-z channel vibration signals measured from the sensor as well as the principal component signal produced by the PCEEMD algorithm for the healthy coupler and fault coupler under the 50% load.

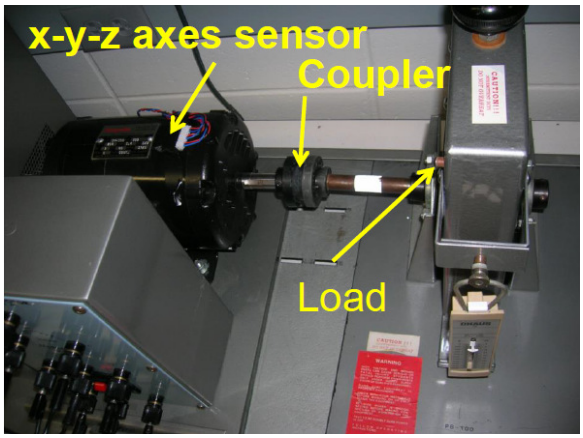

Figure 2. Experimental Setup

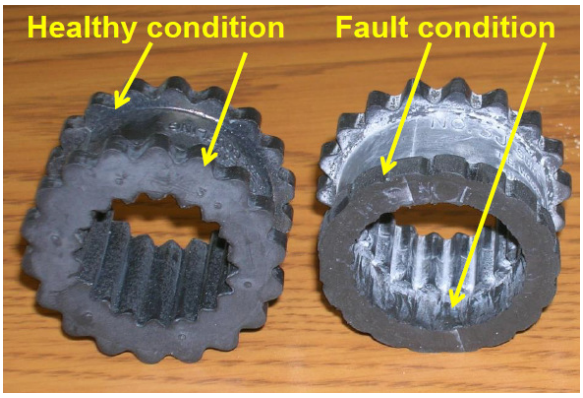

Figure 3. The Healthy and Fault Conditions of the Coupler

The second stage applied the EEMD algorithm to the principal component signals. The principal component signal was added with a white noise sequence and a Gaussian distribution using 20% of the standard deviation of the original signal. The ensemble mean of each IMF was calculated using 50 trials. The achieved corresponding IMFs for both healthy and fault conditions are given in Figure 5 for comparison. It can be seen that, for both cases, there was no significant evidence of mode mixing. The shaft frequency of 30 rev/s can be seen in IMF6 for both cases. For the healthy condition, there were nine IMFs but 10 IMFs for the fault condition.

The corresponding HHT spectra for healthy and fault conditions are depicted in Figure 6. As shown Figure 6(a), the dominant frequency component comes from the shaft rotation of 30 Hz (rev/sec); for the fault condition shown in Figure 6(b), besides the dominant frequency component of the shaft rotation (30 Hz), there appeared to be a fourth harmonic component, irregular pulses, and high frequency noise. As an additional validation, the discrete-Fourier transform spectra were calculated and are displayed in Figure 7. Clearly, the shaft frequency component was dominant for both healthy and fault conditions. Similarly, the fourth harmonic frequency component became significant in the fault condition. However, the DFT spectrum did not show time-scale information.

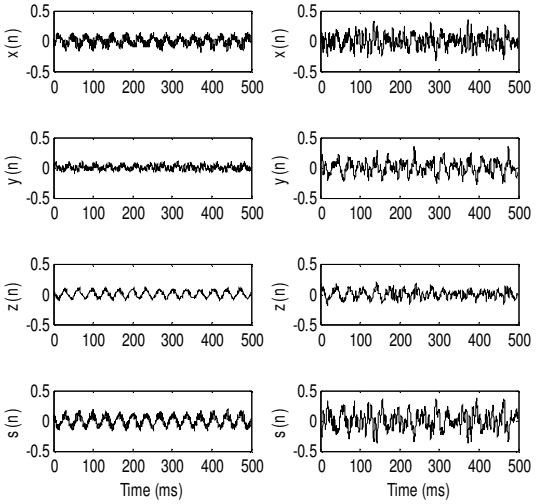

Figure 4. Acceleration Measurements and Generated Principal Component Signal *s*(*n*) (left: healthy condition; right: fault condition)

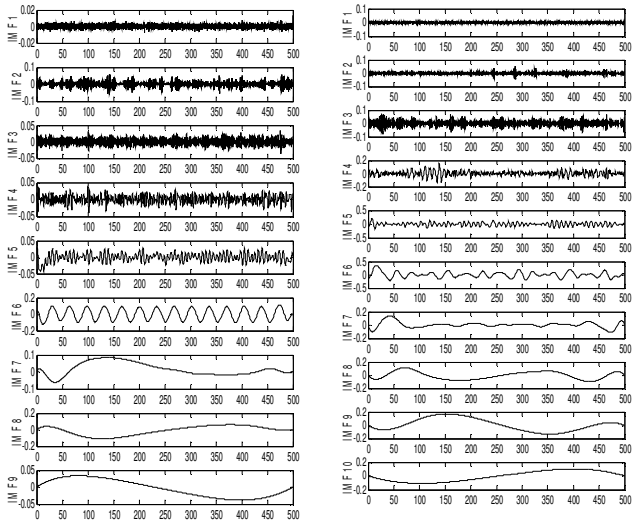

Figure 5. Decomposed IMFs from Two Coupler Conditions Using the PCEEMD Algorithm (left: healthy condition; right: fault condition)

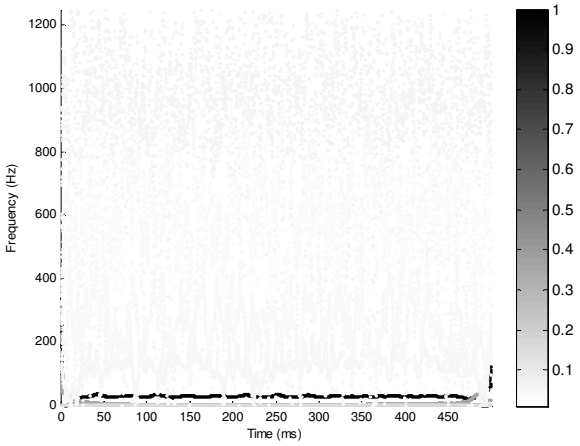

(a) Healthy Condition

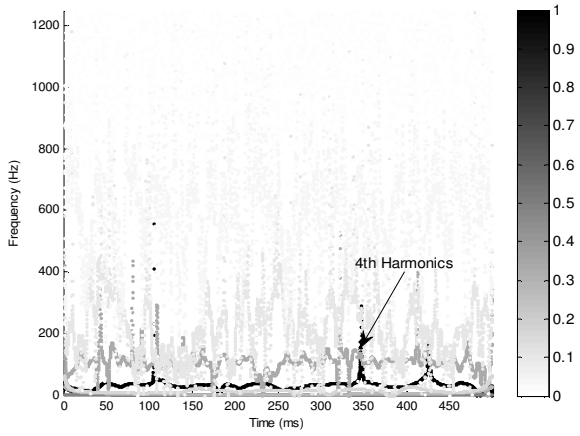

(b) Fault Condition

Figure 6. The HHT Spectra from Two Coupler Conditions Using the PCEEMD Algorithm

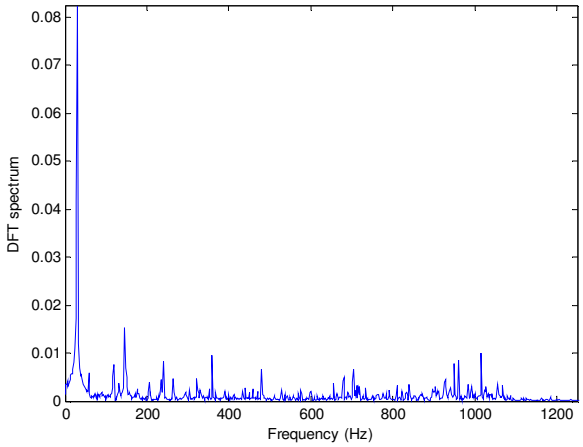

(a) Healthy Condition

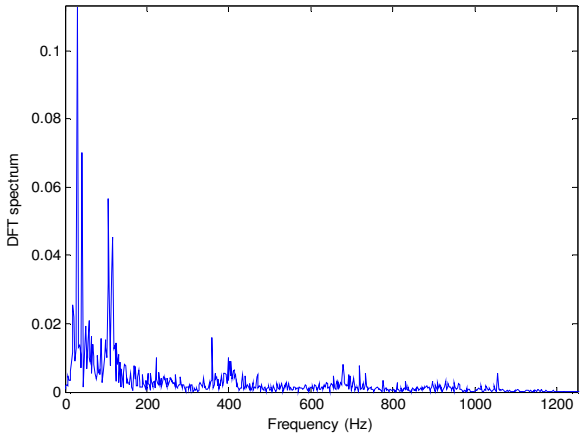

(b) Fault Condition

Figure 7. DFT Spectra from Two Coupler Conditions Using the PCEEMD Algorithm

Table 1. Results from HHT Spectra

Operation Conditions	Dominant frequency	High-order harmonics	Irregular pulses	High frequency noise
Healthy, 0% load	Significant	Not Significant	Not Significant	Not Significant
Faulty, 0% load	Significant	Significant	Significant	Significant
Healthy, 50% load	Significant	Not Significant	Not Significant	Not Significant
Faulty, 50% load	Significant	Significant	Significant	Significant
Healthy, 100% load	Significant	Not Significant	Not Significant	Not Significant
Faulty, 100% load	Significant	Significant	Significant	Significant

Additional Results

Validation of the 0% and 100% loads showed similar results to those of the 50% load. The results are summarized in Table 1.

Since the EEMD process only applies to the principal component signal, the computational load was significantly reduced. Most importantly, the principal component signal contained the sensed vibration signal with its aligned direction so that the obtained IMFs and HHT spectra would present the most meaningful information for fault detection and condition monitoring.

Conclusion

In this paper, the authors proposed a principal component ensemble empirical decomposition (PCEEMD) algorithm for rotational machine fault detection and condition monitoring. The algorithm was very effective for processing data from a single station sensor with x-, y-, and z-axis sensing components. The PCEEMD consisted of two stages. The first stage performed vibrational signal enhancement in order to achieve the principal component signal according to three orthogonal channel recordings. With the principal component signal, the EEMD algorithm was applied in order to obtain the IMFs with the advantage of mixing mode elimination. The Hilbert-Huang transform spectra were then obtained for rotational machine fault detection and diagnosis. The algorithm significantly alleviated the computational load by processing the principal component signal instead of three individual channel recordings. The experimental validations of the proposed method were demonstrated using vibration data acquired from the three-phase electric motor for healthy and fault conditions under various loads.

References

[1] Satish, L. (1998). Short-Time Fourier and Wavelet Transform for Fault Detection in Power Transformers during Impulse Tests. *Proceedings of the Institute of Electrical Engineering, Science, Measurement and Technology*, *145*(2), 77-84.

[2] Wang, C., & Gao, R. (2003). Wavelet Transform with Spectral Post-Processing for Enhanced Feature Extraction. *IEEE Transactions on Instrumentation and Measurement*, *52*(4), 1296-1301.

[3] Tan, L., & Jiang, J. (2013). *Digital Signal Processing: Fundamentals and Applications*. (2nd ed.). Amsterdam: Elsevier.

[4] Huang, N. E., Zheng, S., Long, S. R., Wu, M. C., Shih, H. H., Zheng, Q., et al. (1998). The Empirical Mode Decomposition Method and the Hilbert Spectrum for Non-Stationary Time Series Analysis. *Proceedings of Royal Society of London. Series A: Mathematical, Physical and Engineering Sciences, 454* (1971), 903-995.

[5] Feldman, M. (2011). Hilbert Transform in Vibration Analysis. *Mechanical Systems and Signal Processing*, *25*(3), 735-802.

[6] Lei, Y., Lin, J., He, Z., & Zuo, M. J. (2013). A Review on Empirical Mode Decomposition in Fault Diagnosis of Rotating Machinery. *Mechanical Systems and Signal Processing*, *35*(1-2), 108-126.

[7] Liu, B., Riemenschneider, S., & Xu, Y. (2006). Gearbox Fault Diagnosis Using Empirical Mode Decomposition and Hilbert Spectrum. *Mechanical Systems and Signal Processing*, *20*(3), 718-734.

[8] Li, R., & He, D. (2012, April). Rotational Machine Health Monitoring and Fault Detection Using EMD-Based Acoustic Emission Feature Quantization. *IEEE Transactions on Instrumentation and Measurement*, *61*(4), 990-1001.

[9] Yang, W., Court, R., Tavner, P. J., & Crabtree, C. J. (2011). Bivariate Empirical Mode Decomposition and Its Contribution to Wind Turbine Condition Monitoring. *Journal of Sound and Vibration*, *330* (15), 3766-3782.

[10] Gao, Q., Duan, C., Fan, H., & Meng, Q. (2008). Rotating Machine Fault Diagnosis Using Empirical Mode Decomposition. *Mechanical Systems and Signal Processing*, *22*(5), 1072-1081.

[11] Zhang, J., Yan, R., Goa, R., & Feng, Z. (2010). Performance Enhancement of Ensemble Empirical Mode Decomposition. *Mechanical System and Signal Processing*, *24*, 2104-2123.

[12] Yan, R., Zhao, R., & Gao, R. X. (2012, December). Noise-Assisted Data Processing in Measurement Science: Part Two. *IEEE Instrumentation and Measurement Magazine*, *15*(6), 32-35.

[13] Magotra, N., Ahmed, N., & Chael, E. (1989, January). Single-Station Seismic Event Detection and Location. *IEEE Transactions on Geoscience and Remote Sensing*, *27*(1), 15-23.

Biographies

LI TAN is a Professor in the College of Engineering and Technology at Purdue University North Central. He received the B.S. degree from Southeast University, Nanjing, China, in 1984, and the M.S. degree in Structural Engineering and the M.S. and Ph.D. degrees in Electrical Engineering from the University of New Mexico, Albuquerque, in 1987, 1989, and 1992, respectively. Dr. Tan has been an IEEE Senior Member since 2001. His research interests

include digital signal processing, active noise control and control systems, and digital communications. He co-authored two textbooks: *Digital Signal Processing: Fundamentals and Applications*, 2nd ed., Elsevier, 2013, and *Analog Signal Processing and Filter Design*, Linus Publications, 2009. He holds a U.S. patent. He has served as an associate editor for the *International Journal of Engineering Research and Innovation*, and the *International Journal of Modern Engineering*. Dr. Tan may be reached at lizhetan@pnc.edu

ALEXANDER MUSSA is a senior electrical engineering student at College of Engineering and Technology, Purdue University North Central.

JUSTIN POLING is a senior electrical engineering student at College of Engineering and Technology, Purdue University North Central.

KAI JUSTICE is a senior electrical engineering student at College of Engineering and Technology, Purdue University North Central.

HONGBO XU is a Ph.D. student at the School of Mechanical Engineering, Nanjing University of Science and Technology, Nanjing, China. He is a visiting scholar in spring 2014, at College of Engineering and Technology, Purdue University North Central.

DEVELOPMENT OF A WEB-BASED 3-D VISUALIZATION AND CLUSTER COMPUTING SYSTEM FOR DISASTER MANAGEMENT

Ge Jin, Purdue University, Calumet; Barbara Jean Nicolai, Purdue University, Calumet; Chuck Winer, Purdue University, Calumet; Gerald A. Dekker Jr., Purdue University, Calumet; John Moreland, Purdue University, Calumet

Abstract

Natural disasters can cause huge loss of life and enormous property damage to local communities. Although it is impossible to avoid natural disasters, human suffering can be reduced by adopting information technologies for disaster response missions. In this study, a web-based 3-D visualization and cluster computing system was developed to facilitate and expedite the resource distribution process during a disaster. This disaster management system utilized a state-of-the-art computing cluster with 16 nodes of Intel Xeon-E5 processors (16 cores per node) to process the emergency supply requests from the disaster victims and calculate the optimal resource distribution routes, while considering damaged transportation infrastructures. The optimized resource distribution problem was solved with a distributed all-pair shortest-path algorithm and the vehicle routing algorithm. The web-based 3-D visualization system was developed using the Google Earth engine to display the disaster areas, affected households, and resource distribution routes. The computational results from the cluster were automatically uploaded to the web-based 3-D visualization system, enabling users to immediately see the optimal resource distribution routes in a virtual 3-D environment. The visualization system is flexible and can be easily adapted to Google Earth-enabled mobile devices, desktop monitors, as well as a cave automatic virtual environment (CAVE). Historical disaster data from Northwest Indiana were used to demonstrate the functionalities of the developed system.

Introduction

The sights and sounds of disasters and expectations of rapid response is putting increasing pressure on governments and other institutions to move ever more quickly, whether it be in disaster relief endeavors such as the 2004 Asian tsunami, the Katrina hurricane along the Gulf Coast of the U.S. in 2005, the earthquake in Haiti in 2010, or the most recent earthquake and tsunami in Japan. From the White House report on Hurricane Katrina, state and local governments should develop modern, flexible, and transparent logistic systems for stockpiling commodities and supplies during emergencies [1]. Improvements in emergency management information and decisions will have a positive impact on those most affected by the disaster: the population. The affected population, however, can create difficulties for the decision maker. Each has varying disaster-caused or exacerbated needs and varied demands for services from the response organizations. With a general perception of lack of planning and coordination at both the federal and state levels, the question arose as to the preparedness of local government programs.

Indiana townships are part of state and local government systems, which supply indigent populations with needed services. Research has shown that, at present, many systems lack an emergency plan capable of meeting immediate needs such as basic shelter, food, clothing, and medical services for a large number of people in a short amount of time [2-6]. Better information and decision support to the manager can provide more accurate focus and priority for balancing the emergency response. A risk assessment and loss estimation tool based on a geospatial information system (GIS) has been widely used at federal and local government levels. The Federal Emergency Management Agency (FEMA) has distributed a HAZUS loss estimation tool on top of the integrated geographic information system platform ArcGIS (ESRI). It has been used to estimate the damages created by earthquakes and flooding [7], [8]. Based on lesson-learned research from Hurricane Katrina, federal, state, and local agencies need to maintain locally accurate GIS data that will enhance effective implementation of geospatial technologies for disaster management.

High-performance computing has been utilized for a variety of damage-estimation and simulation-in-disaster management applications. Akhter et al. [9], [10] extended an open-source GRASS (geographic resources analysis support system) library with MPI and OpenMP frameworks to perform distributed processing of satellite images for rapid damage severity and extent estimation. Roy et al. [11] indicated that in the emergency management of the real-time data, it is important to adopt a distributed geo-data processing methodology for effective decision-making. De la Torre et al. [12] reviewed numerous articles in disaster relief routing and suggested the utilization of a high-performance computing approach for disaster relief routing.

Recently, Lecron et al. [13] and Cruz-Chávez et al. [14] exploited a grid-computing method for solving vehicle routing problems.

In this paper, the authors introduce a GIS-based disaster data management, cluster computing, and 3-D visualization system that focuses on the Northwest Indiana region. The web-based disaster data management and communication system can provide communication between local authorities and indigent populations affected by the disaster. The high-performance computing cluster will provide expedited disaster management plans for decision makers. The cluster computing system gathers data during a disaster and disburses that information to the administrators who must make critical decisions for providing emergency food, water, medical, and rescue distribution. The 3-D geospatial information visualization system provides situational awareness and a common operating picture of local disaster areas. Local government agencies can visually acquire disaster-related information and make appropriate decisions based on the proposed disaster management and decision support system. The visualization system is flexible and can be easily adapted to Google Earth-enabled mobile devices, desktop monitors, as well as a cave automatic virtual environment (CAVE).

Although the proposed research focused on the Northwest Indiana region, the generality of the proposed methods and developed prototype system can be easily applied to other regional government agencies across the nation. The optimized resource distribution and route planning algorithm is based on USGS road network data in Arcview Shapefile format, which is open to the general public. The optimal route calculation algorithm utilizes an open-source VRPH (vehicle route planning heuristics) library and is implemented in C++ for a single CPU and in C++/MPI for the computing cluster. The web-based 3-D visualization system adopts an open-source PostgreSQL server with a 3-D Google Earth plugin and is implemented in PHP/Javascript. These software tools and programs are available for regional government agencies across the nation for development of their own disaster management and visualization systems.

Web-based Disaster Management and Communication System

The disaster management and communication module consists of a software/hardware solution. The software consists of a SQL server database and user interface built on the ASP.NET framework. It contains modules for collecting client information and resource information for services such as housing, transportation, emergency assistance, clothing, etc. The resource inventory data can be used by the Homeland Security incident commander in charge of providing support to the affected disaster area. The networking and hardware portion of this system consists of wireless handheld devices or laptops, which can be brought to a disaster site to collect indigent demographic information. This information is then added to the SQL database through a wireless network system.

Built on a Windows server platform, this system was implemented on both portable computers and workstations, which can be easily transported, if necessary. The enhanced entity relationship model describes the relationships between the agency, resources, clients, and service providers during emergencies. The DMCS system was set up as a two -tier application with application screens and class objects residing on a Web server, and the data being stored in a separate SQL server database. The Web server uses an HTTPS security protocol to encrypt the data communication between the client computer and Web server. The application requires a login ID and password validated through the database to gain access to the application. The communication between the DMCS and the database was set up with one connection setup in the Web.cfg file. The security of the data is also enhanced by the use of SQL-stored procedures that reside on the database for getting and sending data to the Web application from the database.

Figure 1 displays the web-based DMCS system described above. Once the disaster manager is assigned to the operation, information about the event can be collected in order to inform their actions. Another feature of the DMCS system is a GIS module, which could be used to display geographic conditions. To obtain the latitude and longitude values of an entered address, the system uses a Web service provided by Yahoo PlaceFinder. This service can convert an address such as “1600 Pennsylvania Avenue, Washington, DC” into geographic coordinates (latitude 38.898717, longitude 77.035974). The geospatial information is part of the situational awareness needed to develop the common operating picture.

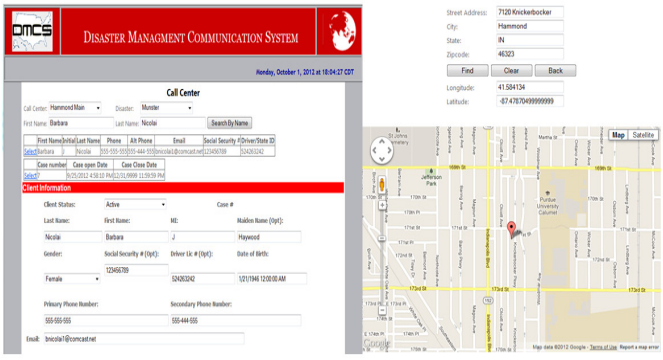

Figure 1. Web-based DMCS Interface and Geo-location API

Automated Data Transmission between the Web-based DMCS and Computing Cluster

The automated data transmission subsystem was developed in order to create a secure channel that connects the database to the remote computing cluster. The subsystem is located at the DMCS database server and runs synchronous operations to search new requests from the customers. When the new requests match, the subsystem extracts and collects the data through SQL scripts and automatically connects to the Linux-based supercomputing cluster using SFTP and SSH protocols. Figure 2 shows a data-flow diagram of automatic data transmission between the web-based DMCS and computing cluster, optimal route computation inside the computing cluster and the web-based 3-D visualization system.

Optimized Resource Distribution Route Computation using a Computing Cluster

It is essential to provide an efficient resource distribution strategy to decision makers after a disaster. A resource distribution center has certain resources including food, water, clothes, emergency medicines, and transportation unit that are typically needed by affected households. There is also an assumption that the amount of available resources are sufficient to serve all of the affected population; thus, minimizing the resource distribution time is equivalent to minimizing the sum of the distance between the resource center and household locations. Therefore, the problem becomes minimizing this sum of traveling distance between resource centers and household locations. Minimizing the sum of traveling distance with the constraint of the capacity is a vehicle routing problem and can be solved by an all-pair shortest-path algorithm and vehicle routing algorithm. Both all-pair shortest-path and vehicle routing problems are fundamentally graph problems. In this study, the graph being processed was the road network structure in the Northwest Indiana region. The GIS road network data were acquired from the U.S. Census Bureau. Unfortunately, these data are only a collection of line segments that do not provide any connectivity information. To solve this problem, a scan conversion algorithm was implemented to rasterize the GIS road data and create an adjacent graph structure. The scan conversion algorithm rasterizes unique road color codes for road segments and identifies intersection points (see Figure 3). This rasterizer is used to generate an adjacency road network graph for calculating all-pair shortest-path and vehicle routing problems.

The all-pair shortest-path algorithm is a graph analysis algorithm used to find the shortest paths between any two nodes in a weighted graph. The original Floyd-Warshall algorithm is a dynamic programming algorithm that finds the summed weights of the shortest paths between all-pairs of vertices, but it does not provide the transition route [15]. In this study, a distributed Floyd-Warshall algorithm was implemented to provide transition route information inside a 16-node computing cluster.

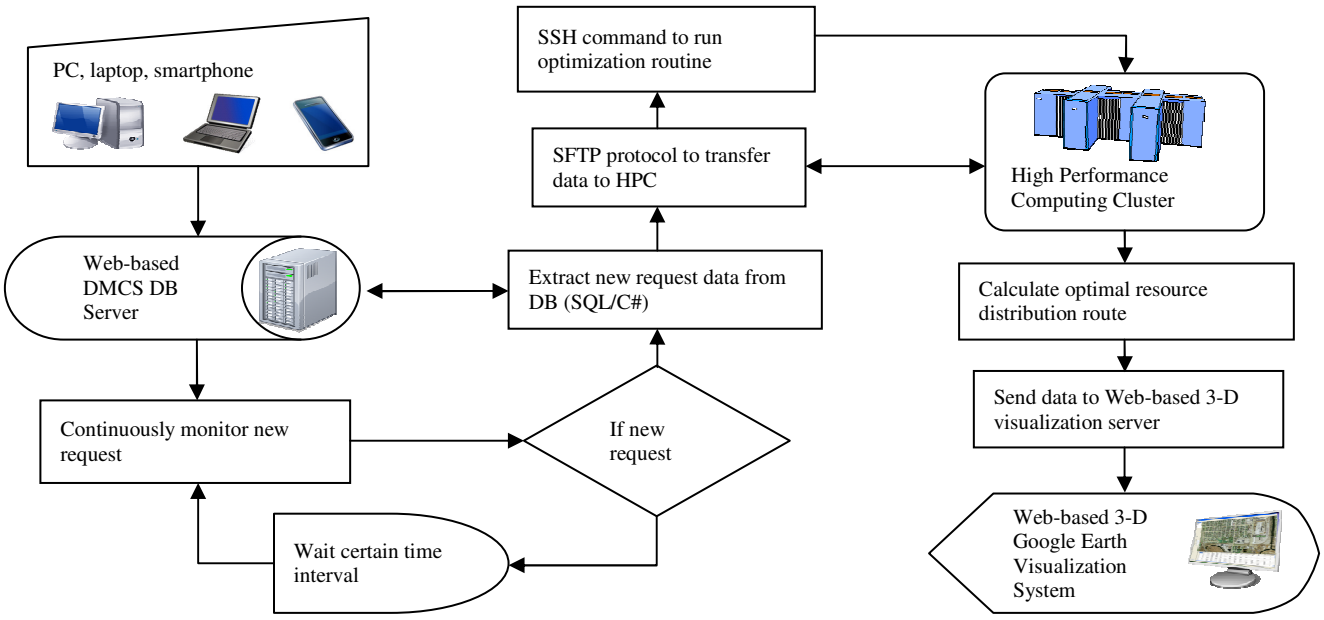

Figure 2. Data Flow of Automatic Data Transmission, Route Planning, and Visualization

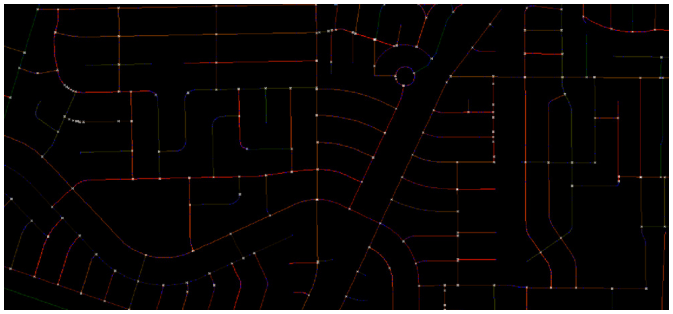

Figure 3. Conversion Algorithm to Generate a Road Network Graph

The distributed all-pair shortest-path algorithm works as follows: Each cluster node obtains a part of the adjacency graph matrix. The shortest-path computation uses a row-first order process. Each node chooses the row that will be shared by multiple nodes and then broadcast it to other nodes. These are candidate transition routes that, if the cumulated distance of passing this graph vertex is shorter than the current accumulated distance, replace the shortest path and put the transition graph vertex into the precedence matrix, P.

The vehicle routing problem (VRP) is to construct a minimum-cost set of routes that meets all customer demands, while minimizing the total distance of the transition routes. Because of the difficulty in solving the VRP and additional constraints, a VRP problem of realistic size was typically solved via heuristic methods. In this project, an open-source C++ package (VRPH) was adopted to solve the vehicle routing problem. VRPH was developed by Chris Groer and provides a modular, well-documented library of local search heuristics for generating solutions to the VRP [16]. The all-pair shortest-path matrix is used as an input to the VRPH software, and it generates an optimized resource distribution route. The optimal distribution route starts from the command center, follows the shortest path to the affected household and resource distribution locations, and returns back to the command center. Different colors indicate the multiple resource distribution routes based on the numbers and capacities of the mobile unit. Figure 4 shows a visualization of the computed resource distribution route in a web-based, 3-D visualization system.

The optimal resource distribution route computation utilizes a state-of-the-art computing cluster with 16 nodes of Intel Xeon-E5 processors to process the emergency supply requests from the disaster victims, and calculate the optimal resource distribution routes with the consideration of the damaged transportation infrastructures. For Munster and Hammond, the HPC can update the optimal route in less than a minute. Considering the flooded area in Lake County, Indiana, the route computation took 15 minutes inside the high-performance computing cluster.

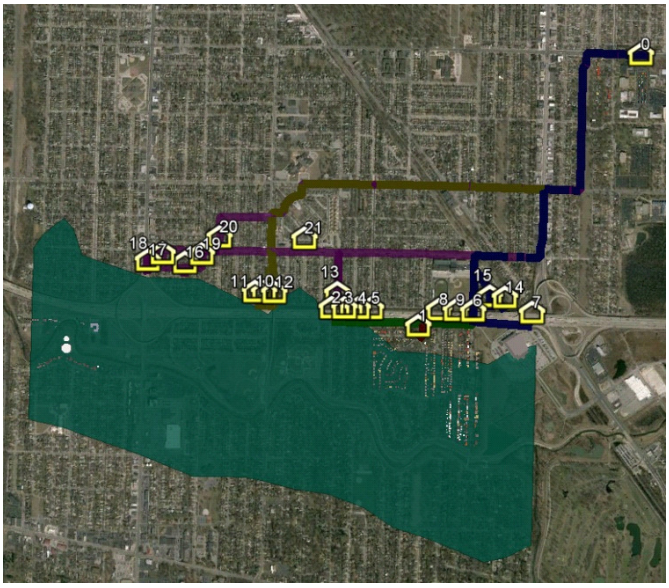

Figure 4. Optimal Route Calculation using the VRPH Method

The disaster management and communication module consists of a software/hardware solution. The software consists of a SQL server database and user interface built on the ASP.NET framework. It contains modules for collecting client information and resource information for services such as housing, transportation, emergency assistance, clothing, etc. The resource inventory data can be used by the Homeland Security incident commander in charge of providing support to the affected disaster area. The networking and hardware portion of this system consists of wireless handheld devices or laptops that can be brought to a disaster site to collect indigent demographic information. This information is then added to the SQL database through a wireless network system. Built on a Windows server platform, this system was implemented on both portable computers and workstations, which can be easily transported if necessary. The enhanced entity relationship model describes the relationships between the agency, resources, clients, and service providers during emergencies.

The DMCS system was set up as a two-tier application with application screens and class objects residing on a Web server, and the data being stored in a separate SQL server database. The Web server uses the HTTPS security protocol to encrypt the data communication between the client computer and Web server. The application requires a login ID and password validated through the database to access the application. The communication between the DMCS and the database was set up with one connection setup in the Web.cfg file. The security of the data is also enhanced by

the use of SQL stored procedures that reside on the database for getting and sending data to the Web application from the database.

Another feature of the DMCS system is a GIS module, which could be used to display geographic conditions. To obtain the latitude and longitude values of an entered address, the system uses a Web service provided by "Yahoo PlaceFinder." This service can convert an address such as "1600 Pennsylvania Avenue, Washington, DC" into geographic coordinates (latitude 38.898717, longitude -77.035974).

3-D Visualization of the Optimal Resource Distribution Route and Disaster Area

The computational result from the computing cluster is automatically uploaded to a Google Earth-based 3-D visualization system. This approach enables the users to immediately see the computational result from a web-based visualization system. The Google Earth software package was chosen as it was both a freely available and reasonably capable GIS suite. Initial testing indicated that selective culling of models would be necessary within the displayed area to ensure program responsiveness. Google Earth supports a large subset of the KML (keyhole markup language) specification. A significant feature of the KML specification used in this visualization system is the network link element. A KML network link allows Google Earth context to be updated periodically from a remote server. The visualization interface initially loads all possible categories of displayable elements as network links. The response files are dynamically generated using PHP and a database backend to reflect the current state of the emergency scenario. Objects that are dynamically generated from the database for display includes emergency relief package sources (EMS centers) as KML models, emergency relief package destinations as KML placemarks, extent of flooded water bodies as KML polygons, calculated optimal package delivery routes as KML lines, and observer photographs inserted as geolocated KML PhotoOverlays. The web-based, 3-D visualization system provides monoscopic and stereoscopic pages, which facilitates the use of both regular monitor and stereoscopic displays such as 3-D monitors and CAVE virtual environments (see Figure 5).

During a disaster, users can upload photos of the disaster areas using mobile and handheld devices. Users can take a photo in the field with a mobile device. Picture info and data could be acquired from phone instrumentation. The photo and geospatial information is uploaded to the server and pictures are automatically updated and placed within the Google Earth interface (see Figure 6), which is dynamically updated or populated with delivery targets, routes, and road obstruction visual indicators via a remote database and computing-cluster-backed Web server.

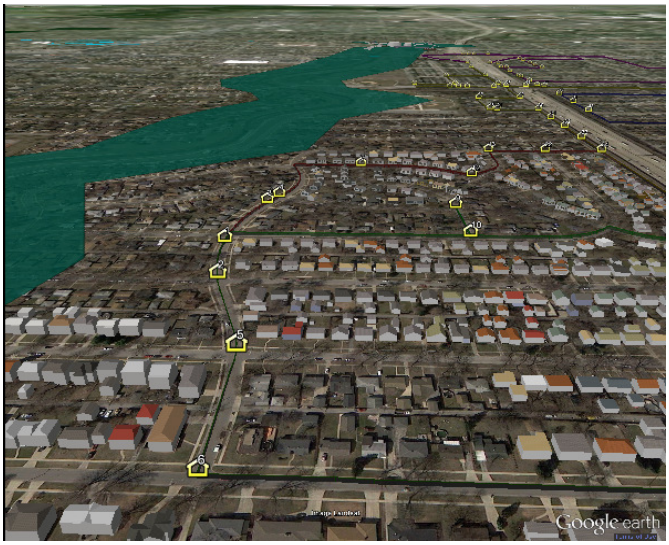

Figure 5. 3-D Visualization of the 2008 Flood Data in Munster, Indiana

To test the developed DMCS system, historical flood data were acquired from the FEMA report from the 2008 Northwest Indiana flood case. The blue area in Figure 7(a) is the flooded area along the Little Calumet River in Munster. The flooded area was imported into the HPC and web-based visualization system in order to compute the optimal resource distribution route. The flooded area rapidly changes during a disaster. The high-performance computing cluster is capable of dynamically updating the optimal resource distribution route with the changes in the flooded area. Figure 8 shows the expansion of the flooded area and resource distribution routes to the affected households over time.

The web-based, 3-D visualization interface was developed in response to two specific criteria: first, that disaster resource requests and locations must be visible to users of the system; and, secondly, that users of the system must have control of the type and quantity of information displayed on the user interface. The new elements of the system were designed to be backward compatible with previous system considerations. An illustration of a typical usage scenario follows: A remote user opens the visualization interface in a HTML 5-compliant Web browser. The interface presented contains the main display surface, based on 3-D Google Earth. A number of sub-panels located around the main display surface allow the user to enable or disable elements visible within the Google Earth environment and view information about each element being displayed.

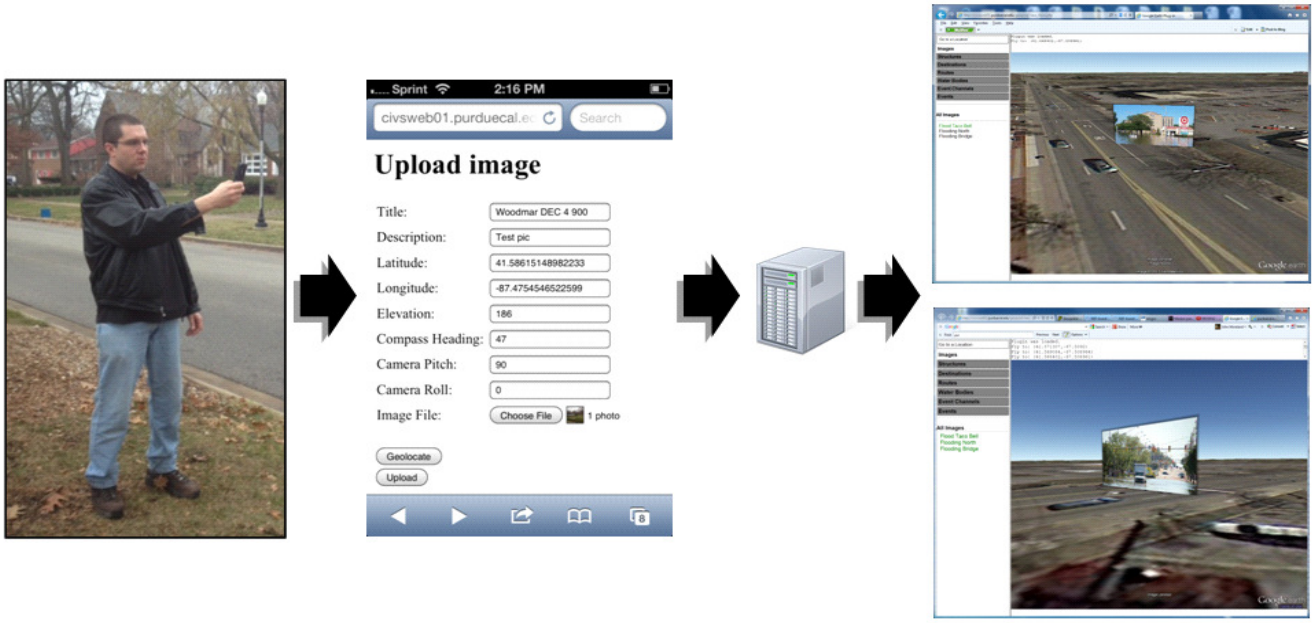

Figure 6. Real-time Update of Disaster-related Photos from Mobile Devices

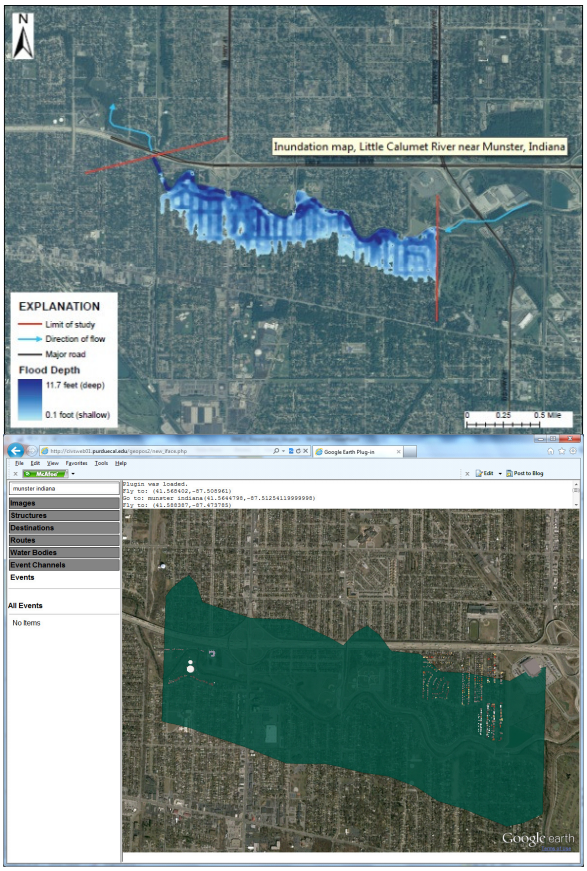

Figure 7. 2008 Flood Data in Munster, Indiana

Project-based Learning for Graduate and Undergraduate Education

Since 2010, more than 30 PUC graduate and undergraduate students have participated in this research project. The authors worked closely with the students to develop a web-based disaster management and communication system and distributed graph partitioning algorithm in the Purdue University Calumet HPC Cluster for disaster decision support. During the project, the students acquired hands-on experience in grid computing as well as interactive visualization techniques. Students developed a HPC-based disaster decision support system to compute the effective resource distribution strategy and prioritize the rescue areas by utilizing a disaster-specific geospatial information system. Three graduate students completed their master's theses based on this project, and more than 10 undergraduate students completed their senior design projects based on this research.

Conclusions

In this paper, the authors describe the development of a web-based, 3-D visualization and cluster computing model for disaster management and rescue efforts. The system is portable and self-supporting with laptops or handheld devices that can be carried into a disaster area. The components of the system could be quickly and easily transported to any disaster terrain site. After deployment, the system could be

Figure 8. Real-time Update of Rescue Routes with Changes in the Disaster Area

operational and functional within just a few hours. In addition, utilization of freely available software packages proved effective as a low-cost solution to the problem. Disaster management systems are currently not installed as a consistent solution across the nation. This research will lay a foundation for disaster preparedness, and a management and decision support system for local and federal governments. Integration of 3-D geospatial visualization and a middle-sized computational cluster with disaster DMCS has the potential to provide innovative disaster management solutions to local and federal government agencies.

This work was supported in part by the Northwest Indiana Computational Grid Project, funded by the Department of Energy.

References

[1] U.S. Government. (2006). The Federal Response to Hurricane Katrina: Lessons Learned. Retrieved from http://georgewbush-whitehouse.archives.gov/reports/katrina-lessons-learned.pdf

[2] Nicolai, B. J., Puntillo, K., & Bilow, B. (2008). Research Design for a Natural Disaster Management Communication System: Local Indiana Government Agency Model. *Proceedings of the Conference on Information Systems Applied Research.* Phoenix, AZ.

[3] Nicolai, B. (2007). Teaching Relational Database Modeling Using A Case Study: Indigent Population Database Project. Can Our Existing Government Agencies Provide Life Support to Our Indigent Population and Survive a National Disaster? *Proceedings of the ATINER 2007 International Conference*. Athens, Greece.

[4] Nicolai, B. (2007). Teaching Citizenship through Database Case Study Application, the Hurricane Katrina Disaster Experience. *Proceedings of the International Conference on Information Society (i-Society 2007)*. Merrillville, IN.

[5] Nicolai, B., & Winer, C. (2006). Indigent Population and Natural or Terrorist Database and Infrastructure Project. *Proceedings of the International Conference on Information Society (i-Society 2006)*. Miami, FL.

[6] Patrick, C. S., & David, M. S. (2009). Technology and Communications in an Urban Crisis: The Role of

Mobile Communications Systems in Disasters. *Journal of Urban Technology*, *16*(1), 133-149.
[7] Kircher, C. A., Whitman, R. V., & Holmes, W. T. (2005). HAZUS Earthquake Loss Estimation Methods. *Natural Hazards Review*, *7*(2), 45-59.
[8] Subrahmanyam, M. (2006). Riverine Flood Modeling in HAZUS-MH: Overview of the Implementation. *Proceedings of the 2005 Georgia Water Resources Conference*. Athens, GA.
[9] Akhter, S., Chemin, Y., & Aida, K. (2006). Satellite Image Processing on Distributed Computing Environments. *HPCS Conference*. Japan.
[10] Akhter, S., Aida, K., & Chemin, Y. (2010). GRASS GIS on High Performance Computing with MPI, OpenMP and Ninf-G Programming Framework. *Proceedings of ISPRS 2010*. Japan.
[11] Roy, P. S., Karnatak, H., & Saran, S. (2012, January). Geospatial Data Processing in Distributed Computing Environment. *Computer Society of India Communication*, *35*(10), 6-10.
[12] de la Torre, L. E., Dolinskaya, I. S., & Smilowitz, K. R. (2012, March). Disaster Relief Routing: Integrating Research and Practice. *Socio-Economic Planning Sciences*, *46*(1), 88-97.
[13] Lecron, F., Manneback, P., & Tuyttens, D. (2010) Exploiting Grid Computation for Solving the Vehicle Routing Problem. *2010 IEEE/ACS International Conference on Computer Systems and Applications (AICCSA)*, (pp. 1-6).
[14] Cruz-Chávez, M. A., Rodríguez-León, A., Rivera-López, R., Juárez-Pérez, F., Peralta-Abarca, C., & Martínez-Oropeza, A. (2012). Grid Platform Applied to the Vehicle Routing Problem with Time Windows for the Distribution of Products. In C. Ortiz Zezzatti, C. Chira, A. Hernandez, & M. Basurto (Eds.), *Logistics Management and Optimization through Hybrid Artificial Intelligence Systems* (pp. 52-81).
[15] Floyd, R. W. (1962, June). Algorithm 97: Shortest Path. *Communications of the ACM*, *5*(6), 345. doi: 10.1145/367766.368168.
[16] Groe, C., Golden, B., & Wasil, E. (2010). A Library of Local Search Heuristics for the Vehicle Routing Problem. *Mathematical Programming Computation*, *2*(2), 79-101.

Biographies

GE JIN, D.Sc., is currently an Assistant Professor in the Department of Computer Information Technology and Graphics at Purdue University, Calumet. He teaches computer game development, computer graphics and animation, as well as computer information technology courses at the undergraduate and graduate levels. Prior to joining Purdue University, Calumet, he was a postdoctoral research scientist at the George Washington University, Department of Computer Science. Dr. Jin holds a B.S. in Computer Science from Peking University, China, and an M.S. in Computer Science from Seoul National University, South Korea. He earned his Doctor of Science degree in Computer Science with a concentration in computer graphics from George Washington University. His research spans the fields of computer graphics, virtual reality, computer animation, medical visualization, and educational game development. Dr. Jin may be reached at ge.jin@purduecal.edu

BARBARA JEAN NICOLAI is currently an Associate Professor in the Department of Computer Information Technology and Graphics at Purdue University, Calumet. Her research focuses on Disaster Management Communication Systems that support any natural or man-made disaster including pandemics, floods, and earthquakes. Her research interests include database modeling and architecture, specifically the study of entities and their correlation with each other; a database perspective of women in technology; and, a database perspective of women and children's health care. Dr. Nicolai may be reached at bnicolai@purduecal.edu

CHUCK WINER is currently a Professor in the Department of Computer Information Technology and Graphics at Purdue University, Calumet. His research interests lie in the shared database utility of the indigent population of the United States. Specifically, those families and individuals in Northwest Indiana and how they can best be serviced in their needs. Of continuing interest is how heterogeneous and homogenous database data may be utilized by both private, non-profit organizations and government agencies. He has published and presented papers on this subject at national and international conferences. Dr. Winer may be reached at winer@purduecal.edu

GERALD DEKKER obtained his master's degree in Computer Science from Purdue University, Calumet, in 2012. He currently works at the Purdue Calumet Center for Innovation through Visualization and Simulation as a postgraduate researcher in virtual reality and computer graphics. Mr. Dekker may be reached at jerrydekker@comcast.net

JOHN MORELAND is a senior research scientist at the Center for Innovation through Visualization and Simulation at Purdue University, Calumet. He holds an M.S. in Technology; a B.S. in Computer Graphics Technology; and, is currently working on a Ph.D. in Technology focusing on the application of mixed reality technologies to education. Mr. Moreland may be reached at morelanj@purduecal.edu

COMPRESSIVE PERFORMANCE OF RECYCLED AGGREGATE MORTAR

Thomas Nicholas II, University of North Carolina at Charlotte; Paul Radford, University of North Carolina at Charlotte;
Tara Cavalline, University of North Carolina at Charlotte; Anthony L. Brizendine, University of North Carolina at Charlotte

Abstract

The use of recycled materials in construction is gaining popularity in efforts to attain net zero status for commercial construction. When investigating the applicability of new materials in building construction, it is prudent to first ensure that the replacement material used equals the strength performance of the natural material being replaced. For concrete masonry systems, the compressive strength of the system, f'_m, is used to describe strength performance. The study used the prism test method to compare the f'_m of prisms made with standard, normal weight masonry sand to the f'_m of prisms made with recycled materials, including crushed demolition rubble and brick manufacturing waste. Several mix designs were tested for each of the recycled aggregates used to determine optimum mix ratios. The crushed demolition rubble was comprised of crushed brick and mortar, while the brick manufacturing waste was solely made up of crushed brick. A sieve analysis for each of the materials was conducted for each of the materials in order to better understand how the distribution of aggregate size affected the overall strength of the mortar.

The effects of workability and bonding in relation to water content for each of these mixes were explored. Alternatives to ASTM C109 for finding accurate mortar strength values using the same mortar from the prism tests were considered. In the case of the crushed demolition rubble and the brick manufacturing waste, the elongation of the aggregates and how they affect the height of the mortar joint were addressed. Compression prism and two inch cube data for each of the recycled materials were analyzed and compared to standard, normal weight masonry sand.

Introduction

As recycled materials continue to gain popularity in the construction industry, it is important to attempt to incorporate these materials into different aspects of construction. As with any new building material, exhaustive testing is needed to ensure that its operating parameters meet the current standards. This study focused on the compression performance of mortar consisting of recycled aggregates in place of natural aggregates. The concept of using recycled aggregates in concrete has grown in popularity while, conversely, the mainstream masonry building community has failed to capitalize. As the cost of new aggregates rises, the need for alternative aggregates of comparable or greater quality will be paramount. The current practice of landfilling demolition rubble is not a sustainable practice, as the amount of landfill space is finite. Overall the ability to recycle and reuse these materials will serve to reduce the amount of material that needs to be quarried, while also reducing the amount of material needing to be disposed of.

One of the common issues that occurred during research with recycled aggregates is the difference in water absorption. Recycled aggregates that are made with brick or other fired clay materials, which were used in this study, have higher moisture absorption than typical normal-weight aggregates [1]. This means that more water needs to be added to the mix in order to achieve the same workability and flow, which has negative impacts on the final strength of the concrete masonry specimens [2].

The use of these materials in concrete has been extensively studied [1-4] with varied results. Some sources of variation in the data retrieved could be credited to inconsistencies in the source materials or differences in testing procedures. Etxeberria et al. [3] reported that concrete made with no more than 25% recycle concrete aggregates could be used in structural applications, while higher percentages had an unacceptable reduction in strength compared to the control. A second study using recycled concrete aggregate from a demolished airport also found that as the percentage of recycled aggregates increased, the strength of the resulting concrete specimens decreased [4].

While research on the use of recycled aggregates in concrete is fairly abundant, the use of recycled materials in masonry mortar is less common. Masonry mortars that include atypical materials ranging from high impact polystyrene [5] to recycled glass and metakaolin [6] have been researched. In mortar or concrete, bonding between the cement paste and the aggregates used is dependent on variables including aggregate angularity and water absorptivity. This presents a possible challenge when using atypical materials as aggregates due to the differences in shape and water retention compared to natural aggregates. If this bond strength is not achieved, slippage between the aggregate particles could cause a decrease in the compressive strength of the mortar.

Although in some cases an adequate bond is made between the new material and the cement paste due to an acceptable aggregate surface roughness [7], [8].

Prism testing, constructed according to ASTM C1314 [9], was used to test and compare the compressive strength of the mortar as part of a concrete masonry building system. Any variability in the concrete masonry units used resulted in a corresponding variability in the prism tests. For this reason, prism compression tests could be used primarily to verify that the performances of the recycled aggregate mixes under compression would be comparable to the standard C-144 sand mix.

Mix Design and Preparation

A mix design of three parts aggregate to one part cement by volume was employed for use in each of the test series. This is due to balancing of the strength of the mortar with the cost of producing. As the cement is the most expensive part of the mortar mix, it is preferred to use the least amount possible, while still maintaining the necessary strength of the material. Any time a material is used in a different application there will be challenges to overcome, and this study was no exception. Over the course of testing, the mortar mixes utilizing crushed brick recycled aggregates provided unique challenges not present in mortar mixes that employ sand. These challenges include: bonding issues, joint height, particle elongation, particle angularity, and water content. The test methods used were improved in order to overcome these challenges and give a more in-depth understanding of the behavior of the recycled materials being used.

Certain particles contained in the recycled demolition brick sand and the brick manufacturing waste have the tendency to be elongated and angular, as shown in Figure 1. This can cause issues when using these materials to construct prisms as the specified mortar joint is only 3/8". Preliminary cube testing indicated that including these long, angular particles in the mortar sample yielded specimens that had a higher compressive strength than those that were made without these particles. In order to prevent premature local failures of the prism specimen due to surface irregularities, it was necessary to provide a uniform bearing area to aid in even-load distribution. This process is referred to as "capping the specimen". The material used for capping the prism test series was a sulfur cement capping compound provided by ASTM C1552-12 [10]. A capped specimen is illustrated in Figure 2.

The effect that water content has on the behavior of masonry mortar is extremely important as it affects nearly every aspect of the mortar's characteristics including workability and bonding to the final compressive strength. To achieve the necessary workability, the mason was given the freedom to dictate the amount of water added to the mix in real time, while the final amount of water added was recorded. Flow tests were performed on a flow table at 1 minute after mixing and 30 minutes after mixing (see Table 1). The mortar sample that was used to create the masonry prisms was the same that was used to create the mortar cubes.

Figure 1. Elongated and Angular Particles

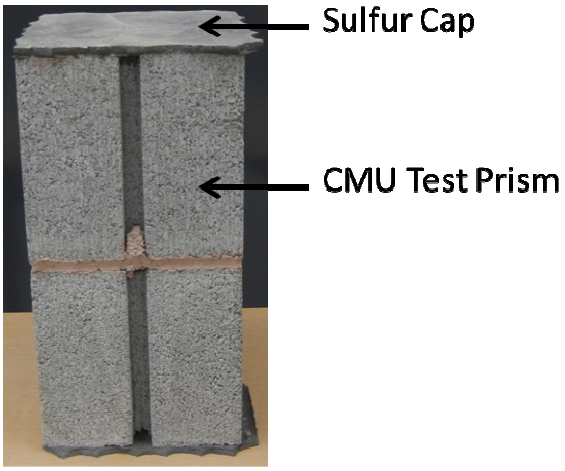

Figure 2. Illustration of Capped Prism Specimen

Table 1. Flow Rates for the Aggregates Tested

Aggregate	@ 1 minute	@ 30 minutes
C-144 Masonry Sand	190	190
Demolition Brick Sand	172	165
Brick Manufacturing Waste	165	159

The prisms that were tested utilized lightweight concrete masonry units that had a higher absorption rate than normal-weight concrete masonry units. This affected the mortar that was used to build the prisms by drawing more water out of the mortar than a normal-weight concrete masonry unit would.

Cube Testing

The standard 2" masonry mortar cube test, as described in ASTM C109 [11], sets a clear guide for creating and testing 2" mortar cubes that utilize typical aggregates. However, the aggregates tested in this study were not typical and, therefore, had different water absorption qualities. Since the brass that makes up the molds used in ASTM C109 will not absorb any water from the specimens they contain, the water content of the sample was accordingly reduced in order to account for this effect.

ASTM C109 specifies that the water content of the sample, prior to being inserted into the brass molds, must produce a flow of 110 ± 5 in 25 drops of the flow table. This results in a very dry state for the mortar and, in the case of the materials tested with the exception of sand, makes it very difficult to obtain a clean, uniform cube. Therefore, an alternative method for creating companion cubes was explored. One of the requirements for the alternative test was that the same mortar sample that was used to create the masonry system prisms could also be used to create the mortar companion cubes, thereby making the companion cubes a more accurate measure of the mortar in the system prisms.

This alternative method is similar to the method for making 4" x 8" grout prisms outlined in ASTM C1019-13 [12]. The masonry units were positioned such that the opening measured 2" x 2". The faces of the lightweight concrete masonry units used in the construction of the molds were first lined with a thin, permeable material in order to prevent the mortar from adhering to the unit. The bottom of the mold was lined with an impermeable material to prevent moisture loss not experienced in-situ. After 24 hours in the molds, the specimens were removed from the molds and placed in a lime bath to cure for 28 days. On day 28 the specimens were removed and cut into three 2-inch-high cubes on a lapidary slab saw before being tested. The goal of this method of making mortar cubes was to more accurately mimic what would be occurring in the field. All specimens of each type of mortar mix were tested within 10 minutes of each other in an attempt to eliminate any variability in moisture content between the specimens.

The results shown in Table 2 and Figure 3 indicate that the mortars made with the recycled brick aggregates were generally stronger than the C-144 masonry sand that was used as the control with the demolition brick sand being 169% stronger and the brick manufacturing waste being 137% stronger. From these data it was expected that this trend would be reflected in the results for the prism testing.

Table 2. Alternative Cube Results

	Ultimate Strength (PSI)		
Cube #	Masonry Sand	Demo. Brick Sand	Brick Manuf. Waste
1	1122	2480	2193
2	1047	2886	2102
3	1335	2775	2535
4	1815	2459	1856
5	1732	2133	2109
6	2074	2683	1743
Average	1521	2569	2090

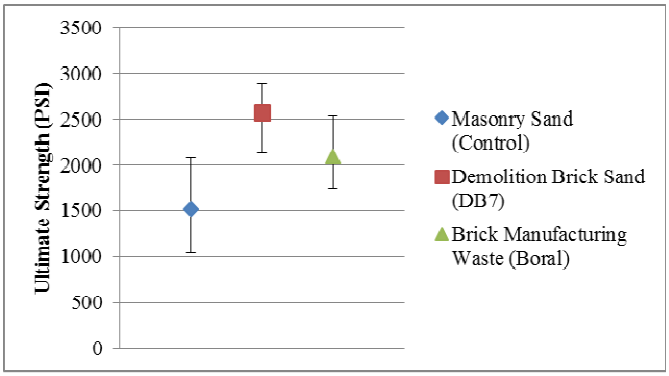

Figure 3. Alternative Cube Results

Prism Testing

Prisms were constructed according to ASTM 1314-12 and tested after 28 days of curing in a lime-water bath. Only 28-day testing was required due to the goal of this test being the validation of the recycled materials in question. Within 24 hours prior to testing the prisms were removed from their airtight bags and capped. The results presented in Table 3 and Figure 4 indicate that the demolition brick sand exhibited 105% of the current standard's compressive strength performance. Meanwhile, the brick manufacturing waste exhibited only 83% of the masonry sand's compressive strength. This could be due to the differences in makeup between these materials. The demolition brick sand was made up of crushed brick and mortar, while the brick manufacturing waste was made up of only crushed brick. The presence of mortar cement particles in the demolition brick sand could have been the reason for the increased compressive strength.

Table 3. Prism Compression Results

	Ultimate Strength (PSI and MPa)					
Prism #	Masonry Sand		Demo. Brick Sand		Brick Manuf. Waste	
	PSI	MPa	PSI	MPa	PSI	MPa
1	1864	12.85	1257	8.67	1104	7.61
2	1182	8.15	1525	10.51	992	6.84
3	887	6.12	2124	14.64	1020	7.03
4	2284	15.75	946	6.52	992	6.84
5	1010	6.96	1192	8.22	1142	7.87
6	1179	8.13	1552	10.70	1671	11.52
7	1646	11.35	1732	11.94	1125	7.76
8	1344	9.27	1380	9.51	1071	7.38
9	1552	10.70	1270	8.76	1299	8.96
10	895	6.17	1596	11.00	1116	7.69
Average	1384	9.54	1457	10.05	1153	7.95

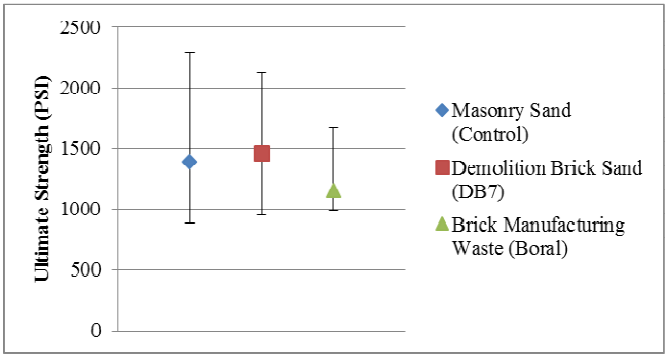

Figure 4. Prism Compression Results

As Figure 5 shows, the block would sometimes exhibit a semi-conical break with the block yielding and leaving the mortar joint intact. Other types of fractures that were exhibited included conical, cone, shear, split, face shell separation, and multiple combinations, as shown in Figure 6.

Conclusions

Results from the strength performance tests indicated that recycled brick aggregate and manufacturing waste would be a suitable substitute for the standard C-144 masonry sand. Specifically:

- Cube testing indicated that the demolition brick sand was 169% stronger than the natural, masonry sand, while the brick manufacturing waste was 137% stronger than the natural, masonry sand.
- Prism testing indicated that demolition brick sand was 105% stronger than the natural, masonry sand, while the brick manufacturing waste was weaker than the standard masonry sand at only 83% of the sand's strength.

Figure 5. Example Break with Exposed Mortar Joint – Adjacent Faces

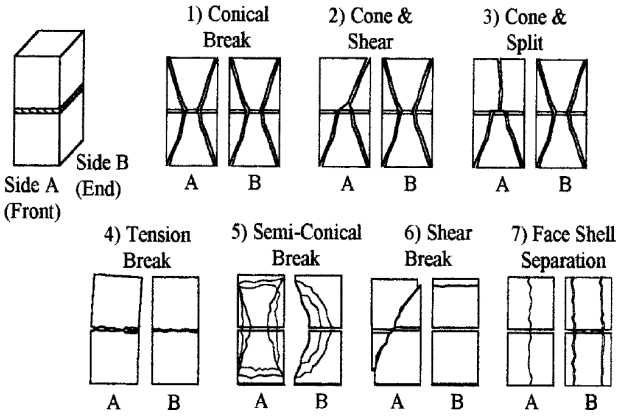

Figure 6. Failure Modes from ASTM C1314-12 [9]

The differences between the test data provided by the cubes and the data provided by the prisms could be explained by several reasons. One reason could be a high variability in the compressive performance of the lightweight concrete masonry units used; more tests should be carried out to attempt to separate the variability of the block from actual differences in mortar strengths. Another reason could be a difference in bond strength between the mortar joint and the concrete masonry units that make up the test prism. During the early stages of testing, there was a lack of bond strength between the mortar and the recycled aggregate. This was mediated by:

- Sieving out the #4 and #8 materials from the samples before creating cubes or prisms;
- Using a capping plate with a finer surface finish to minimize friction between the cap and the plate; and,
- Extending the cure time from seven days to 28 days to ensure full-strength development.

Sieving out the #4 and #8 materials from the crushed brick aggregates served two purposes: It improved the bond strength between the concrete masonry units and the mortar joint, and it improved the workability of the material. The improvement of the capping plate decreased the amount of force it took to get the specimen out of the capping apparatus. This greatly reduced the risk of cracking or damaging the prisms during this process. Lastly, extending the cure time to 28 days improved the quality of the data retrieved by letting the strength of the mortar-block interface and the overall compressive strength of the mortar develop.

Due to the inability of the recycled materials to provide satisfactory cubes using the standard brass molds used in ASTM C109-12, a modified method for creating test cubes was developed. The modified cube process closely followed the established process of creating grout specimens, where stacked block formed cube mold which served as porous media to mimic the moisture absorption found in the prisms. While strength testing shows promising results, further testing beyond strength performance is required to validate these materials as viable substitutions in the building industry. Future efforts should include resistance to freeze/thaw, shear and tensile strength, and thermal performance of the recycled brick aggregates.

References

[1] Cavalline, T. L., & Weggel, D. C. (2013). Recycled Brick Masonry Aggregate Concrete. *Structural Survey, 31*(3), 160-180.

[2] Rahal, K. (2007). Mechanical Properties of Concrete with Recycled Coarse Aggregates. *Building and Environment, 42*(1), 407-415.

[3] Etxeberria, M., Marí, A. R., & Vázquez, E. (2007). Recycled Aggregate Concrete as Structural Material. *Materials and Structures, 40*(5), 529-541.

[4] Xiao, J., Li, J., & Zhang, C. (2005). Mechanical Properties of Recycled Aggregate Concrete under Uniaxial Loading. *Cement and Concrete Research, 35*(6), 1187-1194.

[5] Wang, R., & Meyer, C. (2012). Performance of Cement Mortar Made with Recycled High Impact Polystyrene. *Cement Concrete Composites, 34*(9), 975-981.

[6] Al-Sibahy, A., & Edwards, R. (2012). Mechanical and Thermal Properties of Novel Lightweight Concrete Mixtures Containing Recycled Glass and Metakaolin. *Construction Building Materials, 31*, 157-167.

[7] Meshgin, P., Xi, Y., & Li, Y. (2012). Utilization of Phase Change Materials and Rubber Particles to Improve Thermal and Mechanical Properties of Mortar. *Construction and Building Materials, 28*(1), 713-721.

[8] Debieb, F., & Kenai, S. (2008). The Use of Coarse and Fine Crushed Bricks as Aggregate in Concrete. *Construction and Building Materials, 22*(5), 886-893.

[9] ASTM International. (2012). *Standard Test Method for Compressive Strength of Masonry Prisms* (ASTM Standard C1314). West Conshohocken, PA. doi: 10.1520/C1314-12

[10] ASTM International. (2012). *Standard Practice for Capping Concrete Masonry Units, Related Units and Masonry Prisms for Compressive Testing* (ASTM Standard C1552). West Conshohocken, PA. doi: 10.1520/C1552-12

[11] ASTM International. (2012). *Standard Test Method for Compressive Strength of Hydraulic Cement Mortars* (ASTM Standard C109). West Conshohocken, PA. doi: 10.1520/C109-12

[12] ASTM International. (2013). *Standard Test Method for Sampling and Testing Grout* (ASTM Standard C1019). West Conshohocken, PA. doi: 10.1520/C1019-13

Biographies

THOMAS NICHOLAS II, Ph.D., P.E., is an Assistant Professor of Civil Engineering Technology and Construction Management at UNC Charlotte. Dr. Nicholas holds graduate degrees from West Virginia University (M.S.C.E) and UNC Charlotte (Ph.D.) and is a registered Professional Engineer in North Carolina. Dr. Nicholas may be reached at tnichola@uncc.edu

PAUL D. RADFORD is currently a graduate student in the Electromechanical and Energy Systems program at

UNC Charlotte. He holds an undergraduate degree in Mechanical Engineering Technology from UNC Charlotte. Mr. Radford may be reached at pradford@uncc.edu

TARA L. CAVALLINE, Ph.D., P.E., Co-PI, is an Assistant Professor of Civil Engineering Technology at UNC Charlotte. She holds B.S. and M.S. degrees in Civil Engineering from the Pennsylvania State University and a Ph.D. in Infrastructure and Environmental Systems from UNC Charlotte. Dr. Cavalline may be reached at tcavalline@uncc.edu

ANTHONY L. BRIZENDINE, Ph.D., is chair and Professor of Engineering Technology and Construction Management at UNC Charlotte, a position he has held since 2002. Dr. Brizendine holds graduate degrees from West Virginia University (Ph.D.) and Virginia Tech (M.S.), and is a registered professional engineer. Dr. Brizendine may be reached at albrizen@uncc.edu

EVALUATION OF INITIAL IRI VALUES AS ACCEPTANCE CRITERIA FOR FLEXIBLE PAVEMENTS

Don Chen, University of North Carolina at Charlotte; Michael Dye, University of North Carolina at Charlotte

Abstract

Smoothness of pavements has been used for construction acceptance and pay adjustment by many state highway agencies. Currently, the international roughness index (IRI) has become the most widely accepted standard for evaluating pavement smoothness. To establish acceptance criteria for a pavement, its initial IRI values (the IRI rating occurs right after the pavement is constructed) need to be determined and provided to contractors as a quality assurance measure. The determination of initial IRI values for various pavement types is a challenging task. This is mainly due to the variations in pavement data collected across localities and the limited availability of pavement design and simulation tools. In this paper, the authors present a method for addressing this issue. Flexible pavement terminal IRI values were simulated using AASHTOWare Pavement ME Design, the new AASHTO (American Association of State Highway and Transportation Officials) design software. Then, statistical analyses were conducted in order to derive initial IRI values. Once implemented, this method can be adopted by highway agencies to establish new acceptance criteria for different types of pavements.

Introduction

The ride quality of roadway pavement is extremely important to roadway users [1]. The roughness of the road has been known to reduce satisfaction of the roadway pavement, prove uneconomical to the roadway users, as well as reduce the safety of the travelers [2]. Therefore, setting required smoothness levels, especially the initial smoothness level when the roadway pavement is constructed, increases the chance of improving traveler satisfaction and safety, and saving the roadway users money.

Realizing the importance of the smoothness of pavements, many state agencies have made a large push to adopt quality control/quality assurance (QC/QA) specification programs for pavements in their states. This is done to ensure that roadway pavements are meeting desired performance and to promote better construction of the roadway pavement. This often results in the reduced variability of the asphalt mixtures and can be linked to longer lasting roadway pavements [3].

The construction QC/QAs are known as end-result specifications that specify the standards that the contractor is required to meet or exceed, when supplying or producing a product during the construction of the roadway pavements. These specifications explicitly define what materials, proportions, installation methods, and equipment can be used by the contractor during construction. Once the contractor has built a roadway, it is the state agency's responsibility to accept or reject the roadway as well as attach a price to the completed work, adjusted by adherence to required specifications. Generally, the state highway agency will prescribe the specifications and will accept the finished product, while the contractor is responsible for the quality control process [3].

QC/QAs are excellent tools for verifying that roadway pavement specifications have been met by the contractor and are becoming a practice worldwide. Several QC/QA measurements exist that help state agencies determine if the specifications have been met. The international roughness index (IRI) is the most practiced. IRI was developed as a way for highway agencies to quantify the smoothness of roadway pavements. It is calculated by using mathematical models that accumulate the output of a quarter-car model and dividing by the profile length [2]. IRI values are traditionally expressed in inch/miles in the U.S. and in mm/km in most other countries. They can be used as measurements for accepting or rejecting the roadway pavements as early as seven days after being paved [4]. The concept of IRI was developed in 1982 under the sponsorship of the World Bank. IRI replaced the profile ride index in 1998, so the same specifications would apply to concrete and asphalt [5]. The Federal Highway Administration (FHWA) later adopted the use of IRI for the highway pavement monitoring system [2]. IRI has become a well-recognized tool and standard of measurement for evaluating pavement ride quality [6] and, therefore, was used as the smoothness measurement in this study.

A pavement's IRI can be measured during its service life. However, the initial smoothness (the smoothness right after the pavement is constructed) is the most important QC/QA criterion. It reflects the quality of construction and is an essential condition for the roadway pavements future performance [5]. Several factors can affect a pavement's initial smoothness. Studies have found a wide amount of variation within pavement material properties and within a pave-

ment's base/sub-base support characteristics. Only a small portion of this variation can be attributed to natural aging and environmental effects. The remaining variance in the pavement material properties occurs during construction [7]. A poor initial smoothness rating can cause the newly constructed roadway pavement to fail QC/QA testing and have a shorter service life [8].

Initial IRI values have been used by state agencies to ensure that roadway pavement is meeting design specifications and is meeting the acceptance and payment qualification of roadway construction. Also, contractors have used the initial IRI value as a target to identify and address process control issues quickly and cost effectively [9]. Initial IRI values have been used internationally for QC/QA purposes as well. Currently, the Australian State Road Authorities are using this practice [10]. The New England State Highway Agency offers an incentive for contractors that meet their quality standards and a penalty for roadway pavements that do not meet their quality standards [11].

The objective of this study was to determine initial IRI values as acceptance criteria for various pavement classifications. This is a challenging task, mainly due to the variations in pavement data collected across localities. To address this challenge, initial and terminal IRI values for flexible pavements was studied through design simulations using the AASHTOWare Pavement ME Design software. AASHTOWare Pavement ME Design is the newer version of the AASHTO (American Association of State Highway and Transportation Officials) pavement design software. The implementation of this concept would allow state agencies to use predetermined initial IRI values as the acceptance criteria for pavements.

Research Methodology

Work Flow

The determination of initial IRI values involved the following three steps:

Step One: Design simulations using the AASHTOWare Pavement ME Design software. In this step, three different initial IRI values (40 in./mi., 50 in./mi., and 60 in./mi.), nine different subgrade types as specified by AASHTO (A-1-a, A-1-b, A-2-4, A-2-5, A-2-6, A-2-7, A-3, A-4, and A-5) [12], a sub-base of 8" of lime, a base of 8" of crushed stone, a sub-surface of 4" of asphalt, and a surface of 3" of asphalt, the North Carolina Charlotte International Airport weather station, and default traffic volumes were used to run design simulations. The target reliability was set to 95%, which is the default value used by the AASHTO design guide [12]. The design life was set to 20 years. A total of 26 predicted terminal IRI values and their corresponding predicted reliabilities were obtained.

Step Two: Statistical analyses using the statistical discovery software JMP. Two regression analyses were conducted. The first was to derive the relationship between predicted terminal IRI reliabilities and initial IRI values as well as types of subgrade, and the second was to derive the relationship between predicted terminal IRI values and initial IRI values as well as types of subgrade.

Step Three: Determination of initial IRI values using the risk analysis tool @Risk. Using the first regression equation obtained in Step Two, and setting the goal of predicted terminal IRI reliability to 95%, the goal-seeking function of @Risk was used to determine initial IRI values for different types of subgrade. Then, the corresponding terminal IRI values, which can be used to valid reasonableness of initial IRI values, were calculated using the second regression equation. Figure 1 is an illustration of the research methodology.

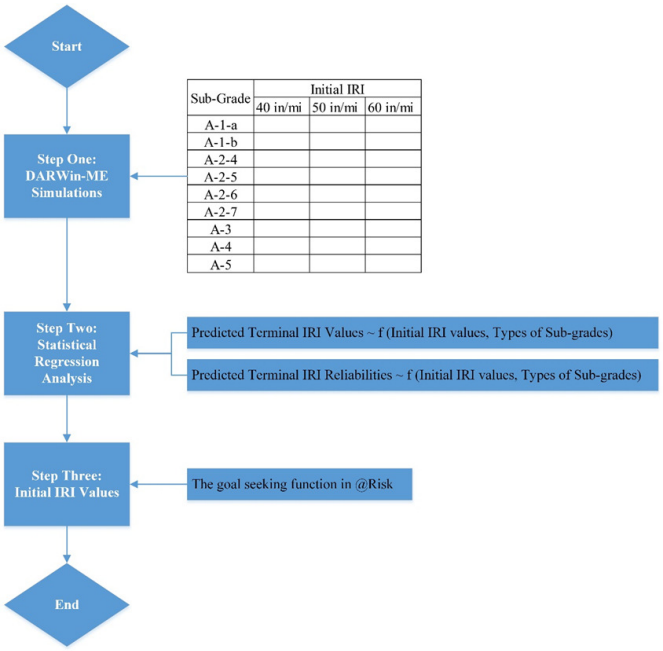

Figure 1. Flowchart of the Research Methodology

Scope of Work

A number of factors can affect a pavement's initial smoothness: the pavement's base/sub-base support characteristics, the pavement's functional classification, material

properties, traffic volume, and climatic conditions. This study selected subgrade as the impact factor because it represents a pavement's support characteristics, and a weak road-bed support can cause poor initial smoothness. Also, flexible pavements were studied in this research. However, these do not impose a limitation on the type of impact factors and pavements that could be used. Instead, the proposed methodology is flexible enough to be applied to other factors, such as those mentioned earlier, as well as rigid and composite pavements.

Data Set

Simulation results are given in Table 1, including the initial IRI values, types of subgrade, and the corresponding terminal reliability and IRI values. A total of 26 observations were obtained. Note that there are missing data, due to an error during the reporting process.

Variables

As described in Step Two, two regression analyses were conducted. In the first analysis, the dependent variable was the predicted terminal IRI reliabilities, while the independent variables were initial IRI values and types of subgrade. In the second regression analysis, the dependent variable was the predicted terminal IRI values, while the independent variables were initial IRI values and types of subgrade.

Results and Discussion

Regression Analysis: Predicted Terminal IRI Reliabilities versus Initial IRI Values and Types of Subgrade

In Figure 2, the y axis (terminal reliability actual) represents the simulation results (see also column 3 in Table 1); the x axis (terminal reliability predicted) represents the reliability values predicted by the regression equation. Figure 2 shows that the majority of the predicted reliability values fall within the bounds of the 95% confidence curves (red-dotted lines). This indicates that the model is significant. Figure 3 shows residual values scattered approximately randomly about zero, which means that the model form is appropriate. Table 2 shows results of effect tests on the null hypothesis, where all parameters associated with the initial IRI values and subgrade types were zero. The effect of initial IRI was statistically significant. In Table 3, an R-square of 0.780 indicates that 78% of the variation in terminal IRI reliabilities can be explained by initial IRI values and subgrade types, which is statistically significant. A p-value of 0.0007 in Table 4 rejects the null hypothesis, indicating that the differences observed in terminal IRI reliabilities are not due to random sampling but rather to different initial IRI values and different types of subgrade, and that the actual strength of the relationship is strong. In this analysis, since there were 10 independent variables (nine different types of subgrade and initial IRI values), there were nine degrees of freedom (see Table 4).

Table 1. AASHTOW Pavement ME Design Simulation Results

Initial IRI (in/mi)	Subgrade	Terminal Reliability (%)	Terminal IRI (in/mi)
40	A-1-a	99.65	133.15
40	A-1-b	99.60	134.04
40	A-2-4	99.41	137.02
40	A-2-5	99.26	138.89
40	A-2-6	99.07	140.92
40	A-2-7	98.98	141.68
40	A-3	99.70	131.96
40	A-4	98.85	142.82
40	A-5	97.52	151.04
50	A-1-a	98.35	146.43
50	A-1-b	99.60	134.04
50	A-2-4	99.41	137.02
50	A-2-5	99.26	138.89
50	A-2-6	99.07	140.92
50	A-2-7	98.98	141.68
50	A-3	99.70	131.96
50	A-4	91.59	168.73
50	A-5	97.52	151.04
60	A-1-a	95.24	159.46
60	A-1-b	94.95	160.31
60	A-2-4	95.74	157.79
60	A-2-5	93.22	164.95
60	A-2-6	92.41	179.15
60	A-2-7		
60	A-3	95.60	158.32
60	A-4	91.59	168.73
60	A-5	92.08	167.63

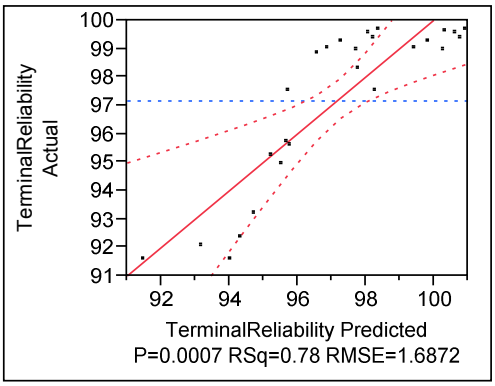

Figure 2. Actual Terminal IRI Reliabilities versus Predicted Terminal IRI Reliabilities

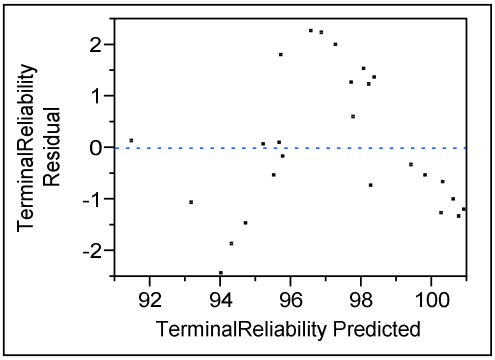

Figure 3. Residual Plot for Terminal IRI Reliabilities

Table 2. Effect Tests

Source	DF	Sum of Squares	F Ratio	Prob > F
Initial IRI	1	108.08321	37.9683	< 0.0001
Subgrade	8	45.46039	2.084	0.1006

Table 3. Regression Analysis Summary of Fit

RSquare	0.780
RSquare Adj	0.657
Root Mean Square Error	1.687
Mean of Response	97.167
Observations	26

Table 4. Analysis of Variance

Source	DF	Sum of Squares	Mean Square	F Ratio	Prob > F
Model	9	161.823	17.980	6.316	0.0007
Error	16	45.547	2.847		
C. Total	25	207.369			

The prediction expression is given in Equation (1):

$$\begin{aligned}\text{Terminal IRI Reliability} = {} & 109.889 - \\ & 0.256*\text{InitialIRI} + \\ & 0.654*\{\text{Subgrade[A-1-a]}\} + \\ & 0.958*\{\text{Subgrade[A-1-b]}\} + \\ & 1.094*\{\text{Subgrade[A-2-4]}\} + \\ & 0.154*\{\text{Subgrade[A-2-5]}\} - \\ & 0.242*\{\text{Subgrade[A-2-6]}\} + \\ & 0.608*\{\text{Subgrade[A-2-7]}\} + \\ & 1.241*\{\text{Subgrade[A-3]}\} - \\ & 3.082*\{\text{Subgrade[A-4]}\}\end{aligned} \quad (1)$$

To understand how to use Equation (1), consider the following example. For subgrade A-1-a, {Subgrade[A-1-a]} = 1, while the rest of the indicator variables are 0. Thus, its terminal IRI reliability can be written as:

Terminal IRI = 109.889 – 0.256*InitialIRI + 0.654 = 110.543 - 0.256*InitialIRI

Similarly, for subgrade A-2-4, its terminal IRI reliability can be written as:

Terminal IRI = 109.889 – 0.256*InitialIRI + 1.094 = 110.983 – 0.256*InitialIRI

In this multiple regression analysis, the coefficient of initial IRI is a constant, and the intercept varies based on the subgrade type.

Regression Analysis: Predicted Terminal IRI Values versus Initial IRI Values and Types of Subgrade

Figures 4 and 5 show the results of the statistical analyses. In Figure 4, the "terminal IRI actual" values are the simulation results (see column 4 in Table 1). Figure 4 shows that the majority of the predicted IRI values fall in the bounds of the 95% confidence curves (red-dotted lines). This indicates that the model was significant. The "terminal IRI predicted" values of Figure 5 are the IRI values predicted by the regression equation. Figure 5 shows the residual values scattered randomly about zero, which means that the model form was appropriate. Table 5 also shows results of the effect tests on the null hypothesis, where all of the parameters associated with the initial IRI values and subgrade types were zero. The effect of the initial IRI values was statistically significant. In Table 6, an R-square of 0.783 indicates that 78.3% of the variation in terminal IRI values can be explained by initial IRI values and subgrade types, which was statistically significant. A p-value of 0.0007 in Table 4 rejects the null hypothesis, indicating that the differences observed in terminal IRI values were not due to random

sampling, but due to different initial IRI values and different types of subgrade; also shown is the fact that the actual strength of the relationship was strong.

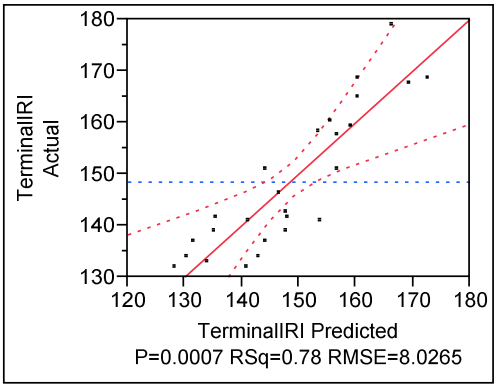

Figure 4. Actual Terminal IRI Values versus Predicted Terminal IRI Values

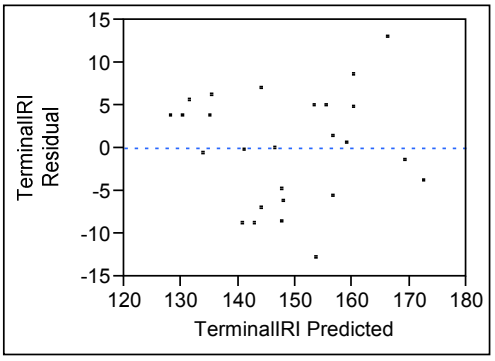

Figure 5. Residual Plot for Terminal IRI Values

Table 5. Effect Tests

Source	DF	Sum of Squares	F Ratio	Prob > F
Initial IRI	1	2584.3788	40.1151	< 0.0001
Sub-grade	8	1031.9227	2.0022	0.1129

Table 6. Regression Analysis Summary of Fit

RSquare	0.783
RSquare Adj	0.660
Root Mean Square Error	8.026
Mean of Response	148.407
Observations	26

Table 7. Analysis of Variance

Source	DF	Sum of Squares	Mean Square	F Ratio	Prob > F
Model	9	3712.432	412.492	6.403	0.0007
Error	16	1030.785	64.424		
C. Total	25	4743.217			

The prediction expression is given in Equation (2):

Terminal IRI = 86.277 +
1.252*InitialIRI –
2.506*{Subgrade[A-1-a]} –
6.056*{Subgrade[A-1-b]} –
4.909*{Subgrade[A-2-4]} – (2)
1.276*{Subgrade[A-2-5]} +
4.811*{Subgrade[A-2-6]} –
0.915*{Subgrade[A-2-7]} –
8.106*{Subgrade[A-3]} +
11.241*{Subgrade[A-4]}

At 95% terminal IRI reliability, initial IRI values and terminal IRI values for nine different types of subgrades were calculated using Equations (1) and (2) and the goal-seeking function of the @Risk program. The results are summarized in Table 8.

Table 8. Initial and Terminal IRI Values for 95% Terminal Reliability

	Initial IRI values (in/mi)	Terminal IRI values (in/mi)
Subgrade [A-1-a]	63	163
Subgrade [A-1-b]	63	159
Subgrade [A-2-4]	63	160
Subgrade [A-2-5]	57	156
Subgrade [A-2-6]	55	160
Subgrade [A-2-7]	63	164
Subgrade [A-3]	63	157
Subgrade [A-4]	49	158
Average	60	160

Discussion

In 2013, a study [13] was conducted to evaluate public perception of the smoothness of pavements in North Carolina. The results indicated that an IRI rating of 156 in/mi was

the threshold for driving public rate roadway ride quality as either acceptable or unacceptable. The average terminal IRI value obtained from this study was 160 in/mi (see Table 8), which was fairly close to this threshold. Therefore, it could be concluded that the results from this study were reasonable. The results in Table 8 also indicate that, for a pavement that is located in Charlotte, North Carolina, designed to have a sub-base of 8" of lime, a base of 8" of crushed stone, a sub-surface of 4" of asphalt, and a surface of 3" of asphalt, while carrying typical traffic volumes, and has one of nine subgrade types, its average initial IRI value should be 60 in/mi.

In this study, three initial IRI values and nine types of subgrade were considered in the statistical analyses. However, the same methodology could easily be applied to pavements having different designs including more initial IRI value variables; various thicknesses and materials of sub-base, base, sub-surface, and surface; differing weather stations and traffic volumes; and, different types of pavements such as rigid and composite.

Conclusions and Recommendations

Previous research indicated that three factors affect pavement roughness: the environment, material behavior, and traffic volume [14]. However, there has been limited research that includes all this data in computer-simulated models. This current study was conducted in order to bridge this gap in knowledge. Initial IRI values for different flexible pavement designs were derived as acceptance criteria using AASHTOWare Pavement ME Design simulations. The results were validated and found to be robust. The contributions of this study are twofold: developing IRI acceptance values for new roadway pavement using simulated models would allow state highway administrations (SHAs) to have a QC/QA based on initial IRI values; and, this also would provide contractors with a way of evaluating their work before presenting their completed projects to the SHAs. Once implemented, the proposed methodology could be applied to rigid and composite pavements having different designs.

For future studies, it is recommended that sensitivity analyses be conducted in order to identify the most important factors among pavement materials, thicknesses, weather stations, and traffic volumes that impact terminal IRI values and reliabilities, and to use model-selection techniques (stepwise, forward, or backward) to develop the final, optimum models.

References

[1] Kohn, S. D., Perera, R. W., Cable, J. K., Karamihas, S. M., & Swanlund, M. (2008). Use of Profile Data to Detect Concrete Paving Problems. *9th International Conference on Concrete Pavements: The Golden Gate to Tomorrow's Concrete Pavements*, (pp. 690-703).

[2] Titi, H. H., & Rasoulian, M. (2008). Evaluation of Smoothness of Louisiana Pavements Based on International Roughness Index and Ride Number. *Jordan Journal of Civil Engineering*, *2*(3), 238-249.

[3] Butts, N. E., & Ksaibati, K. (2003). Asphalt Pavement Quality Control/Quality Assurance Programs in the United States. *Annual Meeting of the Transportation Research Board.*

[4] Stroup-Gardiner, M., Carter, A., Das, T., & Bowman, B. (2005). Part 5: Hot-Mix Asphalt Pavement: Initial Ride Quality of Hot-Mix Asphalt Pavements. *Transportation Research Record*, *1907*(1), 105-112. doi: 10.3141/1907-12.

[5] Thebeau, D., Delisle, M.-C., & Cormier, B. (2005). Quebec's Experience with Smoothness Specifications on Concrete Pavements. *Eight International Conference on Concrete Pavements*, (pp. 718-732). Colorado Springs, CO.

[6] Li, N., Qin, R., & Liu, Z. (2013). Performance Measures and Evaluation of Asphalt Pavements Using the International Roughness Index. *First International Symposium on Pavement and Geotechnical Engineering for Transportation Infrastructure*, (pp. 19-30). doi: 10.1061/9780784412817.002 .

[7] Chatti, K., Manik, A., & Imen, Z. (2011). *Assessment of Pavement Acceptance Criteria and Quantifying its As-Constructed Material and Structural Properties*. (RC-1540). Lansing, MI: Michigan Department of Transportation.

[8] Corley-Lay, J., & Mastin, J. N. (2009*).* Evaluation of Long-Term Pavement Performance Profile Data for Flexible Pavements. *Transportation Research Record: Journal of the Transportation Research Board, 2093*(1), 25-30.

[9] Hand, A., Mondal, A., & Ward, D. (2001). A Performance Evaluation of Lightweight Non-Contact Pavement Profilers. *Journal of Testing and Evaluation*, *29* (2), 161-172.

[10] Wix, R. (2003). Ride Quality Specifications—Smoothing Out Pavements. *Proceedings of the 21st AARB and 11th REAAA Conference. Transport. Our Highway to a Sustainable Future*, (pp. 549-565).

[11] El-Korchi, T., & Collura, J. (1998). A Comparative Study of Ride Quality Measuring Devices. *Transportation Research Record*, *1643*, 125-135.

[12] AASHTO. (2008). *Mechanistic-Empirical Pavement Design Guide, Interim Edition: A Manual of Practice*. Washington, D.C.: AASHTO.
[13] Chen, D., Hildreth, J., & Nicholas, T. (2014). *Development of IRI Limits and Targets for Network Management and Construction Approval Purposes*. Research project funded through the North Carolina Department of Transportation (final report).
[14] Chen, I.-C., & Chou, K.-J. (2009). A Study on the Incentive/Disincentive Schemes of Expressway Pavement Smoothness. *Journal of the Chinese Institute of Civil & Hydraulic Engineering*, *21*(2), 137-153.

Biographies

DON CHEN is currently an Assistant Professor in the Department of Engineering Technology and Construction Management at the University of North Carolina at Charlotte (UNC Charlotte). He has extensive experience in pavement management systems and over 22 years of experience as an engineer, researcher, and educator. He has been a LEED AP since 2009. Dr. Chen may be reached at dchen9@uncc.edu

MICHAEL DYE is currently an M.S. student in construction and facilities management in the Department of Engineering Technology and Construction Management at UNC Charlotte. He earned his B.S. degree from UNC Charlotte. Michael is currently working on two research projects under Dr. Chen's supervision. One of the projects is to develop IRI limits and targets for network management and construction approval purposes. Michael may be reached at mdye2@uncc.edu

VALIDATING THE USE OF TEACHING EFFECTIVENESS DATA IN THE IMPROVEMENT OF TEACHING

Jess Godbey, Jacksonville State University; Terry Marbut, Jacksonville State University

Abstract

Using data as a catalyst for initiating changes that can improve program performance is critical in any effective assessment strategy. Successful assessment programs typically measure performance and implement improvement strategies in the identified areas of student learning, student services, and, to an increasing degree, teacher effectiveness. The U.S. Department of Education's Educational Resources Information Center system cites more than 2000 articles on research that focus on student evaluations. Assuming that the primary goal of such instruments is to actually improve teaching effectiveness, the authors in this current study explored one department's use of statistical analyses in the assessment of faculty teaching ratings from graduating seniors in applied engineering and technology programs. This information was used by the department chair to develop appropriate professional development activities and provide performance feedback to individual faculty members.

Introduction

Successful academic programs must include performance assessments to ensure the implementation of program improvements. In spite of the long-running debate over their usefulness, student evaluation of teaching (SET) has long been a major component in most assessment strategies involving teaching effectiveness [1]. Seldin [2] noted that colleges and universities were moving to concerted and sustained efforts to improve teaching in programs. Since most academic accreditation standards require both student evaluation of the program and application of improvement strategies for teaching effectiveness, continual improvements related to these areas continue to be important to institutions of higher learning. Halloran [3] even pointed out that governments in some countries demand that universities be judged on their performance in teaching to meet both regulatory and funding requirements.

The existing research regarding issues that impact teaching effectiveness is extensive. One such issue is faculty recognizing the need for improvement. Blackburn et al. [4] found in interviews with almost 300 college teachers, that 92% of the teachers believed that their own teaching was above average. It may be that, within a department, faculty members hold these same beliefs and do not actively engage in efforts to improve their teaching effectiveness. While it might be argued that these faculty members could indeed be above average, when compared with all college teachers or with the institutional average, it is a fact that within a given department all cannot be above average.

Another issue is the relationship between teaching styles and learning styles. There is ample research that suggests that students learn best when they are taught in ways that match their style of learning [5-8]. There is also significant research that reveals no such correlation [9-11]. Some of this research suggests that the best correlation is actually between content and teaching style and contends that students learn given content better through a particular teaching style, even if the style does not match the students' preferences [11]. Rinaldi and Gurung [10] suggested that including various teaching styles in a course should provide all students with something that best matches their learning preferences and increase the students' engagement, thereby enhancing learning and student satisfaction.

While this project does not attempt to further investigate any of the noted research, the project was based on the realization that there are very likely faculty members in a given technology and engineering department that utilize more effective teaching styles than others in the same department. Faculty members' ratings on senior surveys were statistically compared in order to identify any such faculty members with the intent of developing improvement strategies to enhance student learning within this particular technology and engineering department.

Survey Description

The graduating senior survey was strongly encouraged, but not mandatory for graduation. The actual response rate was above 90%. The rating scale for the teaching effectiveness of a faculty member ranged from A (excellent) to D (very poor). There was also an E rating (no opinion) if the student did not have the faculty member as an instructor. In order to compare the mean rating of each faculty member, points of 4, 3, 2, and 1 were assigned for answers A through D, respectively. The rating of E, no opinion, was considered a non-rating and was not counted. Since an ordinal rating scale was used, the distinction must be made that the subjects taking the survey may not have felt that the difference between each step was equal. An A rating may have been

considered twice as good as a B rating to some subjects but only marginally better to others. For purposes of this comparison, it was assumed that each step in the ratings scale was equal.

Statistical Analyses

Minitab was selected as the software package for data analysis. An analysis of variance (ANOVA) was used to determine if there was a statistically significant difference in the average ratings of the faculty members. T tests were utilized to compare faculty members' older ratings to their newer ratings to determine if differences over time were significant. Finally, the variances in ratings for faculty members were compared.

Comparison of Mean Scores and Analysis of Variation

To determine if any faculty member had a significantly higher rating than any of the other faculty members, a one-way analysis of variance (ANOVA) was performed. Groupings were made using the Tukey method with a 95% simultaneous confidence interval. Results of this analysis are presented in Table 1, which shows the means and grouping by faculty member. The listed means of faculty members that do not share a letter were significantly different.

Based on these Tukey groupings, faculty members 3 and 7 belonged to group A and were not significantly different. Faculty members 1 and 7 belong to group B and were not significantly different; but, faculty members 1 and 3 were significantly different. The rest of the faculty members, 2, 4, 5, and 6, all belonged to group C and were not significantly different from each other but were significantly different from 1, 3, and 7.

Table 1. Grouping Information using Tukey Method

Faculty	N	Mean	Grouping
3	189	3.7460	A
7	167	3.6886	A B
1	144	3.5139	B
5	133	3.2105	C
4	105	3.2000	C
2	185	3.1838	C
6	66	3.0909	C

The next statistical test that was performed compared the variation associated with each faculty member's student ratings. A standard deviation test was performed to identify significant differences. The results of the test are given in Tables 2 and 3. Analysis of standard deviations for faculty members revealed that faculty member 3 had the lowest variation in student scores and faculty members 2 and 6 seemed to have more variation than most of the others. The standard deviations of faculty members 2 and 6 were significantly higher than the standard deviation of faculty member 3.

Hypothesis Tests: Comparing Past and Present Effectiveness

The final tests were designed to determine if faculty member ratings were different now in comparison with ratings from earlier years. Two-Sample T-Tests were conducted for each faculty member comparing the last two years of ratings with their earliest two years of ratings in the sample. The number of years between present and earliest ratings

Table 2. Faculty Rating Variation

Standard Deviations Test for Faculty 1, Faculty 2, Faculty 3, Faculty 4….. Descriptive Statistics Report				
Statistics				
Sample	Sample Size	Mean	Standard Dev	Ind 95% CI
Faculty 1	117	3.4957	0.63821	(0.56341,0.73526)
Faculty 2	130	3.0615	0.85139	(0.76905,0.95698)
Faculty 3	134	3.7164	0.52904	(0.44057,0.64470)
Faculty 4	76	3.2895	0.74504	(0.63830,0.89265)
Faculty 5	97	3.2680	0.66951	(0.60149,0.76059)
Faculty 6	66	3.0909	0.85444	(0.72882,1.0324)
Faculty 7	123	3.6341	0.59047	(0.48154,0.73578)

varied depending on an individual faculty member's years of service. The hypothesis tested for each faculty member was that the rating means for past and present were equal. The tests were all performed at the alpha equal to the 0.05 level. These tests revealed that most faculty members had lower ratings in recent years as compared to earlier ratings. However, rating means for faculty members 4, 5, and 6 over the last two years were not statistically different than their earliest rating means. The other faculty members did have different rating means for the two time periods and all appeared to be somewhat lower.

Table 3. Summary Report of Faculty Rating Variation Significance

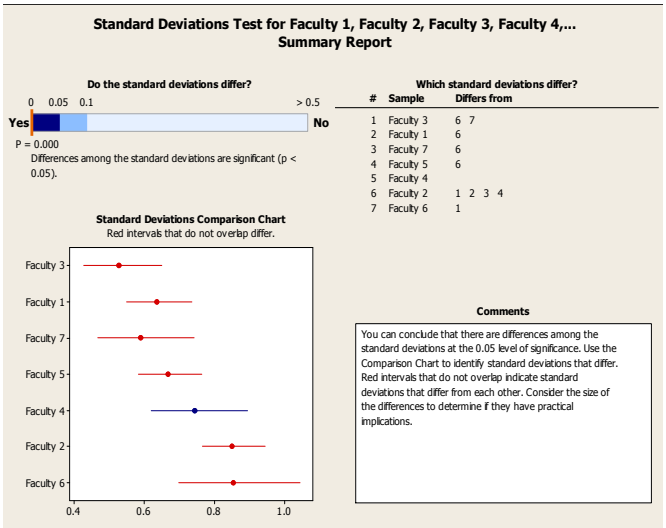

Summary of Statistical Analyses

One faculty member had a mean rating that was significantly ($\alpha = .05$) higher than those of all other faculty members and the smallest variation in rankings. Comparisons of most recent ratings with ratings from earlier years generally revealed that the ratings had decreased over time, but that the decrease was not statistically significant for most faculty members.

Use of Findings

The data clearly indicated that one faculty member received higher ratings from students than other faculty members in the Department of Technology and Engineering. A check of grading patterns for this faculty member revealed that the grades students received were no better than grades received from other faculty members within the department. This fact negates any tendency to suggest that the higher ratings might be the result of easier grading. Upon extensive review, after analysis of the data, it was apparent that the highest-rated faculty member incorporated teaching strategies that related well to departmental students. The consistency of this faculty member's ratings (small standard deviation) was especially intriguing. With the idea that this highly rated faculty member might be able to share some insight with the other members of the department, the department head asked this faculty member to develop and deliver a "Best Practices in Teaching" seminar for the department. The faculty member developed and delivered the seminar and feedback was solicited from faculty members to assess its usefulness. The seminar centered around three key points: course structure and organization, feedback to students, and real-world application.

The second significant discovery was that the scores for the highest-rated faculty members had decreased slightly over a period of years. Each of these faculty members was made aware of these findings and asked to examine their practices to determine if some change in their approach to teaching may be contributing to the lower ratings. During these discussions, it was noted that the student population had changed significantly from non-traditional, older working students to traditional-age college students during this time period. This may be a contributing factor explaining, at least in part, these slight decreases in faculty ratings. Faculty members were encouraged to include teaching methodologies that match the learning styles of these younger students. As a result, the department acquired 25 iPads that were provided to students for portions of selected classes to increase their engagement as active learners.

The third finding was that the scores for the lowest-rated faculty members were not changing significantly up or down. These faculty members were made aware of the findings by the department head to encourage them to explore ways to improve teaching effectiveness, including implementation of methods discussed in the previously mentioned teaching seminar. The department head also reminded faculty members that excellence in teaching is a major criterion for success in a regional institution.

Feedback from Faculty Members

A short survey was administered to all faculty members following the seminar to help assess the effectiveness of the professional development opportunity. Some questions were designed to gather information about the overall effectiveness of the information presented, the format of the seminar, and the time allotted for discussion. One question asked whether faculty members were likely to incorporate an idea presented in the seminar into a class. Survey results were encouraging. All faculty members agreed, and the majority

strongly agreed, that the seminar should be helpful in improving teaching effectiveness and that they were likely to incorporate at least one idea from the seminar into a class that they teach.

Conclusions

Preliminary results from the project indicated that systematic review and analysis of available data can be useful in developing effective strategies for improving teaching effectiveness. A longitudinal study will be needed to determine if teaching effectiveness in the department was actually strengthened as a result of this project.

References

[1] Centra, J. A. (1993). *Reflective Faculty Evaluation: Enhancing Teaching and Determining Faculty Effectiveness.* San Francisco: Jossey-Bass.

[2] Seldin, P. (1995). *Improving College Teaching*. Bolton, MA: Anker Publishing Company.

[3] Halloran, P. (2010). Using Case Studies as a Lens to Observe Teaching Evaluations. *Journal of Computing and Information Technology*, *18*, 133-139.

[4] Blackburn, R. T., Bober, A., O'Donnell, C., & Pellino, G. (1980). *Project for Faculty Development Program Education: Final Report.* Ann Arbor, MI: University of Michigan, Center for the Study of Higher Education.

[5] Lovelace, M. K. (2005). Meta-Analysis of Experimental Research Based on the Dunn and Dunn Model. *The Journal of Education Research*, *98*(3), 176-183.

[6] Mahlios, M. C. (2001). Matching Teaching Methods to Learning Styles. In B. H. Stanford & K. Yamamoto (Eds.), *Children and Stress: Understanding and Helping* (pp. 65-73). Olney, MD, US: Association for Childhood Education International.

[7] Ogden, W. R. (2003). Reaching All the Students: The Feedback Lecture. *Journal of Instructional Psychology, 30*(1), 22-27.

[8] Stanberry, A. M., & Azria-Evans, M. (2001). Perspectives in Teaching Gerontology: Matching Strategies with Purpose and Context. *Educational Gerontology*, *27*(8), 639-656.

[9] Garton, B. L., Spain, J. N., Lamberson, W. R., & Spiers, D. E. (1999). Learning Styles, Teaching Performance, and Student Achievement: A Relational Study. *Journal of Agricultural Education*, *40*(3), 11-20.

[10] Rinaldi, C., & Gurung, R. (2008, 26 October). Should Teaching and Learning Styles Match? *Teaching Forum*. Retrieved from http://www.uwosh.edu/programs/ teachingforum/public_html/?module=displaystory&story_id=648&format=html

[11] Pashler, H., McDaniel, M., Rohrer, D., & Bjork, R. (2008). Learning Styles: Concepts and Evidence. *Journal of Psychological Science in the Public Interest*, *9*(3), 105-119.

Biographies

JESS GODBEY is program coordinator of the Occupational Safety and Health Program at Jacksonville State University. He earned a Ph.D. in Industrial and Systems Engineering from Auburn University, and M.S. and B.S. degrees from the University of Michigan. Dr. Godbey also has experience in the automotive industry, working with both Ford Motor Company and General Motors. Dr. Godbey can be reached at jgodbey@jsu.edu

TERRY MARBUT serves as the department head for Technology and Engineering at Jacksonville State University. He earned B.S. and M.S. degrees in Electrical Engineering from the University of Alabama in Birmingham. He has engineering experience working for Goodyear Tire and Rubber Company and has been teaching at Jacksonville State University for the past twenty six years. Mr. Marbut can be reached at tmarbut@jsu.edu

THE EFFECTS OF UNDERGRADUATE PROJECT-BASED COURSES ON STUDENT ATTITUDES TOWARD STEM CLASSES

Mohammadjafar Esmaeili, University of Dayton; Ali Eydgahi, Eastern Michigan University

Abstract

Low student interest in pursuing Science, Technology, Engineering, and Mathematics (STEM) degrees remains as one of the main concerns of American society in this era. Several researchers have stated that introductory college classes in STEM are very theoretical and provide freshman students with limited opportunities to gain hands-on experience. Also, the tedious teaching styles of faculty talking and students listening along with large class sizes have contributed to freshman students becoming demotivated in pursuing STEM-related programs. A number of studies have attempted to measure the success of project-based and active learning methodologies in respect to students' motivation in the classroom environment. However, few studies have examined the impact of such methodologies on students' tendency toward STEM classes. In this study, the authors attempted to examine the effects of using an active learning methodology on students' tendency to enroll in STEM courses. The Technology Acceptance Model (TAM) was utilized to test the effect of active learning-based classes on students' intentions and attitudes toward STEM courses. The effects of external factors such as social influences as well as internal factors such as anxiety and self-efficacy toward STEM courses were also considered. The results of this research showed that the theoretical framework of TAM could be used to predict student intentions toward pursuing and enrolling in more STEM courses.

Introduction

In recent years, the weakening interest of students in enrolling in fields related to Science, Technology, Engineering, and Mathematics (STEM) has been one of the main concerns of academia as STEM classes are becoming less appealing and are losing attraction to students. The traditional lecturing method [1] in which professors talk and students listen has been the dominating method in college and university classrooms. As a result, this tedious teaching style [2-6] has become a demotivating factor for new generations of college students, who are more technology oriented and active in utilizing technology in their daily life styles.

The new college students need to do more than just "sit and listen" to the tedious lectures. They need to be actively involved [1], [2], [7] in instructional activities, be continuously challenged by real-world problems, and work in a team. It has been reported [2], [8-10] that student retention of information is not only gained by verbally or visually receiving it, but also is complemented through a problem-solving process. Several studies [11], [12] have shown that students in project-based courses not only achieve and attain better knowledge but also are more satisfied. Although utilizing active learning methodologies has shown the overall satisfaction of students, there is not enough evidence to show any students' change of attitude toward STEM courses. Several studies [11], [13] have attempted to measure the success of project-based and active learning methodologies and its relation to student motivation; however, a few have considered the impact of such methodologies on increasing students' tendency toward enrolling in STEM classes.

The Technology Acceptance Model (TAM) along with the theory of reasoned action and theory of planned behavior [13] have been widely used in different domains to predict individual intention to adopt or not adopt a specific behavior. The TAM examines human intention toward adaptation of a particular behavior based on individual perception of usefulness and ease of use. In addition, individual behavior is affected by several other external factors such as peers, parents, and media, to name a few. According to TAM, human behavior has a direct relationship to individual motivation and intention that can be modeled by human attitude. Also, human attitude can be modeled by human belief such as perceived usefulness and perceived ease of use.

This current study examined the relationship between an active learning methodology [11] used in one of the freshman classes (ET100: Introduction to Engineering Technology) and the students' tendency to pursue and enroll in further STEM courses. The study utilized TAM as a core model to assess effectiveness of robotic activities as an active learning tool on increasing student intention and attitude toward STEM courses. Moreover, the authors present here the effects of external and internal factors such as social influences, anxiety, and self-efficacy of students toward STEM courses.

Methodology

This study utilized robotic projects [11], [12], [14], [15] as its active learning methodology. The following constructs [15-17] were utilized for measuring the impact of the hands-on projects of the course on the students' tendency to pursue further STEM courses:

1. Behavioral Intention (IN)—the degree to which a person has formulated conscious plans to perform or not perform some specified future behavior.
2. Attitude Behavior (ATT)—general feeling toward performing a certain action.
3. Perceived Usefulness (PU)—the perception of usefulness toward performing an action.
4. Ease of Use (EU)—the perception of how easy it is to perform a specific action.
5. Social Influence (SI)—an external factor that impacts a person's perception toward the adoption of a behavior.
6. Self-Efficacy (SE)—the judgment of one's ability to organize and execute a course of action required to attain a designated type of performance.
7. Anxiety (ANX)—the feeling of anxiety toward performing an action.

Based on these constructs, a research model—presented in Figure 1—was constructed with the following hypotheses. Then, the constructs were validated and those with higher loading were selected.

H1. There is a significant relationship between Perceived Ease of Use and Perceived Usefulness.
H2. There is a significant relationship between Perceived Usefulness and Intention toward registering in STEM courses and utilizing robotic projects.
H3. There is a significant relationship between Perceived Usefulness and Attitude.
H4. There is a significant relationship between Social Influence and Attitude.
H5. There is a significant relationship between Social Influence and Intention.
H6. There is a significant relationship between Anxiety and Attitude.
H7. There is a significant relationship between Anxiety and Intention.
H8. There is a significant relationship between Ease of Use and Attitude.
H9. There is a significant relationship between Self-Efficacy and Attitude.
H10. There is a significant relationship between Ease of Use and Intention.
H11. There is a significant relationship between Attitude and Intention.
H12. There is a significant relationship between Self-Efficacy and Intention.

The following survey was designed to measure each construct in the research model:

1. Demographics:
   a. Age
   b. Gender
   c. Major
   d. Years of Education
   e. Have you had any exposure to project-based classes?
   f. Have you worked on Mindstorm robotic projects?

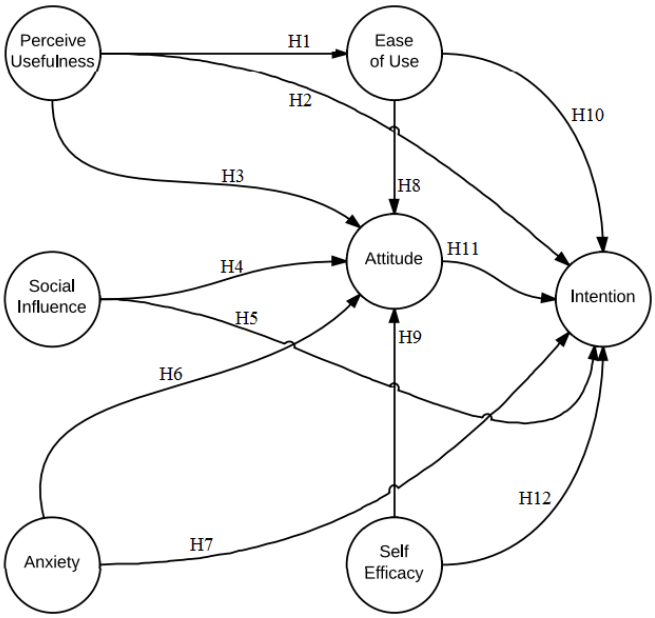

Figure 1. Research Model and Hypotheses

2. Ease of use:
   a. It is easy to use robotic projects in the classroom.
   b. It is easy to build a robotic structure.
   c. It is easy to program a robot.
   d. I can easily figure out how to use robots.
   e. It is easy to learn how to operate a robot.
   f. It is easy to become skillful in using robots.

3. Usefulness:
   a. I believe working on robotic projects helps me to better understand the class concepts.
   b. I believe using robotic projects is beneficial.
   c. I believe working on robotic projects is useful.
   d. I believe using robotic projects helps to increase my performance in the class.

e. I feel my learning in robotics helps my analytical skills.
f. I feel robotic projects improve my problem-solving skills.
g. I feel robotic projects are useless.
h. I feel robotic-based classes help me to work better as a team member.
i. I believe robotic-based classes help me to better communicate my ideas with other team members.

4. Attitude:
   a. Using a robotic project in class is a good idea.
   b. Robotic projects make learning more interesting in class.
   c. Working with a robotic project in class is fun.
   d. I like working with a robotic project in class.

5. Intention:
   a. Assuming I have access to a robotic platform, I intend to use it.
   b. Given that I have access to a robotic platform, I predict that I would use it.
   c. I prefer to register for robotic-based classes, if possible.
   d. This course motivates me to register for more science-oriented classes in the future.
   e. This course motivates me to take more engineering-oriented classes in the future.
   f. This course motivates me to take more mathematic-oriented classes in the future.
   g. This course motivates me to take more technology-oriented classes in the future.
   h. I predict, I would use a robotic platform in the future.

6. Social influences:
   a. People who influence my behavior think that I should use a robotic-based project.
   b. People who are important to me think that I should use a robotic-based project.
   c. My instructors support me to work with robotic-based projects.
   d. My school (professor, peers) encourages me to take more classes in the technology field.
   e. My school (professor, peers) encourages me to take more classes in the engineering field.
   f. My school (professor, peers) encourages me to take more science classes.
   g. My school (professor, peers) encourages me to take more mathematics classes.

7. Anxiety:
   a. I feel apprehensive about using a robot.
   b. It scares me to think that I could break a robot when I am using one.
   c. I hesitate to use a robot for fear of making mistakes that I cannot correct.
   d. Robotic projects are somewhat intimidating to me.

8. Self-efficacy:
   I could complete a task/project using robots.....
   a. If there was no one around to tell me what to do as I go.
   b. If I could call someone for help if I got stuck.
   c. If I had a lot of time to complete the job for which software was provided.
   d. If I had just the robot manual for assistance.
   e. I feel confident to create different programing functions of robots.
   f. I feel confident to build different structure of robots.
   g. I feel confident to learn advanced skills within a robotic field.

The validity of the questionnaire [16] was ensured by carefully selecting each question and consulting with a panel of experts, which was formed by three faculty members at Eastern Michigan University. Finally, an online survey was created and was used to test the research hypotheses by asking all students, who were enrolled in the course either in the fall or in the winter semester, to complete it. The reliability of the questionnaire was tested by utilizing Smart PLS statistical software [17]. The software was used to measure the Cronbach's Alpha and Composite Reliability, as illustrated in table 1.

Table 1. Reliability of the Survey

	AVE	Composite Reliability	R-square	Cronbach's Alpha	Communality
ANX	0.6807	0.8930	0.0000	0.8385	0.6807
ATT	0.7688	0.9430	0.6115	0.9235	0.7688
EU	0.6193	0.9065	0.0000	0.8768	0.6193
INT	0.6457	0.9357	0.7460	0.9212	0.6457
PU	0.6545	0.9443	0.4100	0.9332	0.6545
SE	0.5659	0.9007	0.0000	0.8725	0.5659
SI	0.6430	0.9152	0.0000	0.8889	0.6430

According to Table 1, the values of the Cronbach's Alpha and Composite Reliability for all of the constructs were greater than 0.7, which confirmed the reliability of the constructs [14]. Table 2 presents the outer loading of each factor within each construct, which is a good representation of the questionnaire. From the 98 responses collected during the two semesters, demographic data showed that there were 10 female (10.20%) and 88 male (89.80%) students. The ages of the students varied from 17 to 66; the average age of the students was 21 years; the average length of time attending the college after high school was 2.2 years. The degree programs of students were Simulation and Gaming, Computer Engineering Technology, Electrical Engineering Technology, Mechanical Engineering Technology, and Finance.

Analysis and Results

The Smart PLS software was used to analyze and find the path coefficients in the proposed model, as presented in Figure 2. The numbers inside each construct were R-square values and each construct was presented with its items and factor loading. Also, the Smart PLS software was used to evaluate the loading of each question in each construct, as shown in Figure 3 and Table 2.

In order to examine the hypotheses, the t-values for all paths and hypotheses were calculated, as illustrated in Table 3. Then, the hypotheses with a t-value above 1.96 were accepted. According to the analysis of hypotheses in Figure 3, the H1, H2, H3, H5, H8, H9, H11, and H12 hypotheses

Table 2. Outer Loading of Each Factor within Each Construct

	ANX	ATT	EU	INT	PU	SE	SI
ANX1	0.6124	0	0	0	0	0	0
ANX2	0.8835	0	0	0	0	0	0
ANX3	0.9197	0	0	0	0	0	0
ANX4	0.8493	0	0	0	0	0	0
ATT1	0	0.9008	0	0	0	0	0
ATT2	0	0.8772	0	0	0	0	0
ATT3	0	0.9086	0	0	0	0	0
ATT4	0	0.9376	0	0	0	0	0
ATT5	0	0.7473	0	0	0	0	0
EU1	0	0	0.7998	0	0	0	0
EU2	0	0	0.6929	0	0	0	0
EU3	0	0	0.7011	0	0	0	0
EU4	0	0	0.8266	0	0	0	0
EU5	0	0	0.8344	0	0	0	0
EU6	0	0	0.8512	0	0	0	0
INT1	0	0	0	0.8321	0	0	0
INT2	0	0	0	0.8039	0	0	0
INT3	0	0	0	0.7918	0	0	0
INT4	0	0	0	0.7961	0	0	0
INT5	0	0	0	0.8515	0	0	0
INT6	0	0	0	0.7562	0	0	0
INT7	0	0	0	0.8463	0	0	0
INT8	0	0	0	0.7439	0	0	0

	ANX	ATT	EU	INT	PU	SE	SI
PU1	0	0	0	0	0.848	0	0
PU2	0	0	0	0	0.8545	0	0
PU3	0	0	0	0	0.8195	0	0
PU4	0	0	0	0	0.8029	0	0
PU5	0	0	0	0	0.8604	0	0
PU6	0	0	0	0	0.7984	0	0
PU7	0	0	0	0	0.6537	0	0
PU8	0	0	0	0	0.8114	0	0
PU9	0	0	0	0	0.8133	0	0
SE1	0	0	0	0	0	0.6716	0
SE2	0	0	0	0	0	0.7715	0
SE3	0	0	0	0	0	0.7465	0
SE4	0	0	0	0	0	0.6769	0
SE5	0	0	0	0	0	0.7742	0
SE6	0	0	0	0	0	0.8633	
SE7	0	0	0	0	0	0.745	
SI1	0	0	0	0	0	0	0.7858
SI2	0	0	0	0	0	0	0.7851
SI3	0	0	0	0	0	0	0.7637
SI4	0	0	0	0	0	0	0.8281
SI5	0	0	0	0	0	0	0.8364
SI6	0	0	0	0	0	0	0.8096

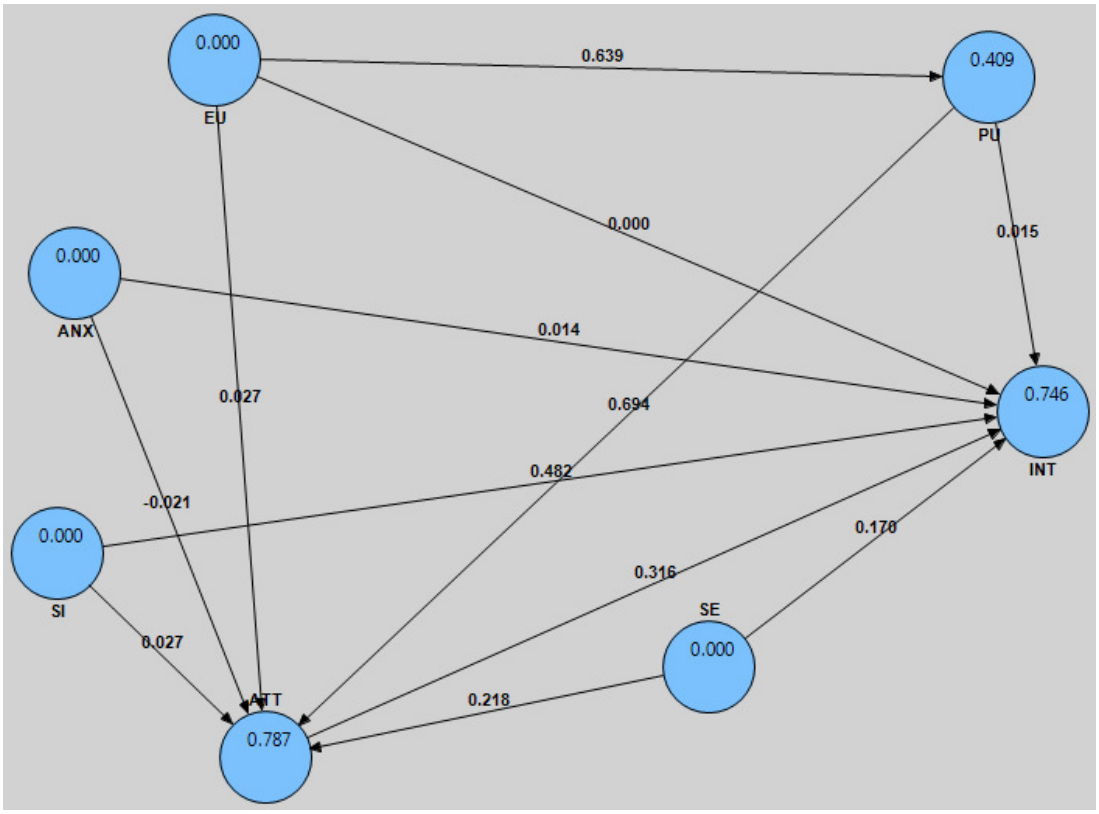

Figure 2. Path Coefficient and R-square

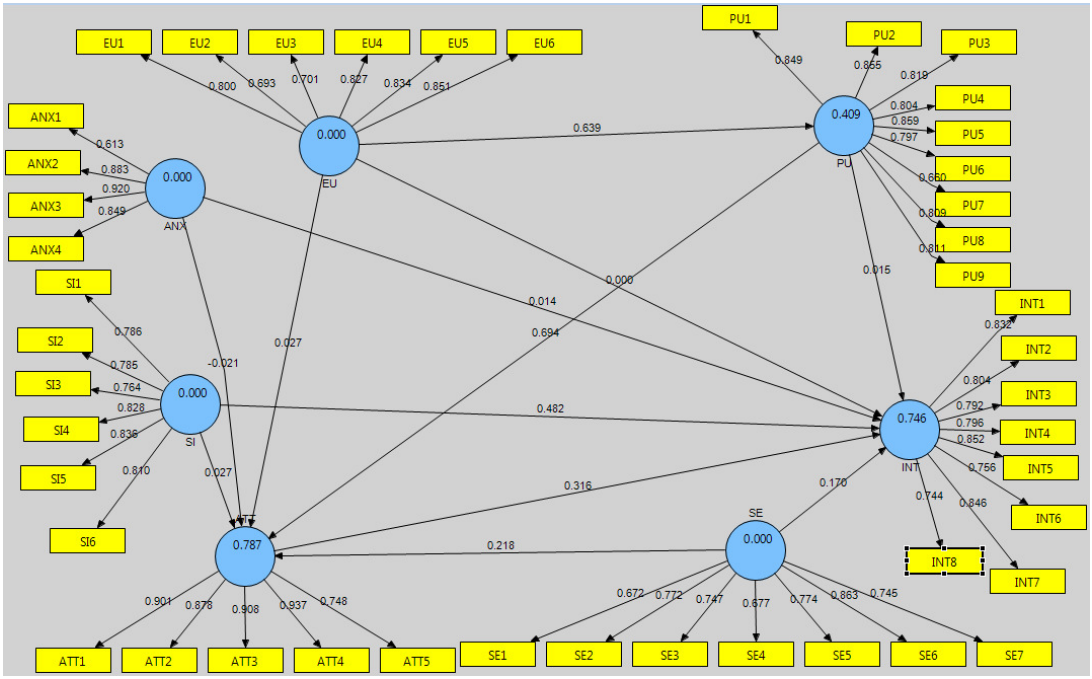

Figure 3. Analysis of the Proposed Model

were confirmed. In other words, the individual perception of Ease of Use of robotic projects had a positive relationship with the students' Attitude and their Perceived Usefulness; Perceived Usefulness has a positive and direct relationship with students' Attitude and Intention toward using robotic projects and enrolling in more STEM classes; Social Influence had a direct and positive relationship with the students' Attitude toward using robotic projects; and, Self-Efficacy had a direct and positive relationship with the students' Attitude and Intention toward enrolling in more STEM-oriented courses.

Table 3. Results of Hypothesis testing

Hypotheses	Path	T-Value	Results
H1	EU -> PU	11.4213	Accepted
H2	PU -> INT	2.005	Accepted
H3	PU -> ATT	8.5484	Accepted
H4	SI -> ATT	0.3387	Rejected
H5	SI -> INT	6.3058	Accepted
H6	ANX -> ATT	0.4678	Rejected
H7	ANX -> INT	0.1194	Rejected
H8	EU -> ATT	6.3023	Accepted
H9	SE -> ATT	3.1517	Accepted
H10	EU -> INT	1.7727	Rejected
H11	ATT -> INT	2.3585	Accepted
H12	SE -> INT	2.5729	Accepted

On the other hand, hypotheses H4, H6, H7, and H10 showed t-values less than 1.96 and, thus, were rejected. This study, then, could not confirm a positive relationship between Social Influence and changing students' Attitude toward using robotic projects; it could not confirm any positive or negative effect of Anxiety toward using robotic projects in the classroom and Attitude and Intention of using robotic projects in the future and/or enrolling in more STEM-related courses; and, it found no positive relationship between perceived Ease of Use and the students' Attitude toward using robotic projects.

Conclusions

This study attempted to address the underlying factors that impact student attitude and intention toward enrolling in more STEM-related courses through a proposed research model that utilized several theoretical frameworks to explain human behavior. Twelve hypotheses were developed for the proposed model, out of which four were rejected and eight were confirmed. This study showed that Perceived Usefulness, Social Influence, Self-Efficacy, and Attitude had a direct and positive relationship with the students' intention toward enrolling in more STEM courses and using robotic projects. It also found no positive relationship between Social Influence and individual Attitude, Anxiety and Attitude, Anxiety and Intention, and Ease of Use and intention of the students to enroll in more STEM-related courses.

In this study, the Social Influences were limited to family members, friends, peers, and instructors. Future studies could focus on the effect of the job market, mass media, and other electronic media on student attitude and intention toward working with robotic projects and enrolling in more STEM courses. Also, data collection was done only over a period of two consecutive semesters for the same course, which makes it impossible to determine the actual behavior of the students as whether or not their intention to enroll in more STEM courses actually led to more registrations in STEM-related courses. Thus, further studies are needed to determine whether student behavior of enrolling in more STEM courses is a function of individual intentions.

References

[1] Bonwell, C. C., & Eison, J. A. (1991). Active Learning: Creating Excitement in the Classroom. *1991 ASHE-ERIC Higher Education Reports*. ERIC Clearinghouse on Higher Education, The George Washington University, Washington, DC.

[2] Chatmon, C., Chi, H., & Davis, W. (2010). Active learning approaches to teaching information assurance. *Proceedings of ACM 2010 Information Security Curriculum Development Conference,* 1-7, Kennesaw, GA.

[3] Habraken, C. L. (2004). Integrating into chemistry teaching today's student's visuospatial talents and skills, and the teaching of today's chemistry's graphical language. *Journal of Science Education and Technology*, *13*(1), 89-94.

[4] Haak, D. C., HilleRisLambers, J., Pitre, E., & Freeman, S. (2011). Increased structure and active learning reduce the achievement gap in introductory biology. *Science*, *332*(6034), 1213-1216.

[5] Scales, A. Y., & Varnado, T. E. (2012). Active Learning for Engineering/Technical Graphics Online Environments. *Proceedings of American Society for Engineering Education*, San Antonio, TX.

[6] Michael, J. (2006). Where's the evidence that active learning works? *Advances in physiology education*, *30*(4), 159-167.

[7] Chickering, A. W., & Gamson, Z. F. (1987). Seven principles for good practice in undergraduate education. *AAHE bulletin*, *3*, 7.
[8] de Graaff, E., Saunders-Smits, G., & Nieweg, M. (Eds.). (2005). *Research and practice of active learning in engineering education*. Amsterdam University Press.
[9] Faust, J. L., & Paulson, D. R. (1998). Active learning in the college classroom. *Journal on Excellence in College Teaching*, *9*(2), 3-24.
[10] Pheeney, P. (1997). Hands on, minds on: Activities to engage our students. *Science Scope 2,* 1(4), 30 -33.
[11] Eydgahi, A., & Esmaeili, M. (2013). Enhancing Engineering Education through Active Learning and Project Based Courses. *Proceedings of 3rd Conference on Engineering Education,* Tehran, Iran.
[12] Esmaeili, M., & Eydgahi, A. (2013). By the Students for the Students: A New Paradigm for Better Achieving the Learning Objectives, *Proceedings of American Society for Engineering Education*, Atlanta, GA.
[13] Taylor, S., & Todd, P. A. (1995). Understanding Information Technology Usage: A Test of Competing Models. *Information Systems Research*, *6*(2), 144-176.
[14] Esmaeili, M., & Eydgahi, A. (2013). An Evaluation Model for Project Based Active Learning in an Engineering Technology Freshman Course. *International Conference on Engineering Education Research.* Marrakesh, Morocco.
[15] Henseler, J., Ringle, C. M., & Sinkovics, R. R. (2009). The use of partial least squares path modeling in international marketing. *Advances in international marketing*, *20*(1), 277-319.
[16] Warshaw, P. R., & Davis, F. D. (1985). Disentangling behavioral intention and behavioral expectation. *Journal of experimental social psychology*, *21* (3), 213-228.
[17] Taylor, S., & Todd, P. A. (1995). Understanding information technology usage: A test of competing models. *Information systems research*, *6*(2), 144-176.

Biographies

MOHAMMADJAFAR ESMAEILI received a Ph.D. degree in Technology with a concentration in information security from Eastern Michigan University in 2014. He holds a B.S. degree in electrical engineering and an M.S. degree in management of information systems. Dr. Esmaeili is currently working as a full-time faculty member in the department of Electrical and Computer Engineering Technology at the University of Dayton. Dr. Esmaeili has over four years of experience in utilizing active learning methodologies in teaching classes. His research interests are in interdisciplinary fields such as information security in automation, robotics, and unmanned systems. He was vice president of IEEE's student branch at Eastern Michigan University and has served as a referee for ASEE conferences. Dr. Esmaeili can be reached at mesmaeili1@udayton.edu

ALI EYDGAHI started his career in higher education as a faculty member at the Rensselaer Polytechnic Institute in 1985. Since then, he has been with the State University of New York, Tehran University, Oakland University, University of Maryland Eastern Shore, and Eastern Michigan University. From 2006 to 2010, he was Chair of the Department of Engineering and Aviation Sciences, Founder and Director of the Center for 3-D Visualization and Virtual Reality Applications, and Technical Director of the NASA-funded MIST Space Vehicle Mission Planning Laboratory at the University of Maryland Eastern Shore. In 2010, he joined Eastern Michigan University as an Associate Dean in the College of Technology and currently is a Professor in the School of Engineering Technology. He has extensive experience in curriculum and laboratory design and development. Dr. Eydgahi has served as a member of the Board of Directors for Tau Alpha Pi; Advisory and Editorial boards for many international journals in engineering and technology; the review panel for NASA and the Department of Education; was the regional and chapter chairman of IEEE and ASEE; and, served as a session chair and as member of scientific and international committees for many international conferences. Dr. Eydgahi can be reached at aeydgahi@emich.edu

THE IMPACT OF PROJECT DELIVERY METHODS USED ON PUBLIC HIGHWAY-RAIL INTERSECTION PROJECTS IN NEW YORK STATE

Osileke O. Osipitan, New York State Department of Transportation; Musibau A. Shofoluwe, North Carolina A&T State University

Abstract

Project delivery methods are used for infrastructure developments based on cost-effective and efficient solutions for meeting project requirements. This study investigated the impact of project delivery methods used by railroad organizations in 256 selected public highway rail intersection (HRI) projects that have similar scope and were completed within a period of ten years in New York State. Specifically, the study sought to assess possible difference between the total costs of HRI when design-build (DB) and design-bid-build (DBB) methods are used by railroad organizations to complete the projects. Public HRI projects were performed at locations where the railroad bisected a highway used by the public and that was maintained by a municipality. Project improvements were funded by the federal government and matched by the states in the U.S. for safety of the public using the intersections. Available funds have remained relatively constant over the years while project costs have escalated. In addition, projects that were similar in scope were being implemented by different project delivery methods that impacted the number of projects approved.

Data for this study were sourced from the New York State Department of Transportation (NYSDOT) and analyzed using SPSS. The hypothesis was tested with a non-parametric test (Mann-Whitney U) to determine the statistical significant difference between the total costs of HRI projects when DB and DBB methods are used. Findings indicated that there was a statistical significant difference between the total project costs when DB and DBB methods were used, based on p=0.004 (p<0.05). Recommendations are provided to assist the NYSDOT as well as other state DOTs in sustaining and improving public HRI projects.

Introduction

Project delivery is a process that defines the relationship between parties involved in a specific project. The method could have an effect on the project and its budget, schedule, and quality as well as the extent of the owner's involvement. While it is applicable in private developments, it is very applicable in providing efficient public projects. Public highway-rail intersections are located at different points along railroad corridors where the railroad bisects the highway (roadway). A highway-rail intersection (HRI) is an infrastructure that impacts the traveling public that uses the rail and road systems. In countries like Australia, the UK, and Nigeria, HRI is called a level crossing. In this study, the term "highway-rail intersection" is used interchangeably with railroad grade crossing. It involves two completely different modes of transportation with different operating authorities and operational characteristics [1]. In the U.S., different railroad companies own the right-of-way along respective corridors of operation. Highways bisect the railroad tracks, which warranted improvements in order to provide warning devices at the bisected locations to alert and bar public users from crossing when a train is approaching the crossing. However, most railroad crossings have been created over the years, but they require continuous improvements. These improvements have been based on different project delivery methods used by railroad organizations. The improvements are necessary to avoid fatalities and injuries to users of the systems.

Federal funds for highway-rail intersections are provided to reduce hazards or risk exposure to the traveling public [2]. It is a cooperative effort between the Federal Highway Administration, states, railroad companies, and municipalities, where required. These funds are matched by each state to afford full upgrades of warning devices. The highway-rail intersections in need of improvements are selected based on a suitable method for a state, using a hazard index such as the USDOT Accident Prediction Formula to prioritize and rank potential high-risk intersections; these are then placed on statewide funding lists. The hazard index is the primary initial factor used to rank and select Section 130 projects [3]. The highest-ranked project locations are funded but limited by the appropriated amounts available each fiscal year. Because of the inadequate funding for all candidate crossings, available funds were only targeted for implementing projects among those that were ranked at the top of the list.

In this study, the authors considered HRI projects consisting of installing flashing lights, gates, and stanchions with their foundations, equipped with signal houses and circuitry systems. The projects had similar scopes and were fully funded by the government. The railroad crossings were lo-

cated at freight and passenger rail corridors, while other projects were being initiated by the states in conjunction with the railroad companies that owned the tracks and/or operated the tracks. There was no targeted cost or specific delivery method applicable to all highway-rail intersection projects, except that it was based on capability, where the railroad uses its workforce to design and build or to use conventional methods. The bottom line is that, recently, the NYSDOT experienced funding constraints to implement all candidate HRI projects. New York State had 2679 public railroad grade crossings [4]. High-risk locations at these crossings continuously require circuitry upgrades and improvements of warning devices, surfaces, and interconnections between highway traffic devices and railroad circuitry systems.

Literature Review

Stakeholders in HRI projects are usually the railroad organizations/contractors/designers and the federal/state/local governments. Ghavamifar [5] defined PDM as a framework of all project stakeholders' legal relationships and responsibilities. It is also defined as a system used within industry to define processes for accomplishing project phases, the contractual relationships, and the parties involved in each phase. In analyzing performance by the City of Los Angeles Bureau of Engineering, project costs were compared based on phases between the DBB method and an in-house construction method. The projects analyzed differed in scope. Further research is recommended for projects with equivalent design, construction scope, and complexity [6]. This study engaged HRI projects that had a similar scope.

PDM is a system designed to achieve satisfactory completion of a construction project from conception to occupancy. However, several fundamental project considerations were impacted by the delivery method selected for a given project. These include adherence to a realistic budget, a schedule that accurately presents the performance period, responsive and efficient design processes that lead to a quality set of documents, thorough risk assessment followed by the proper allocation of risk by the owner, and recognition of the level of expertise within the owner's organization or its availability [7].

The four main criteria for the success of any project delivery method are cost, quality, time, and safety. The responsibilities for meeting these criteria vary by methods and level of risk that a PDM offers to owners or providers [8]. Constraints can allow the use of any contracting format to achieve the delivery. The methods include design-bid-build, design-build, construction management at risk, integrated project delivery, public-private partnership, build operate and transfer, turnkey, fast tracking, partnering, and job order. Each of these project delivery systems has varying responsibilities and risk allocation. In essence, different project delivery systems organize the building process and allocate risks differently [9].

An HRI is either a private or public crossing. Public HRIs are part of the infrastructure, which, when created and/or improved, are funded by the government. Public infrastructure is investment in roads, water and sewage systems, electric power plants, telecommunication facilities, railroads, and airports that are traditionally provided by the public sector to private households and businesses [10]. The HRIs selected for this study were public infrastructure funded by the government to provide safety measures to the public using the crossings.

Limitations of public funds available for infrastructure improvements have led governments to invite private sector entities into long-term contractual agreements for the financing, construction, and/or operation of capital-intensive projects [11]. HRIs are public projects that can only require collaboration between state agencies and railroad organizations so as to share costs for improving high-risk HRI projects. Such collaboration will sustain the current number of project improvements or improve more candidate crossings. Therefore, while there is limited relative research for this study, the results would fill the gap on constraints encountered from the use of different project delivery methods on serial projects, such as HRIs, that have similar scope.

Methodology

This study was conducted to assess the impact of PDMs used on public highway-rail intersection projects in New York State. The study considered all completed projects with the same scope, which were contracted between the NYSDOT and railroad organizations within a 10-year period. In order to assess the impact of the PDMs, the authors used a total population sampling to select the HRI projects, a type of purposive sampling technique that involves examining the total population that has a particular set of characteristics [12]. The authors selected 256 public HRI projects from 368 closed projects. These projects were those installed with flashers and gates and were completed between 2002 and 2012. These projects were installed at independent locations and were not repeated.

The data for the 256 HRI projects were sourced from the NYSDOT project database. The limitation in the study scope was that the database did not distinguish the type of circuitry used for these projects. However, the projects were representative of project delivery methods used to accom-

plish them (see Figure 1). The data types were continuous and categorical. The variable with continuous data for this study was the total project cost (TPC), while the variable with categorical data was the PDM. The PDM was classified based on the method used by the railroad organizations to accomplish the projects. It was classified into DB and DBB. The projects with bid documents used DBB methods, while those without bid documents were completed with DB. The TPC was measured by a ratio scale, while the PDM was measured by a nominal scale.

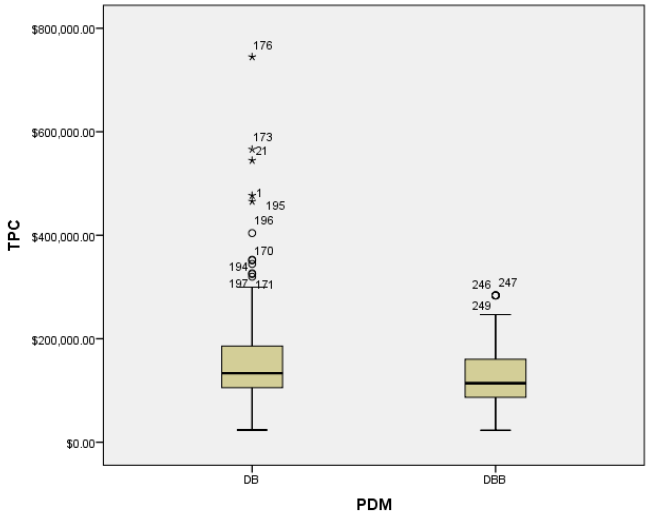

Figure 1. Box Plots of TPC for Methods of Project Delivery

These data were copied into an Excel spreadsheet, sorted and checked for errors, then were imported into SPSS 20 statistical software for statistical inferences. With targeted project population data for the 10-year period, box plots were used to investigate the presence of outliers. Because of the presence of any outliers and/or extreme outliers, unrelated to data errors, a non-parametric test (Mann Whitney U) was used to check the hypothesis. Mann-Whitney was used because the dependent variable, TPC, was continuous, while the independent variable, PDM, was categorical with two levels. The non-parametric test utilizes mean ranks and reports the median. The alpha level was set at 0.05 in order to determine the statistical significance of the data. Hence, the following hypothesis was tested:

Hypothesis

$H_0 1$: There is no statistically significant difference between the total cost of highway-rail intersection projects when design-bid-build methods and design-build methods are used by railroad companies.

$H_1 1$: There is a statistically significant difference between the total cost of highway-rail intersection projects when design-bid-build methods and design-build methods are used by railroad companies.

Findings

Table 1 shows that 256 projects were analyzed. Approximately 74% of the completed projects were performed with the design-build method, while 26% of the completed projects were performed with the design-bid-build method.

Table 1. Projects Performed with Different PDMs Between 2002 and 2012

PDM	Frequency	%
DB	189	73.83
DBB	67	26.17

Note: N = 256

The box plots indicate outliers across levels of PDM. The DB had outliers and extreme outliers, while DBB had only outliers. The total number of outliers shown in the box plots were 13. All outliers indicated in the box plots were total project costs that were not gathered in error and could not be removed. These outliers would cause failure of statistical tests on normality and other parametric assumptions.

A non-parametric test, Mann-Whitney, was used to test the hypothesis and determine if a statistically significant difference existed between the total cost of highway-rail intersection projects when design-bid-build and design-build methods were used by railroad organizations. Figure 2 is an SPSS output for the Mann Whitney U test, which was embedded with a table. It shows the mean ranks and shape of distributions for total project costs for DB and DBB. The mean rank for DB (136.53) was higher than the mean rank for DBB (105.84). The table indicates that the Mann-Whitney test statistic, "U", was 4813. This reflects the difference between the two rank totals. The "U" can be easily reported for small sample data. It also indicates the standardized test statistics, "Z", that are converted from "U". The Z score was -2.916. It was less than the critical value (-1.96) for the set alpha (0.05) for the two-tail test and fell in the rejection region. The "p" value shown was 0.004. This value was less than the set alpha of 0.05. However, the p value of 0.004 indicated was less than the alpha level.

Table 2 reports the median of the TPC when DB and DBB methods were used. It indicates that the median of

TPC reported for DB was 19,177, more than the median of TPC reported for DBB.

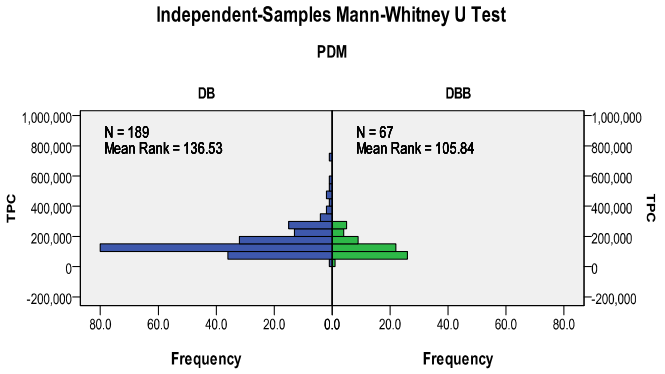

Total N	256
Mann-Whitney U	4,813.000
Wilcoxon W	7,091.000
Test Statistic	4,813.000
Standard Error	520.766
Standardized Test Statistic	-2.916
Asymptotic Sig. (2-sided test)	.004

Figure 2. Mann-Whiney U Test

Table 2. Median Report for PDM Based on TPC

PDM	TPC
DB	$133,316.00
DBB	$114,139.08
Total	$129,898.99

Therefore, based on Figure 2 and Table 2, the total project cost of HRI, when DB (mean rank = 136.53, median 133,316) and DBB (mean rank = 105.84, Median 114,139) were used, was a statistically significant difference, U = 4,813, z = -2.916, p = 0.004. The DB indicated a higher median cost than DBB. The DB was also ranked higher than DBB. Based on the p value (0.004<0.05), the null hypothesis was rejected. Therefore, there was a statistically significant difference between the total cost of highway-rail intersection projects when the DBB and DB methods were used by railroad companies.

Discussion and Recommendations

This study was conducted in order to provide recommendations on ways that HRI projects can continue to improve warning devices to mitigate risks and provide safety for users of railroad grade crossings in New York State. The results shown in Table 1 indicate that most of the projects were based on the DB method, as compared to DBB. The use of DB was basically a result of the capacity of railroad organizations that used their workforce to complete the projects. In essence, most of the projects improved were those of large or commuter railroad organizations. The results indicated a statistically significant difference between the total cost of highway-rail intersection projects when DB and DBB methods were used by railroad companies. The DB methods allow a company to develop the design and perform the construction at the same time. However, that same company assumes design and construction risks, which eventually influence project costs. Moreover, larger railroads' administrative costs and overhead can be higher than those charged by regional or short-line railroads. Furthermore, the project initiation period and the period of cost reimbursement could be financial risk factors considered by the railroad organizations.

Large railroad organizations (Class 1) and regional (Class 2) railroad organizations mostly use DB methods to perform HRI projects because of their resources and workforce. Short-line railroads, which are local and switching railroad organizations, use DBB methods to perform the HRI projects. This study did not recommend a particular PDM to choose for HRI projects for installation of warning devices. Similarly, the NYSDOT cannot mandate that a railroad organization use a particular PDM for completing an HRI project, because the property belongs to the railroad; project implementation was based on railroad capability and the state/railroad agreement was to use the funds to reimburse costs, irrespective of the PDM used.

Hence, in order to sustain and improve HRI projects with available funds, it was recommended that the NYSDOT partner with railroad organizations using the DB method in New York State so as to share costs relative to labor, equipment, and materials. The state agency should adequately monitor railroad organizations, particularly those using the DB method, so that they do not charge for HRI projects simultaneously when performing routine railroad work. A long-term plan could be developed between the NYSDOT and railroad organizations using the DB method to close some crossings at railroad corridors and/or grade separate HRIs so that the railroad can derive safety and maintenance benefits. These will encourage railroad organizations to fund HRI improvements. Finally, the NYSDOT should en-

sure that the billing for cost reimbursement by railroads using DB and DBB methods is standardized.

These recommendations will help the NYSDOT and other state Departments of Transportation to use available funds to sustain the current number of projects implemented and also implement more candidate high-risk HRIs. Furthermore, it would help maintain and improve the overall safety level at highway-rail intersections in New York State.

References

[1] Bowman, B. L., Stinson, K., & Colson, C. (1998). Plan of Action to Reduce Vehicle-Train Crashes in Alabama. *Transportation Research Record, 1648*, 8-18.

[2] *United States Code—Title 23*. (n.d.). Retrieved from https://www.fhwa.dot.gov/ map21/docs/ title23usc.pdf

[3] Indiana State Department of Transportation. (1997). *Rail-Highway Crossing Program (Section 130)*. Retrieved from FINAL--006__Critical Thinking in Technical Decisions (Barry Hoy).docx

[4] USDOT-FRA. (2014). Office of Safety Analysis. Retrieved from http://safetydata.fra.dot.gov/ officeofsafety/publicsite/Query/invpub.aspx

[5] Ghavamifar, K. (2009). *A Decision Support System for Project Delivery Method Selection in the Transit Industry*. Unpublished doctoral dissertation, Northeastern University.

[6] Kuprenas, J. A., & Nasr, E. B. (2007). Cost Performance Comparison of Two Public Sector Project Procurement Techniques. *Journal of Management in Engineering, 23*(3), 114-121.

[7] CMAA. (2012). *An Owner's Guide to Project Delivery Methods*. Retrieved from https://cmaanet.org/ files/Owners%20Guide%20to%20Project% 20Delivery%20Methods%20Final.pdf

[8] AIA & AGC Primer Tax Force. (2011) *Primer on Project Delivery*. (2nd ed.). Retrieved from http:// www.aia.org/aiaucmp/groups/aia/documents/pdf/ aiab093116.pdf

[9] Rubin, R., & Wordes, D. (1998). Risky Business. *Journal of Management in Engineering, 14*(6), 36-44.

[10] Fox, W. F., & Smith, T. R. (1990). Economic Development Programs for the States in the 1990s. *Economic Review, 75*(2), 49-50.

[11] Grimsey, D., & Lewis, M. (2002). Evaluating the Risks of Public Private Partnerships for Infrastructure Projects. *International Journal of Project Management*, *20*(2), 107-118.

[12] Laerd Dissertation (n.d.). *Total Population Sampling*. Retrieved from http://dissertation.laerd.com/total-population-sampling.php

Biographies

OSILEKE OSIPITAN is an intermodal transportation specialist with the New York State Department of Transportation. He received his Ph.D. in Technology Management, specializing in Construction Management, from Indiana State University. He is a professional member of the Royal Institution of Chartered Surveyors. Dr. Osipitan may be reached at osipitan@hotmail.com

MUSIBAU SHOFOLUWE is a professor of Construction Management at North Carolina A&T University. He received his doctorate degree in Industrial Technology, specializing in Construction Management, from the University of Northern Iowa. His research interests include sustainable development and construction practices. Dr. Shofoluwe may be reached at musibaus@ncat.edu

ENERGY INPUTS AND CARBON DIOXIDE EMISSIONS DURING CONSTRUCTION OF A GOLF COURSE

Fariborz M. Tehrani, California State University, Fresno; Athanasios Alexandrou, California State University, Fresno; Diganta Adhikari, California State University, Fresno; Michael Mahoney, California State University, Fresno; Raymond Maestas, California State University, Fresno

Abstract

In this paper, the authors describe the results of a study to evaluate the energy inputs and carbon dioxide emissions from major construction machinery and labor activities during construction of a typical golf course. The primary objective of this study was the earthmoving operations, including excavating, loading, scraping, and grading. An 18-hole golf course in the Central Valley of California was studied. The course contained landscapes, turf grass, greens, roughs, and fairways. Information for identifying major construction machinery and their technical specifications were obtained from the site superintendent and manufacturers, respectively. Productivity, energy input, and carbon dioxide (CO_2) emissions were estimated based on available resources and analysis. These estimates covered both manufacturing and operation processes, and included items like equipment life, energy from labor, and fuel consumption of the equipment. Results included breakdown of outputs per various parameters such as machinery type, construction activity, and pollution source. Findings emphasized the need for careful selection of equipment, based on their environmental impacts.

Introduction

The State of California has been at the self-professed forefront of efforts to control climate change since its landmark California Global Warming Solutions Act of 2006 (AB 32). Subsequently, environmental awareness on the part of stakeholders has increased and companies are becoming more and more environmentally friendly. As the concentration of CO_2 in the atmosphere continues to rise, policy and regulatory agencies work to regulate emissions in order to reduce and/or offset them [1].

There is currently no reliable information estimating the amount of energy invested into the earth-moving phase of a construction project. During this phase, huge amounts of dirt are relocated—depending on the project—by heavy machinery with a corresponding consumption of energy. The energy sequestered in each project depends on the machinery used and its productivity as well as work quantities. Even though the productivity and efficiency of these heavy machines are major factors in determining the total energy consumption and the cost of construction, such data vary significantly from case to case. Further, quantities of moved earth generally depend on the type of golf course layout and the extent of the modification of existing contours [2]. Nevertheless, available mean estimates are often helpful in providing a general baseline for comparison purposes.

Linked to energy consumption is the CO_2 emitted during the construction of a golf course. Despite the fact that earth-moving machines are used often in various projects, limited CO_2 emission data have been gathered from these operations that include the amount of energy sequestered into the equipment. CO_2 emissions and the corresponding energy sequestered into the construction machinery operations from these earth-moving-based systems can be calculated using a model based on the process. Such a model has been used in studies for ammonia emissions [3-5]. In that model, CO_2 emissions within the system were first determined for every process and then summed. The total amount of CO_2 emitted was then calculated. For an earth-moving operation, this means that for a given piece of equipment, CO_2 emissions would be calculated for both operation and manufacturing processes.

Both energy and CO_2 emissions are recognized as measured values in sustainability rating systems, including Envision™ by the Institute of Sustainable Infrastructure (ISI) [6]. Table 1 lists primary and other related credits for these measures in Envision. The total credit for impacted measures was 97 points, nearly 14% of the total 700 points. This shows the significance of controlling energy and CO_2 emissions in a sustainable infrastructure.

Many strategies exist to address energy and CO_2 emissions, such as renewable energy, biochar, and other alternative approaches [7]. The primary objective of this study was to estimate the energy input and the CO_2 emissions. These emissions were measured for earth-moving operations during construction of a typical golf course. The global growth of golf course construction has raised serious environmental concerns including, but not limited to, energy and impacts on land use, water, soil, and air [8], [9]. These impacts are generally linked to the features and construction methods of the course as well as geography and climate of the region.

The Central Valley in California is a typical warm and sunny area, also known as the sun-belt region [10], which has attracted golf course developers in the past several decades [11]. Such attraction has also been an opportunity to address global concerns about golf course impacts on environment, such as air pollution and energy consumption. While golf course construction methods and equipment vary around the globe, similarities in the features and regional characteristics of golf courses justify global approaches to reducing energy input and CO_2 emissions. In this paper, the authors provide a detailed bottom-up analysis to provide baseline data for such approach.

Table 1. Envision Credits for Energy and CO_2 Emissions [6]

Categories	Subcategories (credits)	Energy*	CO_2 Emissions*
Quality of Life	QL2.1 Enhance Public Health and Safety (16)		R
Resource Allocation	RA1.1 Reduce Net Embodied energy (18)	R	R
	RA2.1 Reduce Energy Consumption (18)	P	
	RA2.3 Commission and Monitor Energy Systems (11)	R	
Climate and Risk	CR1.1 Reduce Greenhouse Gas Emissions (18)	R	P
	CR1.2 Reduce Air Pollutant Emissions (11)		P
* P: Primary; R: Related			

Estimating Energy Inputs during Construction of a Golf Course

The project site utilized in this study was an 18-hole golf course on a 216-acre (87.5 hectare) footprint, as reported by Maestas et al. [12]. Turf grass was planted on 116 acres (47 hectares), including 25.4 acres (10.27 hectares) for greens, and 90.8 acres (36.73 hectares) for roughs and fairways. In addition, an area of 90 acres (36.4 hectares) was landscaped—half was planted with woody perennial shrubs and half with unmanaged grasses. Areas dedicated for transport, such as cart paths and walkways, occupied 10 acres (4.1 hectares).

In calculating the energy inputs for various machines used in the construction of a golf course, the machinery used was identified and its engine horsepower was determined (see Table 2). This information was provided by the superintendent of the golf course in private discussions, while some of the technical details were obtained from the manufacturers.

Table 2. Machines used for Various Operations during Construction of the Golf Course

Construction operation	Type	Engine type	Power kW (HP)
Leveling	Caterpillar 637G wheel tractor scraper	Cat C18 ACERT	373 (500)
		Cat C9 ACERT	211 (283)
Grading	Caterpillar 12H motor grader	3306 DINA	104 (140)
Excavating (Hydraulic)	Caterpillar 330DL excavator	Cat C9 ACERT	200 (268)
Excavating (Backhoe)	Caterpillar 416E Backhoe Loader	Cat C4.4 DITA	65 (87)
Excavating (Steer Loader)	Bobcat A300 All Wheel Steer Loader	Kubota V3300 DI T	60 (81)

Productivity of Construction Equipment

The productivity of equipment used for construction of the golf course is a function of machine specifications, site characteristics, and general layout of the golf course. Machine specifications generally include capacity, power, speed, and efficiency. Typical site characteristics for a golf course include earth material properties, slope, and haul distance. The golf course design, e.g., minimalist or sculptured, would also determine the magnitude of the earth-moving operation [2]. Further, project planning and optimized management of time and resources have great impacts on the productivity rate. This is particularly important when multiple machines need to work simultaneously to accomplish certain tasks (e.g., using a combination of scraper, grader, and excavator to move, level, and grade earth). Moreover, development of highly efficient machines has enabled contractors to perform essential construction activities at the same cost levels as before, even though the cost of labor and equipment is on the rise. It can be expected that these highly efficient machines reduce the number of hours per unit of production, thereby reducing the energy input during the construction operation. However, this may not necessarily be the case for the emissions from new machines, or the energy input required to manufacture new machines. Measurement of emissions from heavy-duty construction equipment has shown that same-size equipment often produces similar emission profiles, disregarding their activities. Further, such equipment generally continues to produce emissions and use energy during intermittent idle periods in any working day. Therefore, the presence of ex-

pensive, efficient machines signifies the importance of resource planning to reduce costs as well as emissions and energy impacts [13-15].

Table 3 includes basic characteristics of construction equipment related to its productivity. The productivity rates are obtained from raw data presented by RSMeans [16] and procedures introduced by Peurifoy et al. [14]. Additional adjustments and modifications were implemented, based on machine performance and site characteristics. Generally, the production per hour requires full consideration of the production cycle. Such cycles typically include loading, hauling, unloading, and return. The capacity of the machine, in terms of volume, weight, or size, determines the amount of material displaced, leveled, or graded. Therefore, this capacity is a major factor in productivity. It should be noted that higher capacities appear to increase the loading time for a scraper or backhoe. However, machines with larger capacities often utilize more power that would compensate the time to fill the extra capacity. Further, the speed of the machine is an important factor in hauling time. However, most machines do not reach their maximum speed in short hauling distances (e.g., within a small project). Moreover, contractors often deliver large projects in multiple phases to increase the productivity of the equipment by shortening return times. Therefore, speed will not be a major factor in productivity [2], [14-16].

Table 3. Specifications of Machines used for Various Operations

Type of machine	Capacity	Speed (km/h)	Productivity*	Crew Size (Minimum /8-h day)
Wheel tractor scraper	26 m^3 (heaped)	54.9 (loaded)	130-230 m^3/h	7.0
Motor grader	3.66 m (blade)	7.4/8.1 (3rd gear)	200-1,000 m^2/h	7.5
Excavator	2.55 m^3	5.0	70-180 m^3/h	2.0
Backhoe Loader	0.76 m^3	6.0 (first)	60-80 m^3/h	1.5
All Wheel Steer Loader	0.76 m^3	11.1 (travel)	60-80 m^3/h	1.5

* Assume 4-8% grade, 8% rolling resistance, 3000 lb/cy soil weight, 200 ft haul distance for loader, 1400 ft haul distance for scraper, 80% swell factor, 90% fill factor, and 50 min/h efficiency

Leveling

Large excavators are common for long hauling distances [2]. Productivity also depends on haul grade and rolling resistance. The total resistance of the haul is assumed to be as high as 16%, where 8% is the grade and the other 8% is the rolling resistance. This will substantially affect the travel speed in both the haul and return cycles, as generally reported in the performance chart by the manufacturer. For instance, the travel speed during the haul cycle will be reduced from a nominal speed of 54.9 km/hour to 9.6 km/hour for 16% total resistance (see Table 4). Further, the travel speed at the beginning and the end of the haul/return cycle is generally halved in order to account for acceleration/ deceleration. Moreover, a minimum efficiency factor of 50 min/hour is incorporated into calculations. Hence, the practical efficiency might be lower due to unforeseen down times during operation.

Table 4. Travel Speed of the Scraper for Various Grade Resistances and Cycles

Total Grade (%)	0	4	8	12	16
Haul Cycle Velocity*, km/h	40	42	21	13	10
Return Cycle Velocity*, km/h	53	51	48	26	19

* Caterpillar 631G/637G Wheel Tractor Scrapers Specifications, 2007.

Grading

The productivity of graders is mostly determined by the characteristics of the equipment as well as the skillfulness of the operator. The wide range of potential speeds at various forward/reverse gears enables the operator to maximize the performance of the grader [14]. Typical gear/speed assumptions in determining average productivity of the grader are shown in Table 5.

Table 5. Travel Speed of the Motor Grader for Various Cycles

Cycle Time*	Gear	Forward Velocity** (km/h)	Reverse Velocity** (km/h)
Bank sloping	1st	2.3	1.8
Spreading	3rd	4.6	5.0
	4th	6.4	7.9
Finish	2nd	3.2	5.0
	3rd	4.6	5.0
	4th	6.4	7.9

* Peurifoy et al. [14].
** Caterpillar 12H Motor Grader Specifications, n.d. (accessed 2012).

Excavating

The performance of the backhoe loader is generally related to the digging height, angle of swing, and bucket capacity. Optimizing the size, height, and position of the backhoe

will increase the productivity, as the load, dump, and swing times could be minimized [14]. The hydraulic excavator also follows the same cycle pattern (see Table 6). Additional time should be allowed for the hauling cycle, say, for a distance of 200 feet. Table 7 shows the cycle velocity and times of the backhoe loader and the all-wheel-steer loader.

Table 6. Bucket Fill Cycle Time of the Backhoe Loader and Hydraulic Excavator

Cycle*	Load (sec)	Swing Loaded (sec)	Dump (sec)	Swing Empty (sec)	Total (sec)
Backhoe Loader**	9	4	4	4	21
Hydraulic Excavator***	7	6	4	5	22

* Peurifoy et al. [14].
** Caterpillar 416E Backhoe Loader Specifications, 2008.
*** Caterpillar 330DL Hydraulic Excavator Specifications, n.d. accessed 2012).

Energy Input and CO_2 Emissions from Construction Equipment

The total amount of energy consumed by a machine is made up of: the energy used to manufacture the raw materials; the energy required during the manufacturing process; the energy for any repair and maintenance; and, the energy required to convey the machine from the factory to the consumer and back [17]. There is no literature on energy sequestered by construction equipment. The authors used data from agricultural equipment of similar size. It was presumed that the energy used for manufacturing agricultural equipment, such as tractors, was comparable to the energy used for manufacturing of construction machinery. The amount of energy sequestrated into the manufacturing of farm machinery was calculated by Pimentel et al. [18] to be 86.77 MJ kg^{-1}. The other energy inputs into the construction machinery were the energy for repair and maintenance, which was approximated to be 0.55 times the energy needed to manufacture the machine [19]; and, the energy seized for transportation and distribution of the materials, which was approximated to be 8.8 MJ kg^{-1} [20]. Consequently, the total energy sequestered in the construction machinery was 143.2 MJ kg^{-1}. Wells [21] studied CO_2 emissions from the manufacturing process of all vehicle components and concluded that a mean emission factor of 0.08 kg-CO_2 MJ^{-1} needed to be assessed in order to compensate for the fossil fuel input and deficiencies of the manufacturing process.

It was assumed that all of the machines were parked on the construction site and golf course during construction of the course. Table 8 shows the equipment parameters and the energy coefficients and emissions rates used for this study. An energy coefficient was introduced which represented the amount of energy incorporated into the equipment during the manufacturing process and was used by the machine per hour of operation. The total and daily energy inputs, along with CO_2 emissions for the construction processes, are listed in Table 8. The contractor provided the hours and days during which all machinery was operated.

Table 7. Bucket Fill Cycle of the Backhoe Loader and All-Wheel-Steer Loader

Cycle*	Loaded Velocity (km/h)	Loaded Time (sec)	Cycle Time* (sec)	Empty Velocity (km/h)	Empty Time (sec)	Total Time (sec)
Backhoe Loader**	6.0	46.1	30	9.5	28.9	105
All-wheel-steer Loader***	11.1	24.7	30	19.3	14.2	68.9

* Peurifoy et al. [14].
** Caterpillar 416E Backhoe Loader Specifications, 2008.
*** Bobcat A300 SOP All Wheel Steer Loader Specifications, 2003.

Table 8. Energy Coefficients and Energy Input per Construction Operation for the Entire Course (mass data were obtained from the Caterpillar Performance Handbook, Edition 37)

Construction operation	Mass (kg)	Energy coefficient* (MJ h^{-1})	Emission rate** (kg-CO_2 h^{-1})	10-hour working days (day)	Total construction machinery energy input (MJ)	Total carbon dioxide emissions (kg-CO_2)
Leveling	52,047	373	30.21	15	55,898	4,532
Grading	13,077	94	7.61	15	14,045	1,142
Excavating (Hydraulic)	35,820	256	20.74	132	338,542	27,371
Excavating (Backhoe)	6,792	49	3.97	220	106,988	8,732
Excavating (Steer loader)	5,330	38	3.08	220	83,958	6,772
Total					599,431	48,549

*Assume 20'000-h life ** Emission factor = 0.081 Kg-CO_2 MJ^{-1}

Energy from Labor

Labor is an indispensable part of the construction process. For the purposes of this study, it was assumed that a laborer worked 40 hours per week and consumed 91.1 MJ [18], [22]. To convert hours of labor to energy, a coefficient of 2.28 MJ/hour was used. This coefficient was multiplied by the inverse values of work rate in order to obtain the energy cost of labor in hour/ha (Table 9).

Table 9. Energy Labor Requirements

Operation	No. of workers	No. of 10-hour days per worker	Total human energy inputs* (MJ)
Leveling	12	15	4,104
Grading	12	15	4,104
Excavating (Hydraulic)	3	132	9,029
Excavating (Backhoe)	5	220	25,080
Excavating (Steer loader)	2	220	10,032
Total			52,349
*Labor Energy = 2.28 MJ per hour			

Energy and CO_2 Emissions from Fuel

The fuel requirements from the construction of the golf course were estimated based on the type of construction equipment used for each operation. For the Caterpillar equipment, the hourly fuel consumption given in the Caterpillar Performance Handbook (Edition 37) was utilized for each machine used. For the rest of the equipment, the specific fuel consumption of the particular engines was used to calculate hourly fuel consumption. Data were taken from the manufacturers' brochures for a 75% load factor. The load factor was estimated using data from the operators and the superintendent of the golf course. The energy contained in a liter of diesel fuel was assumed to be 47.8 MJ l^{-1} [23].

Table 10 shows the energy requirements for construction operations. According to EPA (2005), the CO_2 emissions from a gallon of fuel are calculated by multiplying the carbon emissions by the ration of the molecular weight of CO_2 to the molecular weight of carbon (44/12). In accordance with the Intergovernmental Panel on Climate Change guidelines (1996), EPA also recommends that an oxidation factor is assessed to the to the carbon content. For oil and its products the oxidation factor used is 0.99 (99% of the carbon within the fuel is oxidized, while 1% is not) [4], [24]. The value for diesel fuel is 2.668 kg-CO_2 per liter.

Results and Discussion

As can be seen from Table 11, the total amount of energy used in the various operations during golf course construction was almost 4.5 TJ. The same table indicates the percentage share of each operation of the total energy inputs. Most of the input energy was used by the backhoe and steer loader, with over 60% of the total energy input. Leveling and grading were responsible for nearly 20% of the total energy input. This was in line with expectations, since the backhoe and steer loader were engaged in the construction operations for over 2000 hours each.

Table 10. Fuel Energy Requirements for Each Construction Operation

Operation	Fuel consumption ($l\ h^{-1}$)	Total hours of operation (h)	Fuel used* (l)	Total energy used (MJ)	Ratio of energy used (%)	Total CO_2 emissions (kg-CO_2)	Ratio of CO_2 emissions (%)
Leveling	93	150	13,950	666,810	17	37,219	17
Grading	19	150	2,850	136,230	4	7,604	3
Excavating (Hydraulic)	11.4	1320	15,048	719,294	18	40,244	18
Excavating (Backhoe)	11.4	2200	25,080	1,198,824	31	66,914	31
Excavating (Steer loader)	11.3	2200	24,860	1,188,308	30	66,327	30
Total				3,909,466	100	218,308	100
* Energy sequestered in fuels = 47.8 MJ per liter							

Table 11. Total Energy and CO_2 Emissions for Golf Course Construction Operations

Construction operation	Total construction machinery energy from manufacturing (MJ)	Total carbon dioxide emissions from manufacturing (kg-CO_2)	Total energy used from fuel (MJ)	Total CO_2 emissions From exhaust (kg-CO_2)	Total human energy inputs (MJ)	Total energy (MJ)	Ratio of energy (%)	Total CO_2 emissions (kg-CO_2)	Ratio of CO_2 emissions (%)
Leveling	55,898	4,532	666,810	37,219	4,104	726, 812	15.9	41,751	15.6
Grading	14,045	1,142	136,230	7,604	4,104	154,379	3.4	8,746	3.3
Excavating (Hydraulic)	338,542	27,371	719,294	40,244	9,029	1,066,865	23.4	67,615	25.3
Excavating (Backhoe)	106,988	8,732	1,198,824	66,914	25,080	1,330,892	29.2	75,646	28.3
Excavating (Steer loader)	83,958	6,772	1,188,308	66,327	10,032	1,282,298	28.1	73,099	27.4
Total	599,431	48,549	3,909,466	218,308	52,349	4,561,246	100	266,857	100
Ratio (%)	13%	18%	86%	82%	1%	100%		100%	

Table 11 also shows that energy input in the form of fuel was around 86% of the total energy inputs, demonstrating that fuel is by far the most important energy input for golf course construction operations. In second place was the energy sequestered during the manufacturing process, with around 13% of the total energy input to be followed by human energy inputs (1%). Moreover, total CO_2 emissions emitted during various golf course construction operations reached almost 267 tons. Leveling and grading were responsible for almost 19% of the total emissions, while the rest of the operations totaled over 80%. Eighteen percent of carbon emissions came from manufacturing and the rest, 82%, from fuel consumption.

In order to facilitate the use of data for estimation of total energy use or CO_2 emissions, a coefficient of energy and CO_2 emissions per unit of machine productivity is introduced. The productivity of the machine, in terms of volume, weight, or size, determines the amount of material displaced, leveled, or graded. Table 12 shows energy use and CO_2 emissions per hour of operation for the operations involved in golf course construction. The coefficients suggested are in terms of energy use or CO_2 emissions per hour of operation, and also in terms of unit of productivity per MJ or kg-CO_2 unit.

Table 12. Energy and CO_2 Emissions Productivity for Golf Course Construction Operations

Construction operation	Total energy (MJ)	Total CO_2 emissions (kg-CO_2)	Energy per hectare of course (MJ $Hectare^{-1}$)	CO2 emissions per hectare of course (kg-CO_2 $Hectare^{-1}$)	Energy per hour of use (MJ h^{-1})	CO2 emissions per hour of use (kg-CO_2 h^{-1})
Leveling	726,864	41,751	8,307	477	4846	278
Grading	154,434	8,746	1,765	100	1030	58
Excavating (Hydraulic)	1,058,241	67,615	12,094	773	802	51
Excavating (Backhoe)	1,331,704	75,646	15,219	865	605	34
Excavating (Steer loader)	1,284,044	73,216	14,675	837	584	33
Total	4,555,287	266,974	52,060	3,051	757	44

As shown in Table 12, leveling operation used the most energy per hour of operation (nearly 4800 MJ per hour) and emitted the most CO_2 (nearly 280 Kg per hour). The grading operation followed the leveling operation in the aforementioned coefficients, consuming nearly 1000 MJ of energy per hour and emitting nearly 60 Kg of CO_2 per hour. On the other hand, all excavation methods, including backhoe, hydraulic excavator, and steer loader, move less material per unit of energy and emit the most CO_2 during the process, in relation to the other construction operations (Figures 1-4). This is simply due to the large quantity of excavation work and substantial number of hours of operation required during golf course construction.

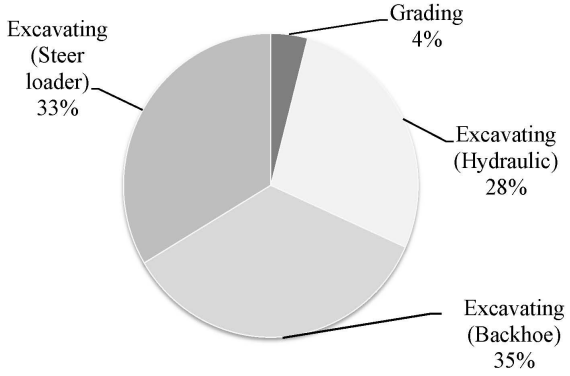

Figure 1. Energy for Golf Course Construction Operations per Hectare

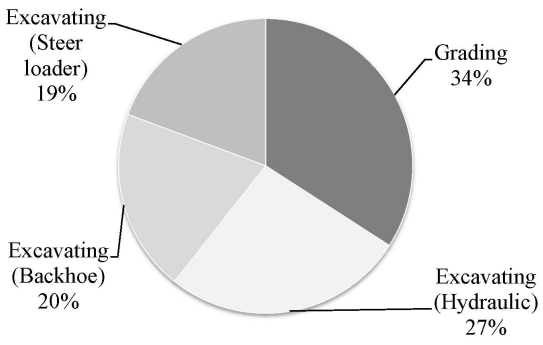

Figure 2. Energy for Golf Course Construction Operations per Hour of Use

Conclusions

The construction of the selected golf course in California's Central Valley caused an estimated release of 267 tons of CO_2 and used approximately 4.5 TJ of energy. This amount included not only the energy and emissions released by the combustion of fuel but also the energy sequestered and CO_2 released during manufacturing and other related processes. From the four construction operations identified in this study, leveling and grading used the most energy per hour of use and emitted the most CO_2. It was followed by excavating (hydraulic), backhoeing, and steer loading. The steer loader emitted the least amount of CO_2 per hour of operation. In general terms, excavating (hydraulic), backhoeing, and steer loading used a quarter of the total energy input and emitted a quarter of the total CO_2 emissions each. In an economic environment where climate change affects economic decisions, the selection of construction equipment may affect the amount of CO_2 released into the environment.

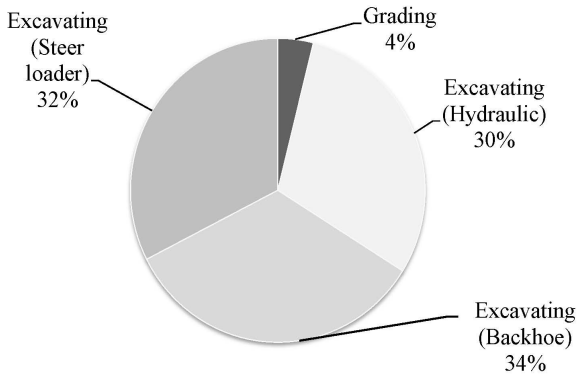

Figure 3. CO_2 Emissions for Golf Course Construction Operations per Hectare

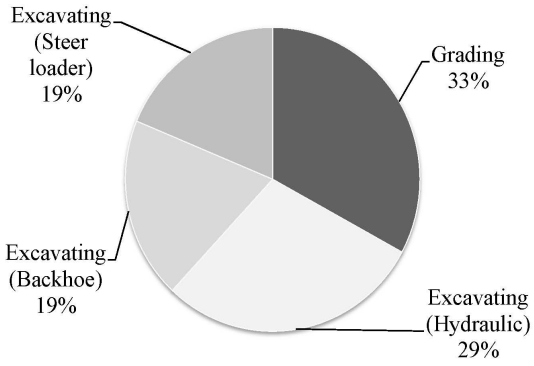

Figure 4. CO_2 Emissions for Golf Course Construction Operations per Hour of Use

The data presented in this paper indicated the need for careful consideration and smart decisions in the selection of equipment used for construction operations. Equipment manufacturing was responsible for 13% of energy use and 18% of CO_2 emissions. In this arena, the manufacturing processes for producing the construction equipment should be considered in the overall performance of the project, with respect to energy use and CO_2 emissions. Sustainable manu-

facturing processes can be measured using energy input coefficients per mass of the equipment, as introduced here. These coefficients might be subject to updates and renewal as manufacturers use innovative materials to reduce the weight of equipment. Further, the fuel efficiency of the produced equipment should be considered in the selection process, as it is responsible for 86% of the energy use and 82% of the CO_2 emissions. Thus, using alternative and green energy to operate heavy machines would be an effective process for reducing those impacts. Increasing the productivity and efficiency of machine operations is another opportunity to reduce the impact of the project on environment. Using the best construction practices to optimize operations facilitates this task by lowering the overall duration of construction. Moreover, the design of the golf course can adapt the existing trends and characteristics of the site to minimize the magnitude of earth-moving activities.

References

[1] Houghton, J. T., Ding, Y., Griggs, D. J., Noguer, M., van der Linden, P. J., Dai, X., et al. (2001). *Climate change 2001: the scientific basis: contribution of working group I to the third assessment*. Report of the Intergovernmental Panel on Climate Change (IPCC). Cambridge, MA: Cambridge University Press.

[2] Graves, R. M., & Cornish, G. S. (1998). *Golf Course Design*. New York, NY: Wiley.

[3] National Research Council. (2003). *Air emissions from animal feeding operations: Current knowledge, future needs*. Washington, DC: National Academies Press.

[4] United States Environmental Protection Agency. (2005). *Emission facts: Average carbon dioxide emissions resulting from gasoline and diesel fuel* (EPA420-F-05-001). United States Environmental Protection Agency. Retrieved August 1, 2012, from: www.carbonsolutions.com/Resources.

[5] Pinder, R. W., Pekney, N. J., Davidson, C. I., & Adams, P. J. (2004). A process-based model of ammonia emissions from dairy cows: Improved temporal and spatial resolution. *Atmospheric Environment*, *38* (9), 1357-1365.

[6] Institute for Sustainable Infrastructure (ISI). (2012). Envision (Version 2.0) [software]. Washington, DC: ISI.

[7] Major, J. (2010). *Guidelines on Practical Aspects of Biochar Application to Field Soil in Various Soil Management Systems*. Westerville, OH: International Biochar Initiative (IBI).

[8] Parsons, B. (2006). The Engineering of Golf Courses. *Canadian Consulting Engineer*, *47*(2), 24-28.

[9] Shen, K., & Xianjuan, K. (2012). Study on Environmental Crisis and Construction of Golf Course. *Advanced Materials Research*, *524-527*, 3251-3255.

[10] Lang, R. E., & Rengert, K. M. (2001). *The Hot and Cold Sunbelts: Comparing State Growth Rates, 1950 -2000* (Fannie Mae Foundation Census Note 02). Washington, DC: Fannie Mae Foundation.

[11] Napton, D. E., & Laingen, C. R. (2008). Expansion of Golf Courses in the United States. *Geographical Review*, *98*(1), 24-41.

[12] Maestas, R., Alexandrou, A., Bushoven, J. T., Goorahoo, D., & Adhikari, D. (2012). Energy inputs and carbon dioxide emissions from turf maintenance equipment on a golf course in California. *Agricultural Engineering International: CIGR Journal, 14*(1), 51-56.

[13] Barth, M., Durbin, T. D., Miller, J. W., & Scora, G. (2008). *Evaluating the emissions from heavy-duty construction equipment* (RTA 65A0197). Riverside, CA: University of California.

[14] Peurifoy, R. L., Schexnayder, C. J., Shapira, A., & Schmitt, R. (2010). *Construction Planning, Equipment, and Methods*. (8th ed.). New York, NY: McGraw-Hill.

[15] Singh, J. (2001). *Heavy Construction: Planning, Equipment, and Methods*. (1st ed.). Lisse, NL: A. A. Balkema Publishers.

[16] Means Engineering Staff (Eds.). (2009). *RSMeans Estimating Handbook*. Kingston, MA: RSMeans Company, Inc.

[17] Bowers, W. (1992). Agricultural field equipment. In R. C. Fluck (Ed.), *Energy in Farm Production: Energy in World Agriculture*. Amsterdam, NL: Elsevier. 6, 117-129.

[18] Pimentel, D., Hurd, L. E., Bellotti, A. C., Forster, M. J., Oka, I. N., Sholes, O. D., et al. (1973). Food production and the energy crisis. *Science*, *182*(4111), 443-449.

[19] Fluck, R. C. (1985). Energy sequestered in repairs and maintenance of agricultural machinery. *Transactions of the ASABE*, *28*(3), 738–744.

[20] Lower, O. J., Benock, G., Gay, N., Smith, E. M., Burgess, S., Wells, L. G., et al. (1977). *BEEF: Production of beef with minimum grain and fossil energy inputs*. (Vol. I, II, and III). Report to National Science Foundation. Lexington, KY: Kentucky University.

[21] Wells, C. (2001). *Total Energy Indicators of Agricultural Sustainability: Dairy Farming Case Study*. Wellington, NZ: Ministry of Agriculture and Forestry.

[22] Fluck, R. C., & Baird, C. D. (1980). *Agricultural Energetics*. Westport, CT: AVI.

[23] Ortiz-Cañavate, J., & Hernanz, J. L. (1999). Energy Analysis and Saving: Energy for Biological Systems. In O. Kitani, T. Jungbluth, R. M. Peart, & A. Ramdani (Eds.), *CIGR Handbook of Agricultural Engineering Vol. V: Energy and Biomass Engineering. The International Commission of Agricultural Engineering* (pp. 13-24). American Society of Agricultural Engineers.

[24] IPCC. (1996). *Guidelines for National Greenhouse Gas Inventories: Reference Manual*. New York, NY: International Panel on Climate Change, United Nations.

Biographies

FARIBORZ TEHRANI is an Assistant Professor, Professional Engineer, and Sustainability Professional in the Department of Civil and Geomatics Engineering at the California State University, Fresno. His research interests are in sustainable and resilient infrastructures, and structural engineering, mechanics, and materials (SEMM). Dr. Tehrani may be reached at ftehrani@csufresno.edu

ATHANASIOS ALEXANDROU is an Associate Professor and Department Chair of Industrial Technology in the Department of Plant Science in the California State University, Fresno. His research focuses on mechanical weed control as part of organic farming, tractor-implement interaction and soil mechanics, with particular interest in soil compaction and its assessment. Dr. Alexandrou may be reached at aalexandrou@csufresno.edu

DIGANTA ADHIKARI is an Adjunct Faculty member in the Center for Irrigation Technology at the California State University, Fresno. He is also a Ph.D. candidate in Environmental Systems at the University of California, Merced. His research includes water management and environmental engineering. He may be reached at dadhikari@ucmerced.edu

MICHAEL MAHONEY is an Associate Professor and the coordinator of the Sports and Entertainment Facility Management Emphasis in the Department of Recreation Administration at the California State University, Fresno. His research interests include venue accessibility, facility, crowd, and security management issues, and patron experience at sport and entertainment venues. Dr. Mahoney may be reached at mmahoney@csufresno.edu

RAYMOND MAESTAS is a graduate Alumni of Plant Science in the California State University, Fresno. He is currently the owner and a research biologist at Precision Ag Research. His research focuses on pesticide, adjuvant, and fertilizer manufacturing. He may be reached at rmaestas@mail.fresnostate.edu

INSTRUCTIONS FOR AUTHORS: MANUSCRIPT REQUIREMENTS

The INTERNATIONAL JOURNAL OF ENGINEERING RESEARCH AND INNOVATION is an online/print publication, designed for Engineering, Engineering Technology, and Industrial Technology professionals. All submissions to this journal, submission of manuscripts, peer-reviews of submitted documents, requested editing changes, notification of acceptance or rejection, and final publication of accepted manuscripts will be handled electronically. The only exception is the submission of separate high-quality image files that are too large to send electronically.

All manuscript submissions must be prepared in Microsoft Word (.doc or .docx) and contain all figures, images and/or pictures embedded where you want them and appropriately captioned. Also, for all accepted manuscripts, each figure, image or picture that was imported into your Word document must be saved individually as a **300dpi or higher JPEG (.jpg)** file and submitted separately; your manuscript and figure numbers must be used in the title of the file (e.g., **J13-F-18 Figure 4**); that means one additional file for each image imported into your manuscript. These 300dpi images do NOT need to be embedded in your manuscript. For tables or graphs created directly in Word, you do not need to submit them as separate files.

Included below is a summary of the formatting instructions. You should, however, review the sample Word document on our website (www.ijeri.org/formatting_guidelines) for details on how to correctly format your manuscript. The editorial staff reserves the right to edit and reformat any submitted document in order to meet publication standards of the journal.

The references included in the References section of your manuscript must follow APA-formatting guidelines. In order to help you, the sample Word document also includes numerous examples of how to format a variety of scenarios. Keep in mind that an incorrectly formatted manuscript will be returned to you, a delay that may cause it (if accepted) to be moved to a subsequent issue of the journal.

1. **Word Document Page Setup**: Two columns with ¼" spacing between columns; Top of page = ¾"; Bottom of page = 1" (from the top of the footer to bottom of page); Left margin = ¾"; Right margin = ¾".

2. **Paper Title**: Centered at the top of the first page with a 22-point Times New Roman (Bold), Small-Caps font.

3. **Page Breaks**: Do not use page breaks.

4. **Body Fonts**: Use 10-point Times New Roman (TNR) for body text throughout (1/8" paragraph indention); 9-point TNR for author names/affiliations under the paper title; 16-point TNR for major section titles; 14-point TNR for minor section titles; 9-point TNR BOLD for caption titles for tables and figures; other font sizes as noted in the sample document.

5. **In-text Referencing**: List and number each reference when referring to them in the body of your document (e.g., [1]). The first entry must be [1] followed by [2], [3], etc., continuing in numerical order to the final entry in your References section. Again, see the sample Word document for specifics. Do not use the End-Page Reference utility in Microsoft Word. You must manually place references in the body of the text.

6. **Tables and Figures**: Center all tables and figures. Captions for tables must be above the table, while captions for figures are below; all captions are left-justified.

7. **Page Limit**: Manuscripts should not be more than 15 pages (single-spaced, 2-column format).

8. **Page Numbering**: Do not use page numbers.

9. **Publication Charges:** Manuscripts accepted for publication are subject to mandatory publication charges.

10. **Copyright Agreement:** A Copyright Transfer Form must be signed and submitted by all authors on a given paper before that paper will be published.

11. **Submissions:** All manuscripts and associated files must be submitted electronically.

    MANUSCRIPTS should be submitted to Dr. Philip D. Weinsier, manuscript editor, at philipw@bgsu.edu along with a copy to editor@ijeri.org.

    FILES containing your high-quality images should ONLY be submitted to philipw@bgsu.edu.

THE LEADING JOURNAL OF ENGINEERING, APPLIED SCIENCE, AND TECHNOLOGY

Print ISSN: 2157-8052
Online ISSN: 1930-6628

www.ijme.us

www.iajc.org

INTERNATIONAL JOURNAL OF MODERN ENGINEERING

ABOUT IJME:

- IJME was established in 2000 and is the first and official flagship journal of the International Association of Journal and Conferences (IAJC).
- IJME is a high-quality, independent journal steered by a distinguished board of directors and supported by an international review board representing many well-known universities, colleges and corporations in the U.S. and abroad.
- IJME has an impact factor of **3.00**, placing it among the top 100 engineering journals worldwide, and is the #1 visited engineering journal website (according to the National Science Digital Library).

OTHER IAJC JOURNALS:

- The International Journal of Engineering Research and Innovation (IJERI)
  For more information visit www.ijeri.org
- The Technology Interface International Journal (TIIJ).
  For more information visit www.tiij.org

IJME SUBMISSIONS:

- Manuscripts should be sent electronically to the manuscript editor, Dr. Philip Weinsier, at philipw@bgsu.edu.

  For submission guidelines visit
  www.ijme.us/submissions

TO JOIN THE REVIEW BOARD:

- Contact the chair of the International Review Board, Dr. Philip Weinsier, at philipw@bgsu.edu.

  For more information visit
  www.ijme.us/ijme_editorial.htm

INDEXING ORGANIZATIONS:

- IJME is indexed by numerous agencies. For a complete listing, please visit us at www.ijme.us.

Contact us:

Mark Rajai, Ph.D.

Editor-in-Chief
California State University-Northridge
College of Engineering and Computer Science
Room: JD 4510
Northridge, CA 91330
Office: (818) 677-5003
Email: mrajai@csun.edu

www.tiij.org

www.ijeri.org

The International Journal of Engineering Research & Innovation (IJERI) is the second official journal of the International Association of Journals and Conferences (IAJC). IJERI is a highly-selective, peer-reviewed print journal which publishes top-level work from all areas of engineering research, innovation and entrepreneurship.

IJERI Contact Information

General questions or inquiries about sponsorship of the journal should be directed to:

Mark Rajai, Ph.D.

Founder and Editor-In-Chief

Office: (818) 677-5003

Email: editor@ijeri.org

Department of Manufacturing Systems Engineering & Management

California State University-Northridge

18111 Nordhoff St.

Room: JD3317

Northridge, CA 91330